NASA TECHNICAL NOTE NASA TN D-5523

NASA TN D-5523

BOUNDARY-LAYER VELOCITY PROFILES DOWNSTREAM OF THREE-DIMENSIONAL TRANSITION TRIPS ON A FLAT PLATE AT MACH 3 AND 4

by John B. Peterson, Jr.

Langley Research Center
Langley Station, Hampton, Va.

NATIONAL AERONAUTICS AND SPACE ADMINISTRATION • WASHINGTON, D. C. • NOVEMBER 1969

1. Report No. NASA TN D-5523	2. Government Accession No.	3. Recipient's Catalog No.
4. Title and Subtitle BOUNDARY-LAYER VELOCITY PROFILES DOWNSTREAM OF THREE-DIMENSIONAL TRANSITION TRIPS ON A FLAT PLATE AT MACH 3 AND 4		5. Report Date November 1969 6. Performing Organization Code
7. Author(s) John B. Peterson, Jr.		8. Performing Organization Report No. L-6486 10. Work Unit No. 720-01-11-02-23
9. Performing Organization Name and Address NASA Langley Research Center Hampton, Va. 23365		11. Contract or Grant No. 13. Type of Report and Period Covered Technical Note
12. Sponsoring Agency Name and Address National Aeronautics and Space Administration Washington, D.C. 20546		14. Sponsoring Agency Code

15. Supplementary Notes

16. Abstract

Boundary-layer profiles were measured downstream of three different configurations of carborundum type transition trips to determine whether the trips caused distortions of the boundary layer. The measured boundary-layer profiles showed that the distortions were very small even for trips larger than the laminar-boundary-layer height at the trip location.

17. Key Words Suggested by Author(s)
Boundary layer
Transition
Transition trips
Velocity profiles

18. Distribution Statement
Unclassified – Unlimited

19. Security Classif. (of this report)	20. Security Classif. (of this page)	21. No. of Pages	22. Price*
Unclassified	Unclassified	87	$3.00

*For sale by the Clearinghouse for Federal Scientific and Technical Information Springfield, Virginia 22151

BOUNDARY-LAYER VELOCITY PROFILES DOWNSTREAM OF THREE-DIMENSIONAL TRANSITION TRIPS ON A FLAT PLATE AT MACH 3 AND 4

By John B. Peterson, Jr.
Langley Research Center

SUMMARY

An investigation was conducted at Mach 3 and 4 and a Reynolds number of 26×10^6 per meter of the effect of three different configurations (locations and widths) of carborundum type transition trips on the boundary-layer profiles downstream of the trips. The three trips tested were as follows: (a) at the 0.0-centimeter station and 0.64 centimeter wide, (b) at the 0.64-centimeter station and 0.64 centimeter wide, and (c) at the 0.64-centimeter station and 0.13 centimeter wide. Several sizes of carborundum grains were tested ranging from a size below that required to trip the boundary layer to a size more than twice as large as the laminar boundary-layer height at the trip location. The boundary-layer profiles were measured at a position 21.6 centimeters from the leading edge of the flat plate.

The results showed that the distortions of the boundary-layer profiles were very small. The variation of the boundary-layer momentum thickness with height of the trip showed that the critical Reynolds number of the trip $R_{k,crit}$ was approximately 600 at Mach 3 and more than 1680 at Mach 4. Further tests are needed to determine how much drag the various trip configurations generate, before a recommendation can be made regarding the best trip configuration to use in a wind tunnel.

INTRODUCTION

One of the most important aspects of wind-tunnel testing of aircraft configurations is the accurate determination of aerodynamic drag. Only with accurate wind-tunnel drag results, together with reliable methods of extrapolating the results to full-scale Reynolds number, can the designer make accurate predictions of full-scale aircraft performance.

Since present-day wind tunnels generally are not capable of duplicating full-scale Reynolds numbers, the boundary layers which develop on wind-tunnel models do not correspond to the boundary layers which develop on full-scale vehicles. For instance the boundary-layer natural-transition position on the wind-tunnel model is downstream of the

corresponding transition position on the full-scale vehicle. Therefore, boundary-layer trips are generally used to fix transition on wind-tunnel models ahead of the natural-transition position in the wind tunnel.

Trips are valuable aids to wind-tunnel testing for many reasons. Three examples of these reasons are as follows:

First, the trips fix the transition position on wind-tunnel models so that the portion of the model in turbulent flow is known. This information allows the designers to calculate the skin friction on the wind-tunnel model so that the wind-tunnel drag results can be extrapolated to full-scale Reynolds numbers.

Second, the changes in wind-tunnel model drag due to small changes in the model configuration can be determined more accurately if the transition position is fixed. If the transition position is not fixed, the changes in drag due to model configuration changes can be masked by the changes in drag caused by shifts of the transition position from one test to another.

Third, tripping the boundary layer on wind-tunnel models insures turbulent boundary layers over the portions of the model which are expected to be turbulent on the full-scale vehicle. Then, characteristics which are sensitive to the condition of the boundary layer, such as control effectiveness, are more closely simulated. In addition, it is sometimes possible to duplicate the relative thickness of the full-scale turbulent boundary layer at certain locations on the wind-tunnel model by fixing transition at the proper location. This procedure was developed in reference 1 to duplicate the full-scale position of the shock wave on a wind-tunnel model wing at transonic speeds. Although tripping the boundary layer will not duplicate full-scale conditions exactly, since there is generally some Reynolds number effect, a turbulent boundary layer will usually duplicate full-scale characteristics more closely than will a laminar boundary layer.

At subsonic Mach numbers it is possible to trip the boundary layer with roughness sizes which are small in comparison with the boundary-layer height. At these Mach numbers the trip drag for properly applied trips is negligible (see ref. 2), and the distortions which the trip might cause to the boundary layer are not of much concern. However, experience has shown that it becomes more difficult to trip the boundary layer at supersonic speeds and larger sizes of roughness are required.

In order to determine whether the roughness sizes required to trip the boundary layer at supersonic Mach numbers cause distortions to the boundary layer, boundary-layer profiles were measured on a flat plate downstream of various sizes of three-dimensional boundary-layer trips made of carborundum particles. In addition to the boundary-layer-profile measurements, an unsuccessful attempt was made to measure the trip drag by measuring the momentum loss in the entire wake behind the trips from the plate surface to the free stream above the leading-edge shock wave.

In addition to a smooth plate without trips, three different trip configurations (locations and widths) were tested. The size of the roughness particles was varied from a size below that required to fix transition to a size larger than the boundary-layer thickness at the trip.

The investigation was conducted in the Langley 20-inch variable supersonic tunnel at Mach 3 and 4 and a Reynolds number of 26×10^6 per meter.

SYMBOLS

H	boundary-layer shape factor, δ^*/θ
k	height of roughness particles in boundary-layer transition trip
$\bar{k}$	average height of roughness particles in boundary-layer transition trip
M	Mach number
n	number of roughness particles in boundary-layer transition trip per unit length
p_t	total pressure
p'	pitot pressure
R_k	Reynolds number of boundary-layer transition trip based on conditions at height of average roughness particle, $u_k\bar{k}/\nu_k$
T_t	total temperature
u	velocity
u_k	velocity in a laminar boundary layer at position x_k and at the height $\bar{k}$
w_k	width of boundary-layer transition trip
x	distance from leading edge
x_k	distance from leading edge of plate to beginning of boundary-layer transition trip

y	distance normal to plate surface
δ	boundary-layer total thickness (see appendix)
δ^*	boundary-layer displacement thickness (see eq. (1))
δ_k	height of laminar boundary layer at position x_k
θ	boundary-layer momentum thickness (see eq. (2))
ν_k	kinematic viscosity in a laminar boundary layer at position x_k and at height $\bar{k}$
ρ	density

Subscripts:

δ	conditions at edge of boundary layer
crit	value which first moves transition from natural-transition location

APPARATUS

Wind Tunnel

The investigation was conducted in the Langley 20-inch (50.8-cm) variable supersonic tunnel. This tunnel is of the blowdown type but the storage reservoir has sufficient capacity for several minutes of running time at the stagnation pressures used in these tests. The maximum stagnation pressure obtainable is 125 lb/sq in. (86 newtons/cm^2). The tunnel has flexible nozzle walls which can be used to vary the Mach number from 2.0 to 4.5. Electrical resistance heaters are available to heat the air to maintain a stagnation temperature above ambient conditions. Further information on the tunnel can be found in reference 3.

Model

The test model was a sharp-leading-edge flat plate mounted vertically in the tunnel at zero angle of attack on a strut off the side wall. This model is the same flat plate used in a previous investigation (ref. 4). A sketch and photographs of the model are shown in figures 1 and 2. The model had removable leading edges 2 inches (5.08 cm) wide, which were used to change the boundary-layer trips during the investigation. The mismatch

step between the leading edge and the flat-plate surface was kept to less than 0.001 inch (0.003 cm), and the joint between the leading edge and the flat plate was sealed with a silicone rubber compound to avoid air leakage. All the leading edges were kept sharp to avoid disturbances from the leading edge. The leading-edge radius was about 0.0003 inch (0.0008 cm).

In addition to a smooth plate without trips, three configurations of boundary-layer trips were tested. The three configurations are shown in the following table:

Configuration	x_k	w_k
(a)	0.00 in. (0.00 cm)	0.25 in. (0.64 cm)
(b)	.25 in. (.64 cm)	.25 in. (.64 cm)
(c)	.25 in. (.64 cm)	.05 in. (.13 cm)

All the trips consisted of carborundum particles glued to the surface with acrylic lacquer. Photographs of the boundary-layer trips enlarged about 2.7 times are shown in figures 3, 4, and 5.

The average size of the carborundum particles tested ranged from 0.0046 centimeter (No. 240 grit) to 0.0491 centimeter (No. 40 grit). A representative number of particles (about 200) were measured (in inches) with a measuring microscope and the results both in inches and centimeters are presented in figure 6. These results show the percentage of measured particles which fell in the range of sizes indicated by the width of the bars on the graphs. Some particles were specially sieved to give average particle sizes which fell between commercially available grit sizes. The No. 240 sieved grit consisted of No. 240 grit sieved through a 0.0041-inch (0.0105-cm) sieve onto a 0.0029-inch (0.0074-cm) sieve. The No. 120 sieved grit was sieved through a 0.0070-inch (0.0177-cm) sieve onto a 0.0059-inch (0.0150-cm) sieve and the No. 70 sieved grit was sieved through a 0.0117-inch (0.0297-cm) sieve onto a 0.0098-inch (0.0248-cm) sieve.

Instrumentation

The tunnel total pressure and total temperature were measured in the tunnel settling chamber ahead of the first minimum. The total pressure was measured with a strain-gage pressure transducer and the total temperature with a thermocouple referenced to an electrically regulated hot junction.

The pressure on the surface of the flat plate was measured with a static-pressure orifice at $x = 20.3$ centimeters (1.3 cm ahead of the boundary-layer-survey position).

Pitot pressures in the boundary layer were measured at a position on the plate center line and 21.6 centimeters from the leading edge. This distance from the leading

edge was the most forward position at which the boundary-layer-survey apparatus could conveniently be located during the test. A single pitot tube was traversed through the boundary layer by the boundary-layer-survey apparatus. The pitot tube was flattened at the end to a height of 0.02 centimeter. The survey apparatus was capable of positioning the pitot pressure tube with an accuracy of approximately ±0.001 centimeter over a range of 2.5 centimeters. All boundary layers encountered in this investigation were less than 0.6 centimeter thick. The probe was electrically insulated from the flat-plate model, and contact with the model surface was indicated by a fouling light on the survey apparatus control console. The pitot pressure was measured with a strain-gage pressure transducer.

In addition to the boundary-layer survey, an attempt was made to survey the flow above the boundary layer with a static and a pitot pressure rake. These rakes were located 2.54 centimeters and 6.85 centimeters off the center line of the flat plate and at a position 21.6 centimeters from the leading edge of the plate. The rakes are shown in figures 1 and 2. The pressures on the pitot rake were measured with an alcohol manometer referenced to a pressure measured by two strain-gage pressure transducers. The pressures on the static rake were measured with two strain-gage pressure transducers mounted on an electrically actuated pressure-scanning valve.

All the pressure transducers and thermocouple outputs were recorded on 10-inch (25.4-cm) self-balancing strip chart recorders. The manometer fluid position was recorded photographically.

TESTS

The tests were conducted at free-stream Mach numbers of approximately 3 and 4. For the Mach 3 test the total temperature and the total pressure were approximately 320° K and 40 newtons/centimeter^2, respectively, and for the Mach 4 tests, approximately 330° K and 71 newtons/centimeter^2, respectively. Both test conditions gave a free-stream unit Reynolds number of approximately 26×10^6 per meter. The total temperatures for both test Mach numbers were chosen to give a recovery wall temperature which was near to ambient temperature (about 300° K) so that there was no heat transfer at the model surface.

The procedure used to obtain the boundary-layer survey was to drive the probe toward the model after the tunnel was started until the fouling light indicated contact of the probe with the model. Then the probe was always moved in a direction away from the plate surface to minimize backlash errors. The data points were taken at several positions above the plate after the pressure settled out.

RESULTS AND DISCUSSION

Reduction of Pitot-Pressure Survey Data

The pitot-pressure survey data at $x = 21.6$ centimeters were used to obtain the boundary-layer velocity profiles, the total thickness δ, the displacement thickness δ^*, and the momentum thickness θ.

In order to determine the height of the pitot probe above the surface of the plate, it was necessary to determine the position of the plate surface as indicated by the probe-position indicator. Although the electrical contact indicator gave some indication of the plate surface, a method used by Coles (ref. 5) was believed to give more accurate results. This method is illustrated in figure 7. Since the probe tip was somewhat flexible, it would deflect when the boundary-layer-survey apparatus was driven beyond the position where the probe touched the flat plate. Therefore, the survey apparatus would give an indication that the probe position was lower than the surface of the plate even though the probe tip remained on the surface. This effect can be seen in figure 7 where the pitot pressure remained constant while the height indication changed from 0.45 to 0.48 centimeter. A plot similar to the plot shown in figure 7 was used to find the surface of the plate for each run. The plate surface is indicated in figure 7 by the point where a line through the points of constant pressure intersects with a line faired through the points above the surface.

The Mach number at the edge of the boundary layer M_δ was used as the reference Mach number in the calculation of θ and δ^*.

The value of M_δ was determined from the ratio of the pitot pressure above the boundary layer p'_δ to the total pressure p_t. Since the wind-tunnel model was a flat plate at zero degrees to the free stream, the total pressure above the boundary layer was assumed to be equal to the total pressure measured in the settling chamber. Although the static pressure on the plate was measured during the investigation and this pressure together with the pitot pressure above the boundary layer could have been used to calculate M_δ, the value of M_δ that could be obtained with the ratio of p'_δ to p_t was believed to be more accurate.

In order to determine the Mach numbers and velocities in the boundary-layer profile, the static pressure and the total temperature were assumed to be constant and equal to the values in the flow just above the boundary layer. The static pressure was calculated from the M_δ determined by the method previously discussed and the measured total pressure.

The boundary-layer thickness δ was determined from the boundary-layer profiles by the method outlined in the appendix.

With the boundary-layer thickness δ and the assumption that the static pressure and total temperature are constant through the boundary layer, the displacement thickness δ^* and momentum thickness θ were determined from the following equations:

$$\delta^* \equiv \int_0^{\delta} \left(1 - \frac{\rho u}{\rho_\delta u_\delta}\right) dy = \int_0^{\delta} \left(1 - \frac{M}{M_\delta}\sqrt{\frac{1 + 0.2M^2}{1 + 0.2M_\delta{}^2}}\right) dy \tag{1}$$

$$\theta \equiv \int_0^{\delta} \frac{\rho u}{\rho_\delta u_\delta}\left(1 - \frac{u}{u_\delta}\right) dy = \int_0^{\delta} \frac{M}{M_\delta}\left(\sqrt{\frac{1 + 0.2M^2}{1 + 0.2M_\delta{}^2}} - \frac{M}{M_\delta}\right) dy \tag{2}$$

The boundary-layer-survey pitot-pressure data were reduced with the aid of a digital electronic computer.

Boundary-Layer Distortions

The boundary layer on the smooth plate without trips was turbulent at the measuring station ($x = 21.6$ cm). Other tests indicated that natural transition occurred on this model at about 5 centimeters from the leading edge at the Reynolds number of this test. The distortions in the profiles measured behind the boundary-layer trips were determined by comparison with the smooth flat-plate turbulent profiles.

Boundary-layer profiles were measured behind the three different trip configurations described in the "Model" section. The first two configurations ((a) $x_k = 0.0$ cm and $w_k = 0.64$ cm and (b) $x_k = 0.64$ cm and $w_k = 0.64$ cm) were tested as examples of trips which are sometimes used but are not recommended (ref. 2). The third configuration ($x_k = 0.64$ cm and $w_k = 0.13$ cm) is an example of the recommended configuration, which is a narrow band of sparsely distributed particles placed at a distance from the leading edge greater than the position of the minimum critical Reynolds number. The Mach numbers and velocities obtained from the boundary-layer surveys are presented in table I, and a summary of the boundary-layer profile parameters is presented in table II. Plots of the boundary-layer Mach number and velocity profiles measured at the 21.6-centimeter station downstream of the three different trip configurations are presented in figures 8 to 19. The data of these figures were plotted on an automatic plotting machine from the results obtained on the electronic digital computer. The smooth-plate turbulent profiles are indicated on each of the figures by a dashed line for comparison with the profiles measured behind the boundary-layer trips. The figures are arranged in the following order:

The effect of trip size on boundary-layer profiles at $x = 21.6$ centimeters, for –

As expected, except for the trips of smaller size, the boundary-layer trips thickened the boundary layer as indicated in figures 8 and 11 and table II. The largest increases in thickness were caused by the trips at the leading edge, both because they cause transition sooner and because the roughness particles have the greatest drag, since they are entirely exposed to the free-stream dynamic pressure and are not shielded by the boundary layer which is present at the other two trips.

The distortion of the boundary-layer profiles as indicated by the plots using the nondimensional heights y/θ or y/δ is very much less than expected. Generally, the profiles are similar in shape to the smooth-flat-plate reference profiles. The largest size roughness was more than twice the laminar boundary-layer height at the most rearward trip location $(x_k = 0.64$ cm) as calculated by the curves in reference 6. The calculated laminar boundary-layer thickness was 0.015 centimeter at $M_\delta = 3$ and 0.020 centimeter at $M_\delta = 4$. Evidently any distortions which were introduced into the boundary layer by the smaller trips had washed out by the time the flow reached the survey station at $x = 21.6$ centimeters. The slight distortions in the profiles behind the larger trips caused the Mach numbers and velocities in the lower part of the nondimensional profile (below $y/\theta \cong 5$) to be slightly higher than those in the flat-plate reference profile. (See figs. 9(a), (b), and (c), and fig. 12(c).)

Since the largest trips greatly increased the boundary-layer thickness, they would be expected to reduce the skin friction behind these trips greatly. However, the distortions in the boundary layer behind the largest trips are in a direction to increase the skin friction, as indicated by the velocities in the boundary layer near the surface, and therefore the skin friction reduction was not as much as it would have been if the profiles had been undistorted. In one case the distortion was large enough to increase the skin friction more than the thickening of the profile decreased the skin friction. This case is shown in figure 8(c) where the profile for the largest roughness size shows Mach numbers greater than the flat-plate reference profile at heights between 0.01 and 0.10 centimeter.

Boundary-Layer Momentum Thickness

The variation of the boundary-layer momentum thickness at the survey station with trip average height $\bar{k}$ is shown in figure 20. The odd behavior of the momentum thickness behind the trips beginning at the leading edge shown in figure 20(a) is discussed subsequently. The curves shown in figures 20(b) and (c) are typical of the expected variation of θ as the trip height is increased. The level of θ remains constant and equal to the value for the smooth flat plate until the trip height reaches the critical value necessary to trip the boundary layer. As the trip height is increased above the critical value the momentum thickness is increased, so that transition appears to have been moved forward by the trip. At subsonic and low supersonic speeds the critical height of a boundary-layer trip is reached when the roughness Reynolds number R_k equals approximately 600. (See ref. 2.) The height necessary for an $R_k = 600$ is indicated by tick marks in figures 20(b) and (c). As can be seen in these figures the critical Reynolds number $R_{k,crit}$ is approximately 600 at Mach 3 but is higher than 600 at Mach 4. This result is in agreement with the values of $R_{k,crit}$ shown in reference 2, which indicates that the $R_{k,crit}$ is approximately 600 from Mach 0 to Mach 3 and increases sharply above Mach 3. Apparently, the transition position is unaffected by the trip at Mach 4 until the trip height is above 0.0155 centimeter. This result indicates that the $R_{k,crit}$ at $M_\delta = 4$ was greater than 1680 in this test.

The height of the laminar boundary layer at the trip location $(x_k = 0.64 \text{ cm})$ calculated from the curves of reference 6 is also indicated by tick marks in figures 20(b) and (c). As can be seen the momentum thickness at $M_\delta = 3$ increases again as the trip height is increased above the laminar-boundary-layer height and indicates that the trip is generating drag; that is, there is an increase in drag above that associated with moving transition forward.

It must be emphasized that the boundary-layer momentum thickness does not indicate the entire drag. There is a possibility of some loss in momentum in the flow above the boundary layer as a result of wave drag. An attempt was made to measure this wave

drag with rakes, but the rake static pressures were not accurate enough to determine the boundary-layer-trip drag. Therefore, determination of the total drag in these tests is not possible. However, an increase in the momentum thickness such as that which occurs at $M_\delta = 3$ when the trip height is greater than δ_k does indicate an increase in the total drag. Since the total drag cannot be determined it is not known whether any trip drag was present at $M_\delta = 3$ when $\bar{k}$ was below δ_k. A comparison between figures 20(b) and 18(c) shows that the momentum thickness is slightly higher for the 0.64-centimeter-wide trip than for the 0.13-centimeter-wide trip at $M_\delta = 3$ when $\bar{k}$ is between $R_{k,crit}$ and δ_k. This result indicates that some trip drag is probably present on the 0.64-centimeter-wide trip at $M_\delta = 3$.

Since the trip was not effective at $M_\delta = 4$ until the trip height was approximately equal to δ_k and since only one increase in the momentum thickness curve is shown in figures 20(b) and (c), it is not possible to determine whether the increase in drag at this point included a trip drag.

In an attempt to determine the cause of the erratic behavior of the momentum thickness shown in figure 20(a), it was noticed that there was a relationship between the measured momentum thickness and the density of the carborundum grains in the pictures of the trips in figure 3. The trips which were abnormally dense corresponded to the points which were abnormally high in figure 20(a). The momentum thickness was found to be a nonlinear function of $n\bar{k}^2$, a parameter proportional to the total frontal area of the carborundum grains in a unit length of the trip as shown in figure 21. The value of n for the various trips is given in the following table:

NUMBER OF CARBORUNDUM GRAINS PER CENTIMETER OF TRIP

$[x_k = 0.0 \text{ cm}; \quad w_k = 0.64 \text{ cm}]$

Carborundum grit No.	$\bar{k}$, cm	n, 1/cm
240 sieved	0.0079	178
120	.0091	382
120 sieved	.0155	63
80	.0194	14
70	.0286	21
40	.0491	19

The curves of figure 21 show a much smoother variation of momentum thickness than those of figure 20(a) indicating that the momentum thickness downstream of the trip at $x_k = 0.0$ centimeter is dependent on the number of particles per unit length of the trip n as well as the average particle height $\bar{k}$.

The variation in density of the carborundum grains found in the trips at $x_k = 0.0$ centimeter can also be seen in the pictures of the trips at $x_k = 0.64$ centimeter. (See fig. 4.) However, the momentum thicknesses shown in figure 20(b) do not show the variation that was noted in figure 20(a). Evidently θ is dependent on n only for trips which start at the leading edge.

CONCLUDING REMARKS

Measurements were made of the turbulent boundary-layer profiles at a station x = 21.6 centimeters downstream of three different configurations of carborundum type boundary-layer trips on a flat plate at Mach 3 and 4 and a Reynolds number of 26×10^6 per meter. The trips were identified by longitudinal position x_k and trip width w_k. The three configurations were (a) $x_k = 0.0$ centimeter and $w_k = 0.64$ centimeter, (b) $x_k = 0.64$ centimeter and $w_k = 0.64$ centimeter, and (c) $x_k = 0.64$ centimeter and $w_k = 0.13$ centimeter. The first two configurations were examples of trips which are sometimes used but not recommended. (See NASA TN D-3579.) The third configuration is an example of the recommended configuration of a narrow band of sparsely distributed particles placed at a distance from the leading edge greater than the minimum critical Reynolds number.

As expected, the trips thickened the boundary layer at the 21.6-centimeter station when they tripped the boundary layer ahead of the natural-transition location. Very large increases in thickness were caused by the trips at the leading edge. The distortions of the boundary-layer profiles downstream of the trips, indicated by nondimensional plots of the Mach number and velocity profiles were very small even for trips larger than the laminar-boundary-layer height at the trip location. Evidently, most of the distortions which were introduced into the boundary layer by the trips had washed out by the time the flow reached the survey station at the 21.6-centimeter station.

The variation of the boundary-layer momentum thickness with height of the trip showed that the critical Reynolds number of the trip $\left(R_{k,crit}\right)$ was approximately 600 at Mach 3 and more than 1680 at Mach 4, which is in agreement with the curves previously published in NASA TN D-3579. The momentum-thickness variations also showed that at a Mach number at the edge of the boundary layer of 3 the trip produced trip drag when the trip height was larger than the laminar-boundary-layer height at the trip location. Whether trip drag was present for trip heights less than the boundary-layer height was not determined. Further tests are needed to determine how much drag the various trip configurations generate, before a recommendation can be made regarding the best trip configuration to use in a wind tunnel.

The results for the trip at the leading edge showed that the momentum-thickness variation was a function of the number of roughness particles in the trip per unit length n as well as of the average height $\bar{k}$.

Langley Research Center,
National Aeronautics and Space Administration,
Langley Station, Hampton, Va., August 21, 1969.

APPENDIX

DETERMINATION OF THE BOUNDARY-LAYER THICKNESS δ

Determination of the total boundary-layer thickness δ has always been a difficult problem in boundary-layer experiments. Theoretically, the boundary layer extends to infinity in incompressible flow and to a Mach line from the leading edge in compressible flow. However, the δ of practical interest is generally much less.

Several different methods for determining δ were examined in this investigation. Each method has its advantages and disadvantages but none was entirely satisfactory. For this reason, a new method of finding δ was developed which is explained below.

Two important characteristics were required of a method for determining δ in this investigation. First, the method should give a realistic δ so that the displacement-thickness integration in equation (1) and momentum-thickness integration in equation (2) includes almost all of the momentum loss in the boundary layer. Second, the method should give consistent and unambiguous values for δ.

The present method was developed from a solution to the velocity profile in a two-dimensional wake behind a single body given by Schlichting (ref. 7, p. 494). This solution gives

$$1 - \frac{u}{u_\infty} = F\left[1 - \left(\frac{y}{b}\right)^{3/2}\right]^2 \tag{A1}$$

where

F a function which determines the center-line velocity of the wake

b width of the wake

y distance from the wake center line

u_∞ free-stream velocity

Writing this equation in terms of the boundary-layer profile gives

$$\left(1 - \frac{u}{u_\delta}\right)^{1/2} = \text{Constant}\left[1 - \left(\frac{y}{\delta}\right)^{3/2}\right] \tag{A2}$$

APPENDIX

If the outer portion of the boundary-layer profile is assumed similar to a wake, then the profile obtained by plotting $\left(1 - \frac{u}{u_\delta}\right)^{1/2}$ against $y^{3/2}$ should be a straight line and the point on the straight line where $\left(1 - \frac{u}{u_\delta}\right)^{1/2} = 0$ will occur where $y^{3/2} = \delta^{3/2}$.

This procedure is illustrated in figure 22(a) for the $M_\delta = 3$ profile without roughness. Also shown in figure 22 are the results of two other methods of determining δ. Figure 22(b) shows the method suggested by Coles (ref. 8) where y is plotted against $\left(1 - \frac{u}{u_\delta}\right)^{2/3}$. Figure 22(c) shows the logarithmic method which assumes that the profile is a power profile of the form $\frac{u}{u_\delta} = \left(\frac{y}{\delta}\right)^n$. As can be seen in figures 22 and 23 the method used in this report gives a more realistic δ and the value of δ is reasonably unambiguous.

The δ was determined by this method for each of the profiles measured in this investigation and the values obtained are listed in table II.

REFERENCES

1. Blackwell, James A., Jr.: Preliminary Study of Effects of Reynolds Number and Boundary-Layer Transition Location on Shock-Induced Separation. NASA TN D-5003, 1969.

2. Braslow, Albert L.; Hicks, Raymond M.; and Harris, Roy V., Jr.: Use of Grit-Type Boundary-Layer-Transition Trips on Wind-Tunnel Models. NASA TN D-3579, 1966.

3. McRee, Donald I.; Peterson, John B., Jr.; and Braslow, Albert L.: Effect of Air Injection Through a Porous Surface and Through Slots on Turbulent Skin Friction at Mach 3. NASA TN D-2427, 1964.

4. Peterson, John B., Jr.; McRee, Donald I.; Adcock, Jerry B.; and Braslow, Albert L.: Further Investigation of Effect of Air Injection Through Slots and Porous Surfaces on Flat-Plate Turbulent Skin Friction at Mach 3. NASA TN D-3311, 1966.

5. Coles, Donald: Measurements in the Boundary Layer on a Smooth Flat Plate in Supersonic Flow – II. Instrumentation and Experimental Techniques at the Jet Propulsion Laboratory. Rep. No. 20-70 (Contract No. DA-04-495-Ord 18), Jet Propulsion Lab., California Inst. Technol., June 1, 1953.

6. Braslow, Albert L.; and Knox, Eugene C.: Simplified Method for Determination of Critical Height of Distributed Roughness Particles for Boundary-Layer Transition at Mach Numbers From 0 to 5. NACA TN 4363, 1958.

7. Schlichting, Hermann (J. Kestin, trans.): Boundary Layer Theory. McGraw-Hill Book Co., Inc., 1955.

8. Coles, Donald: Measurements in the Boundary Layer on a Smooth Flat Plate in Supersonic Flow – I. The Problem of the Turbulent Boundary Layer. Rep. No. 20-69 (Contract No. DA-04-495-Ord 18), Jet Propulsion Lab., California Inst. Technol., June 1, 1953.

TABLE I.- DATA FROM BOUNDARY-LAYER SURVEYS

(a) $M_\delta = 3$; Smooth flat plate

$\bar{k} = 0.0$ cm; $M_\delta = 3.078$

y, cm	M/M_δ	u/u_δ
0.0102	0.3826	0.5759
.0159	.4204	.6191
.0251	.4656	.6670
.0413	.5466	.7431
.0600	.6081	.7934
.0730	.6399	.8170
.0886	.6686	.8370
.1207	.7256	.8735
.1864	.8474	.9384
.2518	.9560	.9841
.3962	1.0005	1.0002
.5112	.9996	.9999
.7591	1.0001	1.0000
1.0182	.9996	.9999
1.3335	.9987	.9995

$\bar{k} = 0.0$ cm; $M_\delta = 3.075$

y, cm	M/M_δ	u/u_δ
0.0102	0.3986	0.5943
.0171	.4367	.6366
.0251	.4767	.6779
.0327	.5188	.7181
.0483	.5812	.7720
.0632	.6165	.7996
.0803	.6501	.8241
.1130	.7125	.8654
.1791	.8288	.9294
.2381	.9301	.9741
.3651	.9998	.9999
.4921	1.0000	1.0000
.7449	1.0001	1.0001
.9934	1.0004	1.0001
1.3075	.9991	.9997

TABLE I.- DATA FROM BOUNDARY-LAYER SURVEYS - Continued

(b) $M_\delta = 3$; $x_k = 0.0$ cm; $w_k = 0.64$ cm

$\bar{k} = 0.0079$ cm; $M_\delta = 3.076$

y, cm	M/M_δ	u/u_δ
0.0102	0.3867	0.5807
.0117	.3980	.5938
.0197	.4423	.6426
.0301	.4835	.6847
.0406	.5375	.7350
.0572	.5914	.7802
.0753	.6277	.8080
.1086	.6780	.8433
.1387	.7199	.8700
.1689	.7750	.9017
.2311	.8676	.9477
.2994	.9637	.9870
.3610	.9948	.9982
.4245	.9988	.9996
.9198	1.0008	1.0003
1.3913	1.0015	1.0005

$\bar{k} = 0.0091$ cm; $M_\delta = 3.083$

y, cm	M/M_δ	u/u_δ
0.0102	0.3788	0.5719
.0168	.4156	.6142
.0229	.4385	.6392
.0390	.5091	.7098
.0562	.5480	.7447
.0721	.5770	.7691
.0895	.6050	.7913
.1213	.6533	.8268
.1838	.7394	.8819
.2515	.8466	.9381
.3832	.9870	.9954
.5131	.9996	.9998
.7639	.9988	.9996
1.0268	1.0015	1.0005
1.3411	1.0020	1.0007

$\bar{k} = 0.0155$; $M_\delta = 3.088$

y, cm	M/M_δ	u/u_δ
0.0102	0.3852	0.5798
.0146	.4175	.6166
.0184	.4392	.6402
.0251	.4768	.6790
.0419	.5468	.7440
.0616	.6066	.7929
.0876	.6479	.8233
.1184	.6780	.8439
.1546	.7253	.8737
.1772	.7627	.8953
.2394	.8521	.9408
.2991	.9319	.9749
.3651	.9825	.9939
.4315	.9979	.9993
.9106	1.0023	1.0008
1.3900	1.0015	1.0005

$\bar{k} = 0.0194$ cm; $M_\delta = 3.084$

y, cm	M/M_δ	u/u_δ
0.0102	0.3959	0.5920
.0174	.4435	.6445
.0241	.4753	.6772
.0413	.5446	.7419
.0597	.5940	.7828
.0781	.6339	.8131
.0933	.6570	.8294
.1257	.7020	.8592
.1892	.7833	.9065
.2521	.8632	.9458
.3788	.9695	.9892
.5089	.9978	.9992
.7614	1.0019	1.0006
1.0217	1.0007	1.0002
1.3370	1.0017	1.0006

TABLE I.- DATA FROM BOUNDARY-LAYER SURVEYS - Continued

(b) $M_\delta = 3$; $x_k = 0.0$ cm; $w_k = 0.64$ cm - Concluded

$\bar{k} = 0.0286$ cm; $M_\delta = 3.084$

y, cm	M/M_δ	u/u_δ
0.0102	0.3751	0.5675
.0130	.3878	.5825
.0184	.4110	.6091
.0352	.4952	.6966
.0495	.5432	.7406
.0657	.5868	.7770
.1019	.6517	.8257
.1353	.6904	.8518
.1702	.7416	.8832
.2324	.8350	.9326
.3004	.9274	.9731
.3607	.9798	.9929
.4178	.9941	.9979
.8525	1.0002	1.0001
1.0481	.9994	.9998

$\bar{k} = 0.0491$ cm; $M_\delta = 3.085$

y, cm	M/M_δ	u/u_δ
0.0102	0.3837	0.5778
.0155	.4104	.6086
.0207	.4298	.6299
.0327	.4824	.6843
.0486	.5435	.7409
.0670	.5877	.7778
.0842	.6130	.7975
.1165	.6455	.8214
.1470	.6748	.8416
.1778	.7120	.8655
.2403	.7780	.9036
.3004	.8399	.9350
.3654	.8964	.9604
.4302	.9479	.9811
.9230	1.0007	1.0002
1.4249	.9986	.9995

TABLE I.- DATA FROM BOUNDARY-LAYER SURVEYS - Continued

(c) $M_\delta = 3$; $x_k = 0.64$ cm; $w_k = 0.64$ cm

$\bar{k} = 0.0046$ cm; $M_\delta = 3.094$

y, cm	M/M_δ	u/u_δ
0.0102	0.3720	0.5647
.0121	.3863	.5817
.0181	.4380	.6395
.0346	.5168	.7176
.0521	.5779	.7706
.0692	.6270	.8085
.0867	.6633	.8343
.1216	.7224	.8723
.1854	.8422	.9363
.2492	.9518	.9827
.3743	.9998	.9999
.5029	1.0006	1.0002
.7553	.9973	.9991
1.0031	1.0012	1.0004
1.3221	1.0041	1.0014

$\bar{k} = 0.0079$ cm; $M_\delta = 3.086$

y, cm	M/M_δ	u/u_δ
0.0102	0.3894	0.5846
.0127	.4072	.6050
.0267	.4868	.6886
.0384	.5429	.7405
.0616	.6134	.7979
.0746	.6441	.8205
.1051	.6921	.8529
.1457	.7540	.8904
.1727	.8050	.9178
.2296	.8928	.9589
.2965	.9788	.9926
.3623	.9998	.9999
.4283	1.0006	1.0002
.9169	.9993	.9998
1.3967	1.0000	1.0000

$\bar{k} = 0.0091$ cm; $M_\delta = 3.089$

y, cm	M/M_δ	u/u_δ
0.0102	0.3693	0.5610
.0137	.3945	.5907
.0229	.4481	.6498
.0368	.5121	.7130
.0552	.5715	.7650
.0724	.6079	.7940
.0873	.6316	.8117
.1184	.6790	.8446
.1803	.7814	.9057
.2477	.8920	.9586
.3794	.9985	.9995
.5067	1.0010	1.0003
.7452	1.0015	1.0005
.9998	.9995	.9998
1.3205	.9995	.9998

$\bar{k} = 0.0155$ cm; $M_\delta = 3.087$

y, cm	M/M_δ	u/u_δ
0.0102	0.3856	0.5802
.0200	.4339	.6345
.0260	.4618	.6637
.0454	.5466	.7438
.0581	.5849	.7757
.0775	.6220	.8044
.1130	.6731	.8405
.1480	.7229	.8722
.1756	.7713	.9001
.2381	.8650	.9467
.3038	.9564	.9843
.3867	.9948	.9982
.4382	1.0007	1.0002
.9134	.9990	.9997
1.3814	.9997	.9999

TABLE I.- DATA FROM BOUNDARY-LAYER SURVEYS - Continued

(c) $M_\delta = 3$; $x_k = 0.64$ cm; $w_k = 0.64$ cm - Concluded

$\bar{k} = 0.0194$ cm; $M_\delta = 3.094$

y, cm	M/M_δ	u/u_δ
0.0102	0.3784	0.5723
.0146	.4065	.6049
.0238	.4577	.6601
.0416	.5221	.7225
.0575	.5648	.7597
.0740	.5923	.7821
.0921	.6202	.8035
.1254	.6702	.8389
.1889	.7763	.9030
.2553	.8816	.9542
.3851	.9970	.9990
.5204	1.0017	1.0006
.7769	1.0022	1.0007
1.0176	1.0006	1.0002
1.3303	1.0005	1.0002

$\bar{k} = 0.0286$ cm; $M_\delta = 3.075$

y, cm	M/M_δ	u/u_δ
0.0102	0.3666	0.5566
.0124	.3752	.5669
.0165	.3845	.5780
.0235	.4137	.6114
.0352	.4738	.6750
.0536	.5478	.7440
.0676	.5924	.7809
.1022	.6616	.8321
.1340	.7018	.8586
.1588	.7382	.8808
.2118	.8129	.9215
.2769	.9062	.9643
.3375	.9703	.9894
.4023	.9977	.9992
.8807	1.0014	1.0005
1.3595	1.0037	1.0013

$\bar{k} = 0.0491$ cm; $M_\delta = 3.089$

y, cm	M/M_δ	u/u_δ
0.0102	0.3783	0.5717
.0159	.4101	.6085
.0232	.4437	.6451
.0387	.5152	.7158
.0578	.5752	.7680
.0749	.6049	.7916
.1099	.6547	.8281
.1416	.6982	.8570
.1730	.7451	.8854
.2372	.8351	.9328
.3010	.9256	.9724
.3632	.9781	.9923
.4578	1.0000	1.0000
.9268	.9995	.9998
1.4173	1.0009	1.0003

TABLE I.- DATA FROM BOUNDARY-LAYER SURVEYS - Continued

(d) $M_\delta = 3$; $x_k = 0.64$ cm; $w_k = 0.13$ cm

$\bar{k} = 0.0046$ cm; $M_\delta = 3.054$

y, cm	M/M_δ	u/u_δ
0.0102	0.3619	0.5492
.0162	.3954	.5889
.0238	.4378	.6360
.0397	.5299	.7266
.0549	.5949	.7816
.0711	.6416	.8168
.0870	.6748	.8399
.1200	.7380	.8799
.1825	.8491	.9386
.2426	.9429	.9789
.3708	.9978	.9992
.4981	1.0001	1.0000
.7540	1.0007	1.0002
1.0080	.9996	.9998
1.3230	1.0015	1.0005
1.6421	1.0011	1.0004

$\bar{k} = 0.0079$ cm; $M_\delta = 3.077$

y, cm	M/M_δ	u/u_δ
0.0102	0.3976	0.5933
.0117	.4104	.6079
.0184	.4549	.6559
.0375	.5556	.7508
.0514	.6138	.7976
.0683	.6581	.8297
.1019	.7041	.8602
.1406	.7670	.8973
.1724	.8255	.9279
.2366	.9283	.9734
.3029	.9882	.9959
.3680	.9989	.9996
.4293	1.0007	1.0003
.9134	1.0012	1.0004
1.3913	.9992	.9997

$\bar{k} = 0.0091$ cm; $M_\delta = 3.080$

y, cm	M/M_δ	u/u_δ
0.0102	0.3348	0.5175
.0130	.3552	.5431
.0229	.4366	.6369
.0387	.5137	.7138
.0546	.5693	.7626
.0689	.6014	.7884
.0873	.6356	.8140
.1175	.6837	.8472
.1835	.8011	.9157
.2445	.8932	.9589
.3667	1.0004	1.0002
.4937	1.0004	1.0002
.7515	.9997	.9999
.9922	.9991	.9997
1.3160	.9980	.9993
1.6421	1.0011	1.0004

$\bar{k} = 0.0155$ cm; $M_\delta = 3.085$

y, cm	M/M_δ	u/u_δ
0.0102	0.3831	0.5772
.0146	.4127	.6111
.0225	.4521	.6536
.0375	.5183	.7184
.0565	.5885	.7785
.0778	.6327	.8122
.1153	.6866	.8494
.1480	.7357	.8798
.1772	.7826	.9062
.2423	.8845	.9553
.3061	.9695	.9892
.3727	1.0004	1.0002
.4439	1.0003	1.0001
.9017	.9995	.9998
1.3811	.9982	.9994

TABLE I.- DATA FROM BOUNDARY-LAYER SURVEYS - Continued

(d) $M_\delta = 3$; $x_k = 0.64$ cm; $w_k = 0.13$ cm - Concluded

$\bar{k} = 0.0194$ cm; $M_\delta = 3.066$

y, cm	M/M_δ	u/u_δ
0.0102	0.3319	0.5126
.0133	.3527	.5389
.0216	.3897	.5833
.0375	.4899	.6902
.0597	.5637	.7569
.0733	.5903	.7787
.0867	.6158	.7985
.1197	.6664	.8349
.1816	.7664	.8966
.2477	.8704	.9487
.3683	.9937	.9978
.4959	.9998	.9999
.7483	.9999	1.0000
1.0585	1.0002	1.0001
1.3789	1.0002	1.0001
1.6421	1.0011	1.0004

$\bar{k} = 0.0286$ cm; $M_\delta = 3.072$

y, cm	M/M_δ	u/u_δ
0.0102	0.3574	0.5452
.0146	.3648	.5542
.0213	.4007	.5965
.0368	.4788	.6798
.0540	.5324	.7302
.0679	.5738	.7658
.1010	.6424	.8185
.1327	.6851	.8478
.1670	.7371	.8801
.2267	.8334	.9316
.2940	.9351	.9760
.3569	.9868	.9954
.4248	.9990	.9996
.8915	1.0006	1.0002
1.3890	1.0015	1.0005

$\bar{k} = 0.0298$ cm; $M_\delta = 3.082$

y, cm	M/M_δ	u/u_δ
0.0102	0.3291	0.5103
.0137	.3550	.5430
.0244	.4308	.6307
.0292	.4532	.6545
.0438	.5317	.7303
.0600	.5739	.7665
.0835	.6134	.7977
.0994	.6411	.8180
.1305	.6839	.8474
.1946	.7817	.9055
.2661	.8794	.9530
.3962	.9942	.9980
.5566	.9993	.9997
.8122	1.0001	1.0000
1.0401	1.0024	1.0008
1.3287	.9975	.9991

$\bar{k} = 0.0491$ cm; $M_\delta = 3.087$

y, cm	M/M_δ	u/u_δ
0.0102	0.4034	0.6008
.0159	.4464	.6478
.0248	.5050	.7062
.0349	.5564	.7522
.0508	.6164	.8002
.0654	.6460	.8219
.1000	.6866	.8494
.1368	.7304	.8767
.1619	.7682	.8984
.2254	.8470	.9384
.2905	.9253	.9723
.3543	.9799	.9930
.4127	.9976	.9992
.9557	1.0019	1.0007
1.4643	1.0031	1.0011

TABLE I.- DATA FROM BOUNDARY-LAYER SURVEYS - Continued

(e) $M_\delta = 4$; Smooth flat plate

$\bar{k} = 0.0$ cm; $M_\delta = 4.109$

y, cm	M/M_δ	u/u_δ
0.0102	0.3356	0.5976
.0130	.3703	.6405
.0194	.4188	.6944
.0416	.5156	.7830
.0568	.5574	.8146
.0702	.5864	.8345
.0860	.6107	.8500
.1190	.6621	.8795
.1895	.7931	.9387
.2568	.9154	.9786
.3797	.9984	.9996
.5058	1.0019	1.0004
.7616	.9991	.9998
1.0315	1.0007	1.0002
1.3716	1.0023	1.0005
1.6856	.9952	.9989

$\bar{k} = 0.0$ cm; $M_\delta = 4.105$

y, cm	M/M_δ	u/u_δ
0.0102	0.3637	0.6323
.0111	.3782	.6494
.0178	.4291	.7047
.0263	.4777	.7508
.0473	.5436	.8044
.0619	.5756	.8271
.0768	.6047	.8460
.0914	.6250	.8585
.1257	.6851	.8913
.1984	.8135	.9462
.2613	.9152	.9785
.3946	.9967	.9992
.5210	.9929	.9984
.7826	.9993	.9998
1.0379	.9988	.9997
1.3497	.9994	.9999

$\bar{k} = 0.0$ cm; $M_\delta = 4.111$

y, cm	M/M_δ	u/u_δ
0.0102	0.3555	0.6228
.0178	.4112	.6864
.0263	.4541	.7296
.0428	.5210	.7874
.0638	.5678	.8220
.0816	.6001	.8434
.0987	.6270	.8599
.1368	.6895	.8937
.2096	.8194	.9484
.2762	.9255	.9814
.4083	.9988	.9997
.5337	.9961	.9991
.7921	.9983	.9996
1.0449	1.0026	1.0006
1.3656	1.0000	1.0000
1.6859	1.0050	1.0011

TABLE I.- DATA FROM BOUNDARY-LAYER SURVEYS - Continued

(f) $M_\delta = 4$; $x_k = 0.0$ cm; $w_k = 0.64$ cm

$\bar{k} = 0.0079$ cm; $M_\delta = 4.101$

y, cm	M/M_δ	u/u_δ
0.0102	0.3124	0.5663
.0175	.3690	.6384
.0219	.3980	.6715
.0400	.5058	.7746
.0543	.5593	.8156
.0721	.6076	.8477
.1051	.6551	.8755
.1318	.6993	.8982
.1683	.7691	.9292
.2276	.8759	.9669
.2991	.9595	.9903
.3610	.9964	.9992
.4490	.9985	.9997
.9395	1.0090	1.0020
1.4176	1.0009	1.0002

$\bar{k} = 0.0091$ cm; $M_\delta = 4.110$

y, cm	M/M_δ	u/u_δ
0.0102	0.3390	0.6020
.0137	.3643	.6334
.0235	.4145	.6899
.0387	.4657	.7403
.0546	.5006	.7709
.0708	.5272	.7923
.0870	.5458	.8063
.1191	.5866	.8347
.1905	.6975	.8976
.2575	.8037	.9427
.3804	.9700	.9929
.5077	.9983	.9996
.7662	1.0000	1.0000
1.0179	1.0005	1.0001
1.3345	.9989	.9997
1.6520	1.0011	1.0002

$\bar{k} = 0.0155$ cm; $M_\delta = 4.107$

y, cm	M/M_δ	u/u_δ
0.0102	0.3104	0.5640
.0117	.3250	.5836
.0191	.3768	.6480
.0250	.4030	.6774
.0377	.4562	.7312
.0584	.5180	.7848
.0730	.5508	.8098
.1025	.5940	.8394
.1460	.6550	.8756
.1768	.7045	.9009
.2321	.7970	.9402
.2991	.9035	.9752
.3622	.9758	.9943
.4255	.9979	.9995
.9042	1.0020	1.0004
1.3821	1.0024	1.0005

$\bar{k} = 0.0194$ cm; $M_\delta = 4.106$

y, cm	M/M_δ	u/u_δ
0.0102	0.3281	0.5876
.0165	.3593	.6270
.0232	.3776	.6488
.0419	.4452	.7207
.0572	.4768	.7500
.0747	.5008	.7707
.0899	.5163	.7834
.1213	.5444	.8050
.1902	.6154	.8527
.2540	.6998	.8986
.3861	.8922	.9719
.5067	.9891	.9975
.7845	.9974	.9994
1.0462	.9996	.9999
1.3678	1.0019	1.0004
1.6837	1.0008	1.0002

TABLE I.- DATA FROM BOUNDARY-LAYER SURVEYS - Continued

(f) $M_\delta = 4$; $x_k = 0.0$ cm; $w_k = 0.64$ cm - Concluded

$\bar{k} = 0.0286$ cm; $M_\delta = 4.095$

y, cm	M/M_δ	u/u_δ
0.0102	0.2898	0.5341
.0111	.2889	.5328
.0184	.3462	.6101
.0248	.3796	.6504
.0454	.4719	.7450
.0565	.5093	.7771
.0746	.5530	.8107
.1077	.5957	.8399
.1407	.6376	.8654
.1686	.6836	.8902
.2375	.7981	.9403
.3032	.9004	.9742
.3693	.9729	.9936
.4385	.9911	.9979
.9074	.9993	.9998
1.3767	1.0015	1.0003

$\bar{k} = 0.0491$ cm; $M_\delta = 4.096$

y, cm	M/M_δ	u/u_δ
0.0102	0.2974	0.5450
.0120	.3123	.5658
.0181	.3454	.6092
.0247	.3823	.6535
.0368	.4250	.6999
.0527	.4690	.7424
.0705	.5031	.7721
.0997	.5430	.8034
.1409	.5880	.8350
.1724	.6280	.8599
.2314	.7076	.9021
.2972	.7859	.9357
.3626	.8724	.9658
.4184	.9342	.9837
.9011	.9988	.9997
1.4090	1.0024	1.0005

TABLE I.- DATA FROM BOUNDARY-LAYER SURVEYS - Continued

(g) $M_\delta = 4$; $x_k = 0.64$ cm; $w_k = 0.64$ cm

$\bar{k} = 0.0079$ cm; $M_\delta = 4.104$

y, cm	M/M_δ	u/u_δ
0.0102	0.3253	0.5838
.0143	.3547	.6213
.0216	.4003	.6743
.0384	.4931	.7641
.0549	.5567	.8139
.0797	.6161	.8531
.1048	.6511	.8734
.1327	.6963	.8969
.1746	.7710	.9300
.2397	.8866	.9702
.3035	.9660	.9919
.3686	.9976	.9995
.4308	1.0017	1.0004
.9033	1.0021	1.0005
1.3684	1.0003	1.0001

$\bar{k} = 0.0091$ cm; $M_\delta = 4.114$

y, cm	M/M_δ	u/u_δ
0.0102	0.3288	0.5891
.0225	.4190	.6949
.0276	.4518	.7275
.0419	.4984	.7692
.0616	.5520	.8110
.0740	.5836	.8328
.0956	.6115	.8507
.1261	.6609	.8791
.1899	.7793	.9335
.2549	.8938	.9725
.3775	.9965	.9992
.5061	.9998	1.0000
.7617	.9994	.9999
1.0322	1.0004	1.0001
1.3522	1.0022	1.0005
1.6811	1.0032	1.0007

$\bar{k} = 0.0155$ cm; $M_\delta = 4.107$

y, cm	M/M_δ	u/u_δ
0.0102	0.3155	0.5708
.0108	.3249	.5834
.0155	.3563	.6235
.0267	.4262	.7018
.0451	.5076	.7764
.0610	.5653	.8201
.0787	.6012	.8439
.1108	.6458	.8705
.1375	.6911	.8944
.1772	.7636	.9271
.2489	.8860	.9701
.3140	.9707	.9931
.3829	.9979	.9995
.4515	1.0019	1.0004
.9277	1.0010	1.0002
1.4068	1.0006	1.0001

$\bar{k} = 0.0194$ cm; $M_\delta = 4.119$

y, cm	M/M_δ	u/u_δ
0.0102	0.3161	0.5725
.0140	.3638	.6335
.0232	.4247	.7011
.0464	.4988	.7698
.0603	.5250	.7910
.0787	.5552	.8136
.0936	.5745	.8270
.1257	.6232	.8579
.1876	.7274	.9119
.2537	.8462	.9577
.3791	.9902	.9977
.5039	.9989	.9997
.7664	.9977	.9995
1.0204	1.0005	1.0001
1.3268	1.0011	1.0002
1.6475	1.0027	1.0006

TABLE I.- DATA FROM BOUNDARY-LAYER SURVEYS - Continued

(g) $M_\delta = 4$; $x_k = 0.64$ cm; $w_k = 0.64$ cm - Concluded

$\bar{k} = 0.0286$ cm; $M_\delta = 4.105$

y, cm	M/M_δ	u/u_δ
0.0102	0.2759	0.5146
.0191	.3529	.6191
.0257	.3922	.6653
.0413	.4589	.7337
.0600	.5197	.7860
.0743	.5529	.8111
.1121	.5990	.8425
.1372	.6352	.8644
.1711	.6889	.8932
.2375	.8013	.9417
.3013	.9070	.9762
.3648	.9792	.9951
.4280	.9984	.9996
.9011	1.0020	1.0005
1.3805	1.0006	1.0001
1.4068	1.0006	1.0001

$\bar{k} = 0.0491$ cm; $M_\delta = 4.131$

y, cm	M/M_δ	u/u_δ
0.0102	0.3054	0.5588
.0152	.3527	.6208
.0216	.3941	.6693
.0394	.4736	.7488
.0549	.5228	.7900
.0762	.5668	.8223
.1137	.6122	.8519
.1445	.6581	.8782
.1731	.7051	.9020
.2337	.8007	.9420
.3032	.9119	.9778
.3680	.9741	.9939
.4365	.9939	.9986
.9191	.9990	.9998
1.4065	1.0022	1.0005

TABLE I.- DATA FROM BOUNDARY-LAYER SURVEYS — Continued

(h) $M_\delta = 4$; $x_k = 0.64$ cm; $w_k = 0.13$ cm

$\bar{k} = 0.0079$ cm; $M_\delta = 4.087$

y, cm	M/M_δ	u/u_δ
0.0102	0.3208	0.5765
.0114	.3313	.5904
.0193	.3815	.6519
.0238	.4056	.6788
.0406	.4887	.7593
.0593	.5631	.8175
.0771	.6008	.8428
.1114	.6574	.8761
.1384	.7016	.8988
.1743	.7669	.9280
.2390	.8841	.9693
.3032	.9650	.9916
.3686	.9945	.9987
.4369	1.0007	1.0002
.9223	.9989	.9997
1.4163	.9999	1.0000

$\bar{k} = 0.0091$ cm; $M_\delta = 4.098$

y, cm	M/M_δ	u/u_δ
0.0102	0.2723	0.5087
.0121	.2858	.5285
.0197	.3539	.6199
.0324	.4353	.7105
.0489	.5064	.7750
.0632	.5503	.8090
.0804	.5865	.8341
.1108	.6392	.8664
.1788	.7810	.9339
.2388	.8777	.9675
.3711	.9932	.9984
.5010	.9998	1.0000
.7550	.9997	.9999
1.0611	1.0003	1.0001
1.3853	1.0003	1.0001
1.6974	.9998	1.0000

$\bar{k} = 0.0155$ cm; $M_\delta = 4.093$

y, cm	M/M_δ	u/u_δ
0.0102	0.3108	0.5635
.0159	.3541	.6198
.0229	.3993	.6725
.0289	.4312	.7060
.0435	.4988	.7683
.0619	.5687	.8218
.0730	.5983	.8415
.1042	.6448	.8694
.1362	.6965	.8966
.1683	.7598	.9252
.2280	.8682	.9644
.2937	.9581	.9899
.3588	.9939	.9986
.4219	.9999	1.0000
.8970	.9994	.9999
1.3792	1.0016	1.0004

$\bar{k} = 0.0194$ cm; $M_\delta = 4.102$

y, cm	M/M_δ	u/u_δ
0.0102	0.2602	0.4906
.0127	.2897	.5345
.0191	.3464	.6108
.0270	.3897	.6623
.0406	.4481	.7232
.0597	.5068	.7755
.0734	.5439	.8044
.1051	.6011	.8437
.1715	.7184	.9073
.2314	.8234	.9497
.3572	.9840	.9963
.4858	.9975	.9994
.7430	1.0009	1.0002
1.0763	1.0014	1.0003
1.3741	1.0009	1.0002
1.7148	1.0009	1.0002

TABLE I.- DATA FROM BOUNDARY-LAYER SURVEYS - Concluded

(h) $M_\delta = 4$; $x_k = 0.64$ cm; $w_k = 0.13$ cm - Concluded

$\bar{k} = 0.0286$ cm; $M_\delta = 4.109$

y, cm	M/M_δ	u/u_δ
0.0102	0.2781	0.5180
.0143	.3107	.5644
.0207	.3525	.6189
.0302	.4105	.6856
.0517	.4991	.7695
.0667	.5423	.8036
.0810	.5708	.8240
.1127	.6074	.8479
.1460	.6594	.8781
.1762	.7112	.9042
.2451	.8303	.9522
.3080	.9325	.9833
.3715	.9889	.9974
.4302	.9999	1.0000
.9064	.9994	.9999
1.3859	1.0017	1.0004

$\bar{k} = 0.0298$ cm; $M_\delta = 4.114$

y, cm	M/M_δ	u/u_δ
0.0102	0.2533	0.4807
.0140	.2965	.5451
.0200	.3417	.6057
.0409	.4484	.7243
.0597	.5054	.7751
.0711	.5295	.7942
.0899	.5667	.8214
.1209	.6239	.8582
.1845	.7318	.9137
.2480	.8411	.9559
.3803	.9974	.9994
.5134	.9986	.9997
.7645	.9997	.9999
1.1033	1.0008	1.0002
1.4033	1.0030	1.0007
1.7062	1.0036	1.0008

$\bar{k} = 0.0491$ cm; $M_\delta = 4.109$

y, cm	M/M_δ	u/u_δ
0.0102	0.3278	0.5875
.0169	.3857	.6584
.0270	.4509	.7264
.0423	.5256	.7909
.0518	.5607	.8170
.0692	.5972	.8415
.0886	.6164	.8535
.1185	.6544	.8754
.1537	.7038	.9007
.1807	.7430	.9185
.2416	.8347	.9537
.3061	.9180	.9794
.3680	.9781	.9949
.4360	.9954	.9989
.9129	.9999	1.0000
1.4075	1.0003	1.0001

TABLE II.- SUMMARY OF PARAMETERS FROM PROFILE MEASUREMENTS

$[M_\delta = 3]$

Run no.	x_k, cm	w_k, cm	Grit no.	$\bar{k}$, cm	p_t, N/cm^2	T_t, ^oK	M_δ	u_δ, m/sec	θ, cm	δ^*, cm	δ, cm	H
32	-	-	-	0.0000	40.2	322	3.078	650	0.0174	0.101	0.303	5.8
50	-	-	-	.0000	40.3	324	3.075	652	.0179	.103	.315	5.8
117	0.00	0.64	240S	.0079	40.3	323	3.076	651	.0203	.116	.358	5.7
30	↓	↓	120	.0091	40.1	321	3.083	650	.0241	.139	.398	5.8
128			120S	.0155	40.0	323	3.088	652	.0221	.125	.393	5.7
29			80	.0194	40.2	321	3.084	650	.0228	.129	.407	5.7
108			70S	.0286	40.5	323	3.084	652	.0228	.130	.396	5.7
131			40	.0491	40.0	322	3.085	651	.0295	.165	.534	5.6
39	0.64	0.64	240	.0046	40.2	323	3.094	653	.0175	.102	.306	5.8
121	↓	↓	240S	.0079	39.9	322	3.086	652	.0186	.107	.335	5.8
38			120	.0091	40.1	322	3.089	652	.0209	.121	.354	5.8
127			120S	.0155	40.1	322	3.087	651	.0212	.122	.370	5.8
35			80	.0194	40.3	322	3.094	652	.0223	.129	.370	5.8
112			70S	.0286	40.3	323	3.075	651	.0222	.127	.390	5.7
122			40	.0491	40.0	322	3.089	652	.0230	.131	.400	5.7
26	0.64	0.13	240	.0046	40.1	322	3.054	649	.0174	.100	.313	5.7
124	↓	↓	240S	.0079	40.2	322	3.077	651	.0173	.099	.317	5.7
24			120	.0091	40.1	323	3.080	652	.0204	.118	.348	5.8
116			120S	.0155	40.2	322	3.085	652	.0203	.117	.361	5.8
23			80	.0194	40.1	323	3.066	650	.0223	.129	.371	5.8
104			70S	.0286	40.2	317	3.072	646	.0224	.129	.379	5.8
20			60	.0298	40.0	322	3.082	651	.0232	.133	.395	5.7
133	↓	↓	40	.0491	39.8	321	3.087	651	.0209	.117	.399	5.6

TABLE II.- SUMMARY OF PARAMETERS FROM PROFILE MEASUREMENTS - Concluded

$[M_\delta = 4]$

Run no.	x_k, cm	w_k, cm	Grit no.	k, cm	p_t, N/cm^2	T_t, ^oK	M_δ	u_δ, m/sec	θ, cm	δ^*, cm	δ, cm	H
33	-	-	-	0.0000	71.5	335	4.109	720	0.0142	0.128	0.337	9.0
49	-	-	-	.0000	71.5	335	4.105	720	.0142	.126	.341	8.9
51	-	-	-	.0000	71.6	335	4.111	721	.0147	.132	.355	9.0
118	0.00	0.64	240S	.0079	70.2	328	4.101	712	.0139	.124	.327	8.9
31	↓	↓	120	.0091	71.4	335	4.110	721	.0188	.169	.404	9.0
129	↓	↓	120S	.0155	71.6	331	4.107	716	.0173	.155	.396	9.0
28	↓	↓	80	.0194	71.5	333	4.106	718	.0240	.214	.507	8.9
110	↓	↓	70S	.0286	70.5	329	4.095	714	.0178	.159	.401	8.9
132	↓	↓	40	.0491	71.4	330	4.096	715	.0229	.203	.507	8.9
120	0.64	0.64	240S	.0079	71.8	331	4.104	716	.0141	.126	.337	8.9
37	↓	↓	120	.0091	71.5	333	4.114	719	.0149	.134	.344	9.0
126	↓	↓	120S	.0155	71.4	330	4.107	715	.0147	.132	.346	9.0
36	↓	↓	80	.0194	71.6	333	4.119	719	.0169	.152	.372	9.0
111	↓	↓	70S	.0286	70.4	329	4.105	714	.0174	.157	.394	9.0
123	↓	↓	40	.0491	71.5	330	4.131	716	.0170	.154	.397	9.1
125	0.64	0.13	240S	.0079	71.5	330	4.087	714	.0144	.128	.337	8.9
25	↓	↓	120	.0091	71.4	335	4.098	720	.0145	.131	.331	9.0
115	↓	↓	120S	.0155	70.4	329	4.093	713	.0142	.127	.330	8.9
22	↓	↓	80	.0194	71.4	335	4.102	721	.0162	.147	.354	9.1
107	↓	↓	70S	.0286	70.5	329	4.109	714	.0167	.151	.337	9.0
21	↓	↓	60	.0298	71.2	334	4.114	719	.0167	.152	.370	9.1
134	↓	↓	40	.0491	71.6	332	4.109	717	.0163	.143	.406	8.8

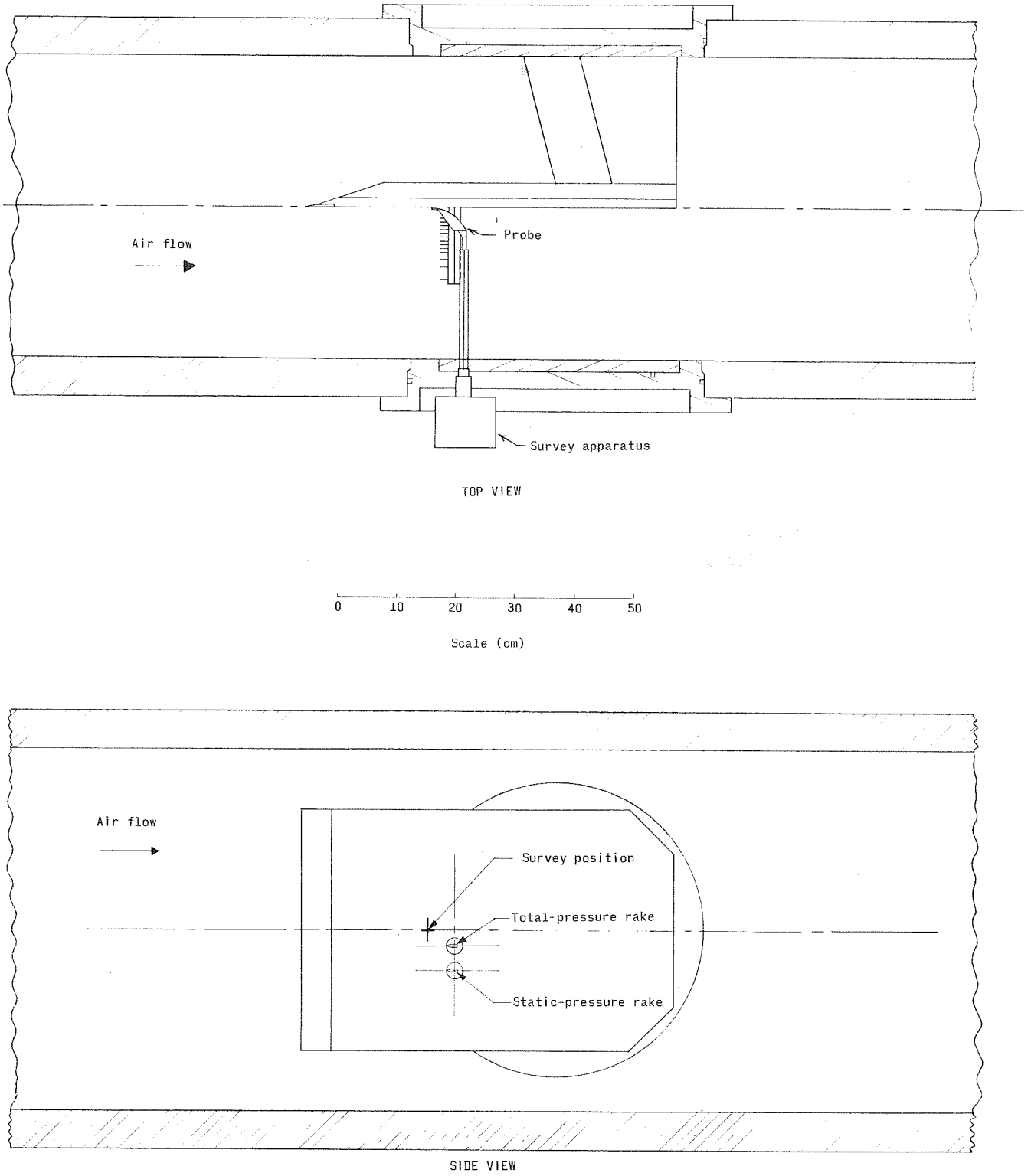

Figure 1.- Diagram of the model in the 20-inch variable supersonic tunnel.

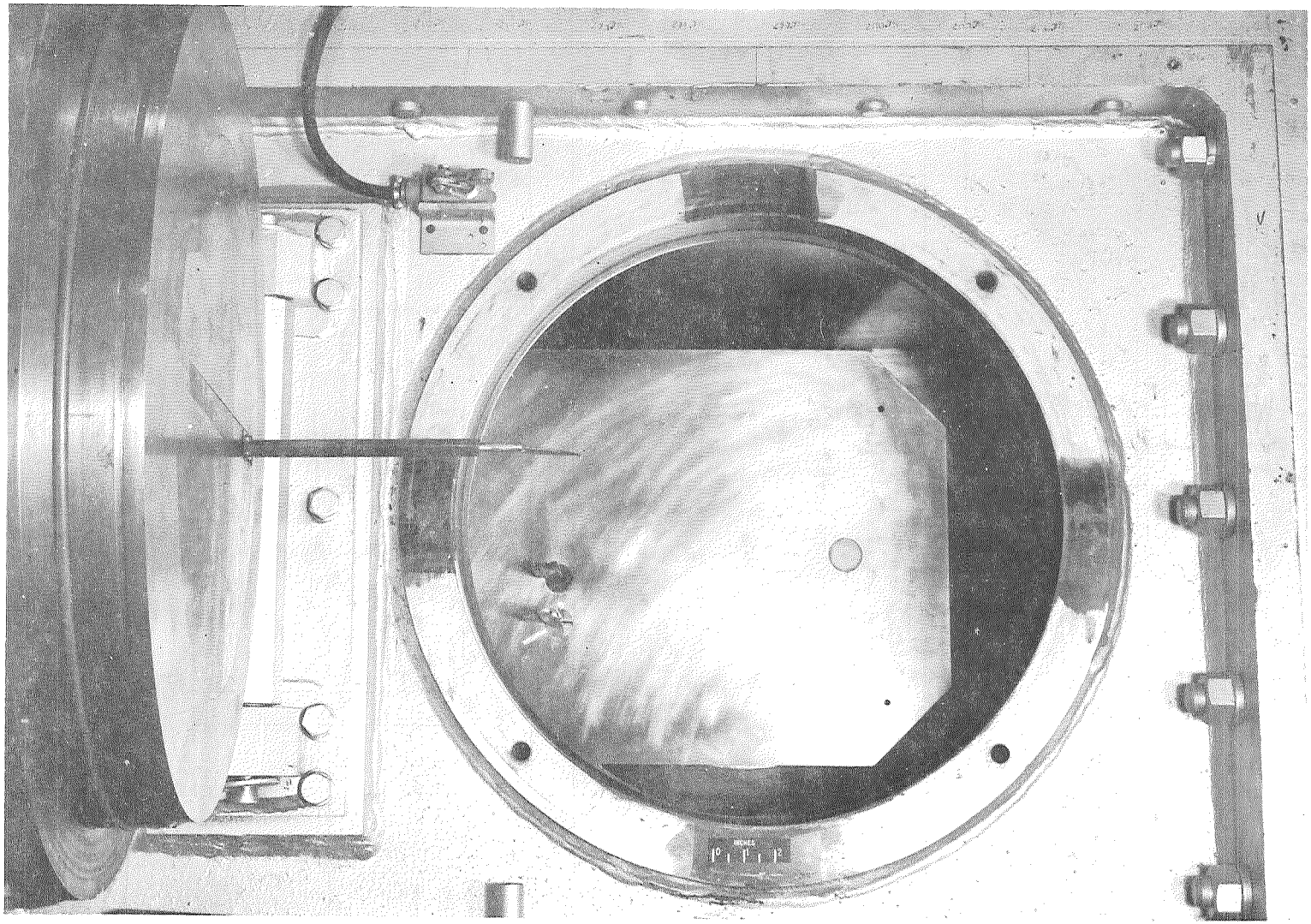

(a) Left side of the tunnel with the probe out.

L-63-8161

Figure 2.- Photograph of the model in the tunnel.

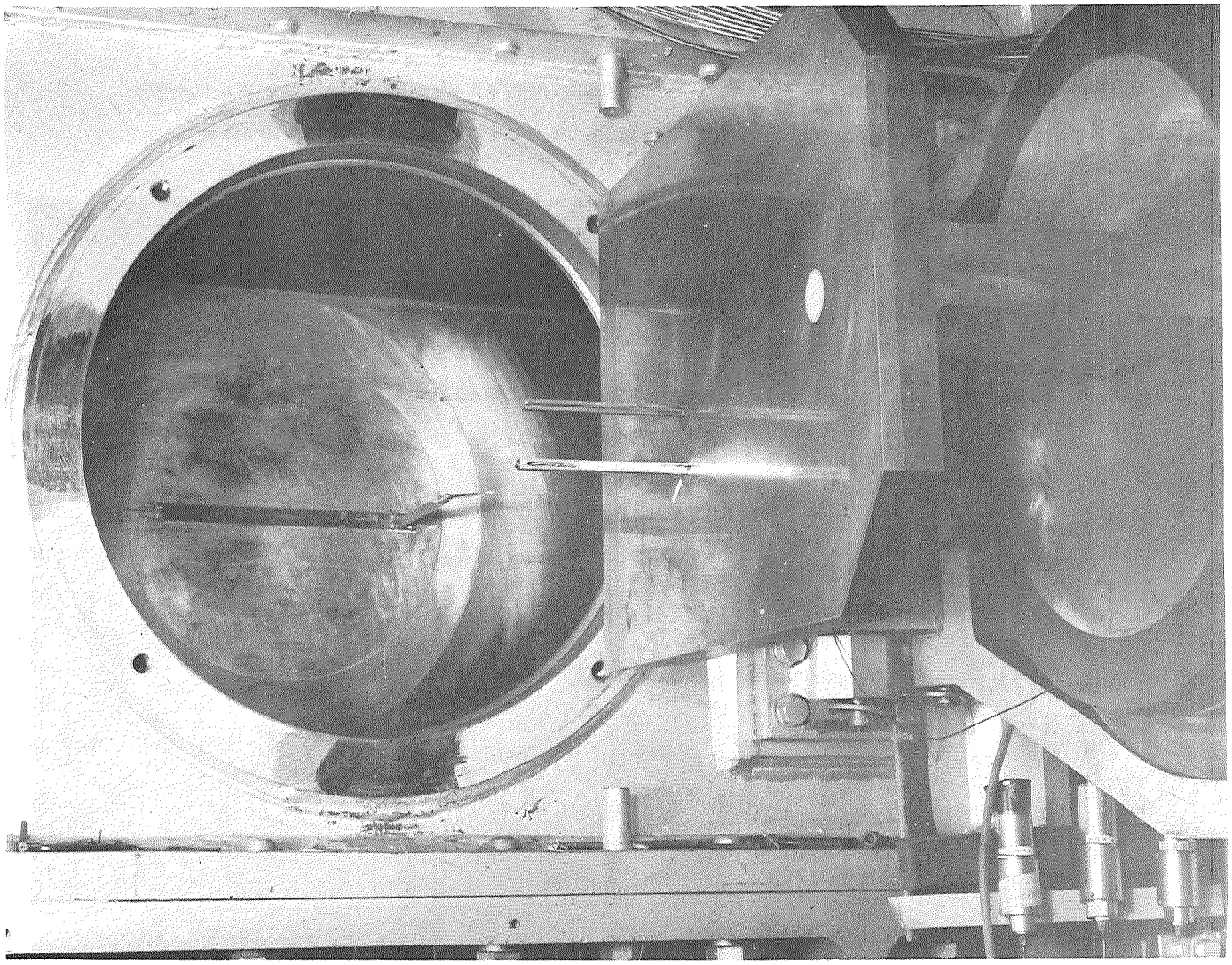

(b) Right side of the tunnel with the model out. L-63-8159

Figure 2.- Concluded.

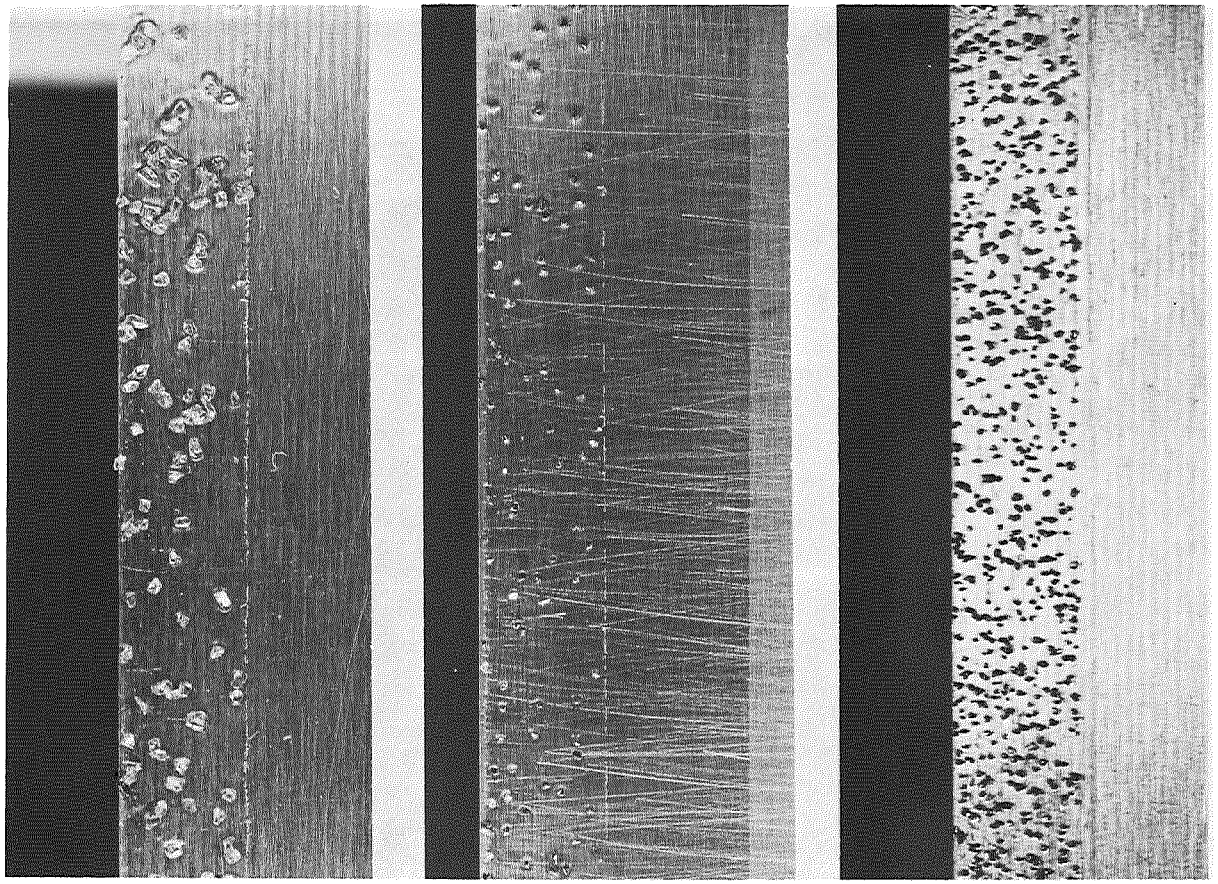

(a) Grit No. 40. (b) Grit No. 70, sieved. (c) Grit No. 80. L-69-5080

Figure 3.- Photographs of boundary-layer transition trips. x_k = 0.0 cm; w_k = 0.64 cm. (Magnified approximately 2.7 times.)

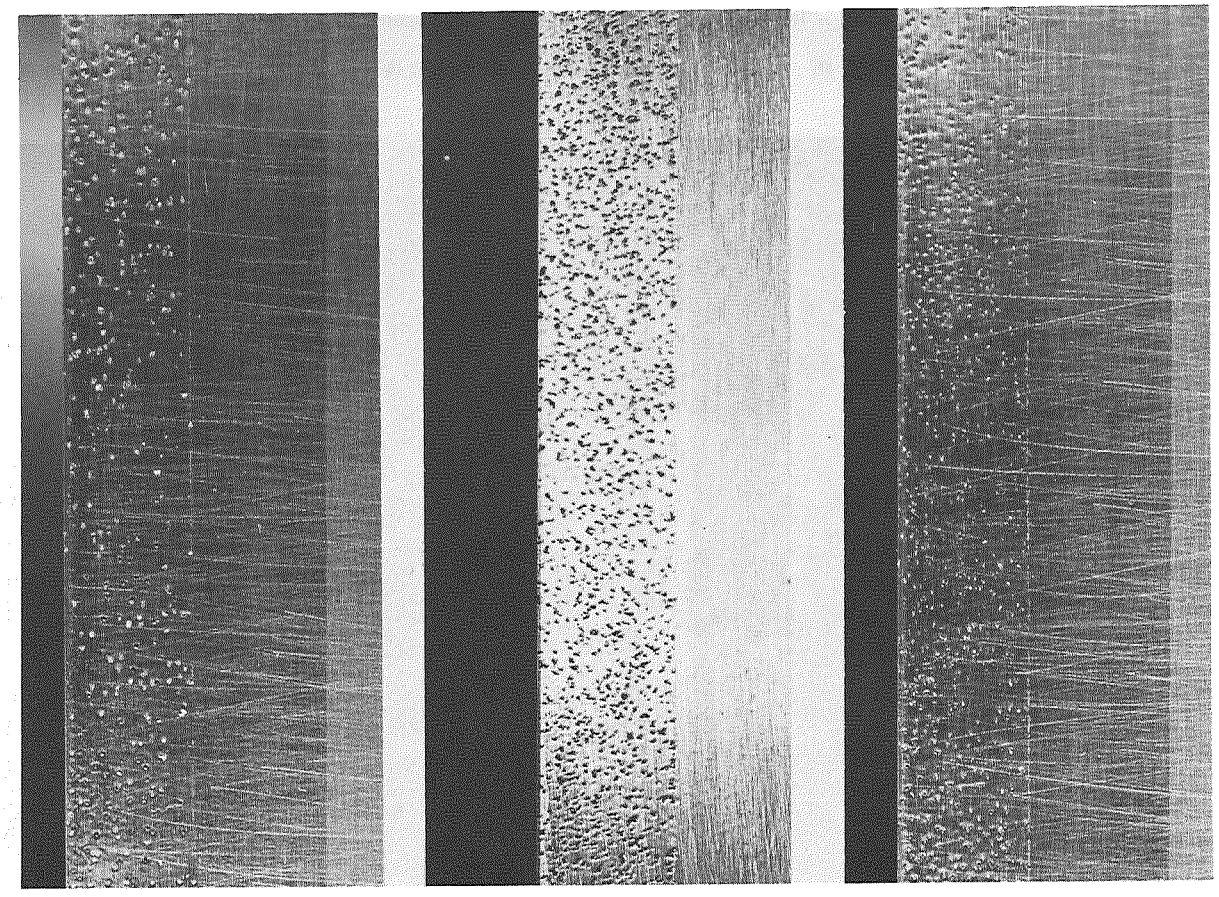

(d) Grit No. 120, sieved.

(e) Grit No. 120.

(f) Grit No. 240, sieved.

Figure 3.- Concluded.

L-69-5081

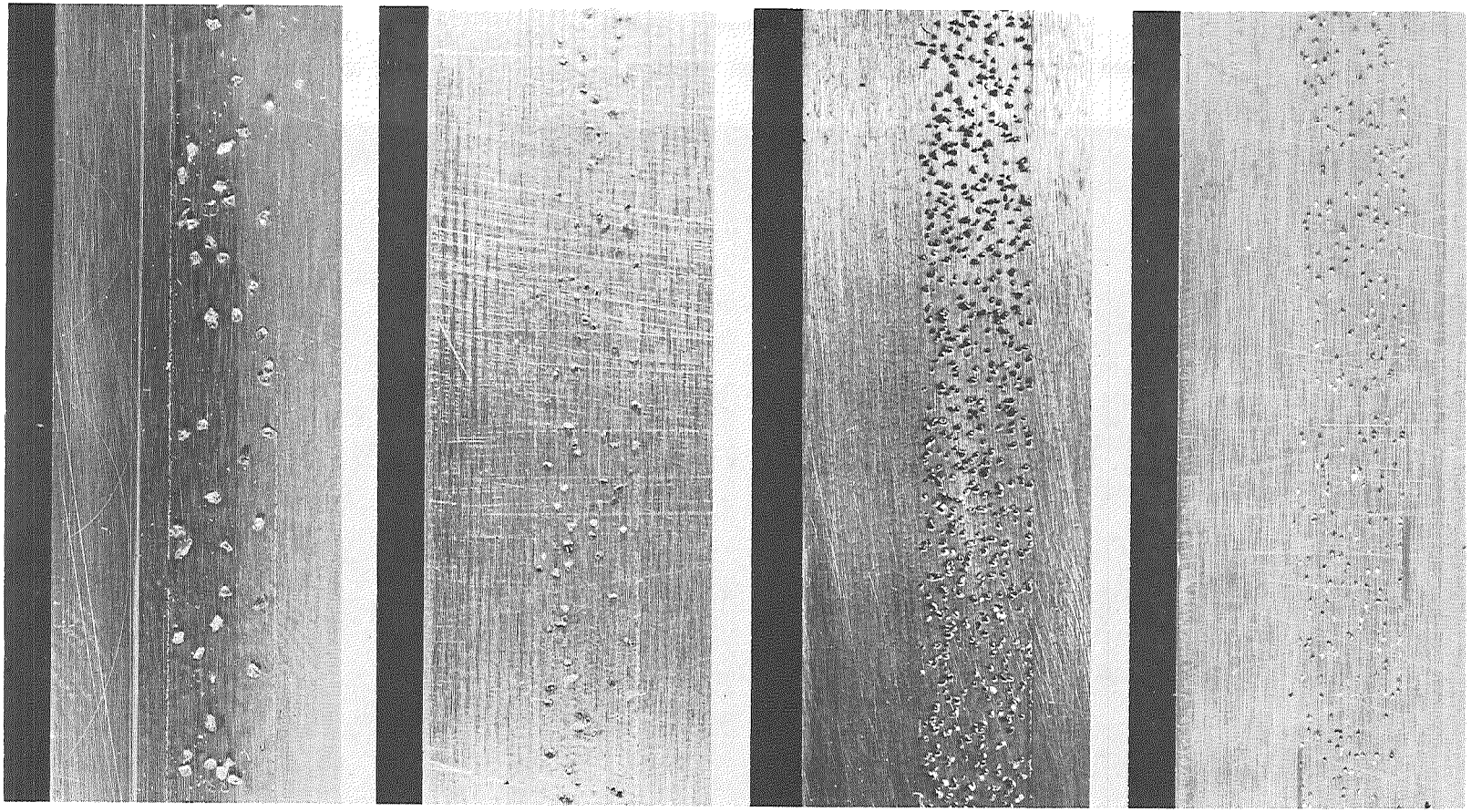

(a) Grit No. 40. (b) Grit No. 70, sieved. (c) Grit No. 80. (d) Grit No. 120, sieved.

Figure 4.- Photographs of boundary-layer transition trips. x_k = 0.64 cm; w_k = 0.64 cm. (Magnified approximately 2.7 times.)

L-69-5082

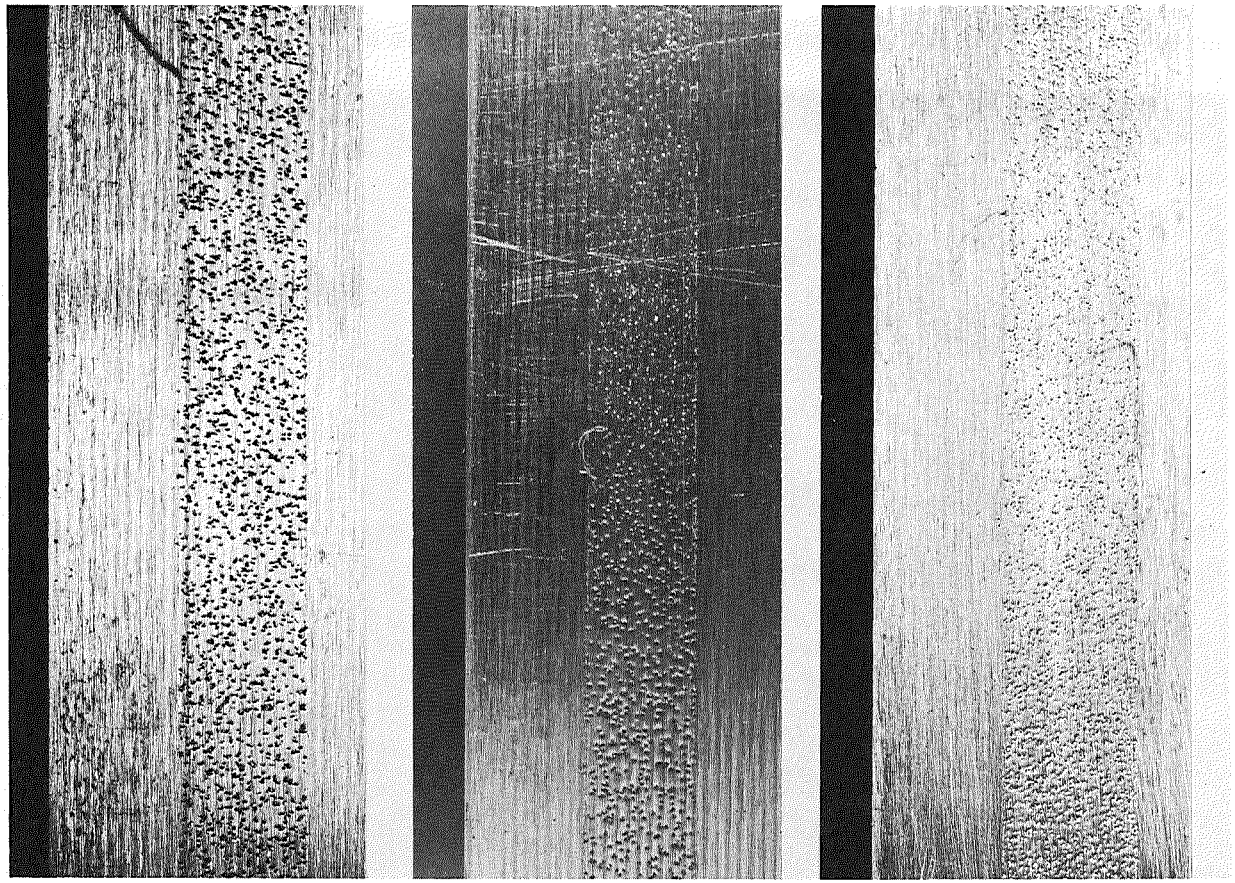

(e) Grit No. 120.

(f) Grit No. 240, sieved.

(g) Grit No. 240.

L-69-5083

Figure 4.- Concluded.

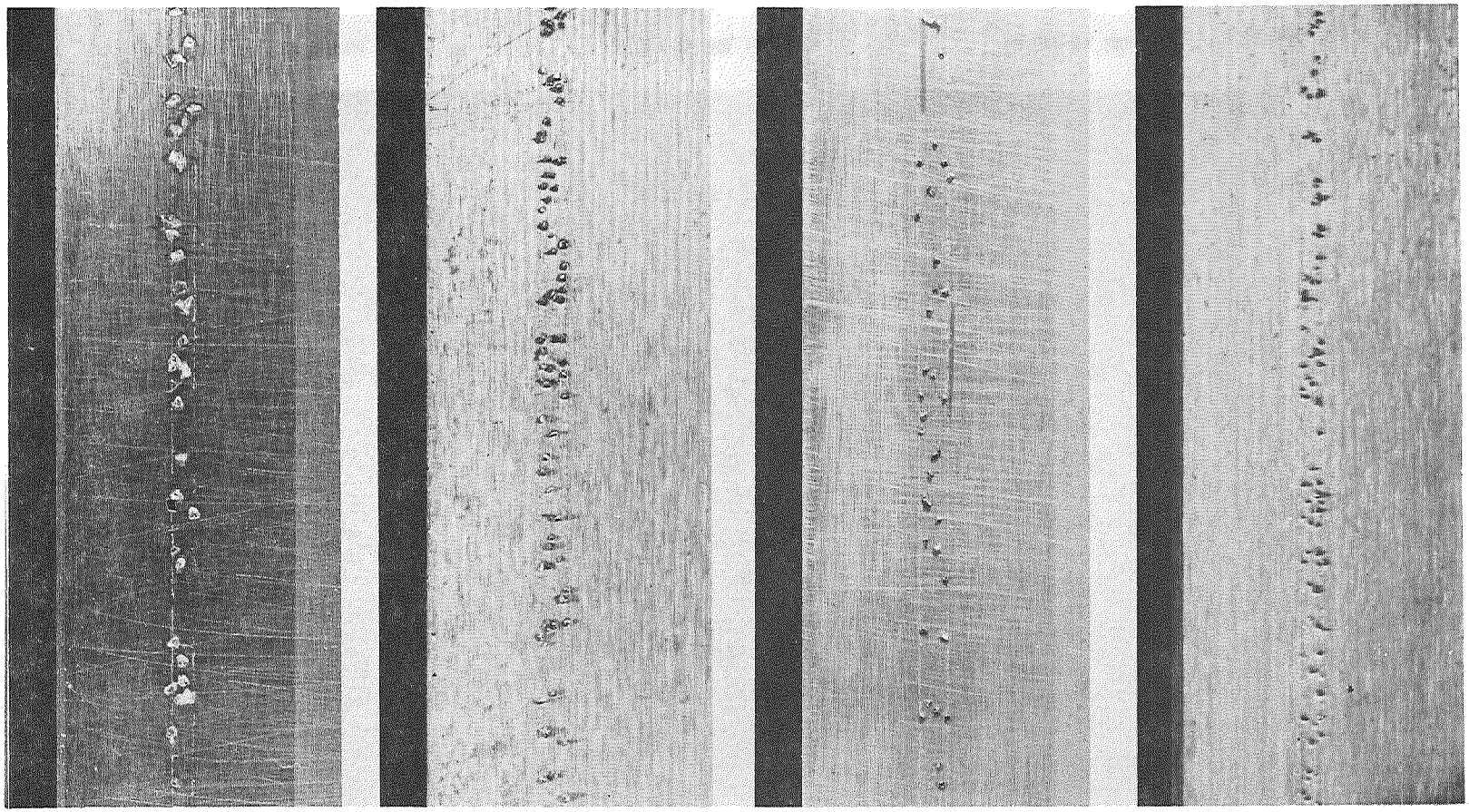

(a) Grit No. 40. (b) Grit No. 60. (c) Grit No. 70, sieved. (d) Grit No. 80.

L-69-5084

Figure 5.- Photographs of boundary-layer transition trips. x_k = 0.64 cm; w_k = 0.13 cm. (Magnified approximately 2.7 times.)

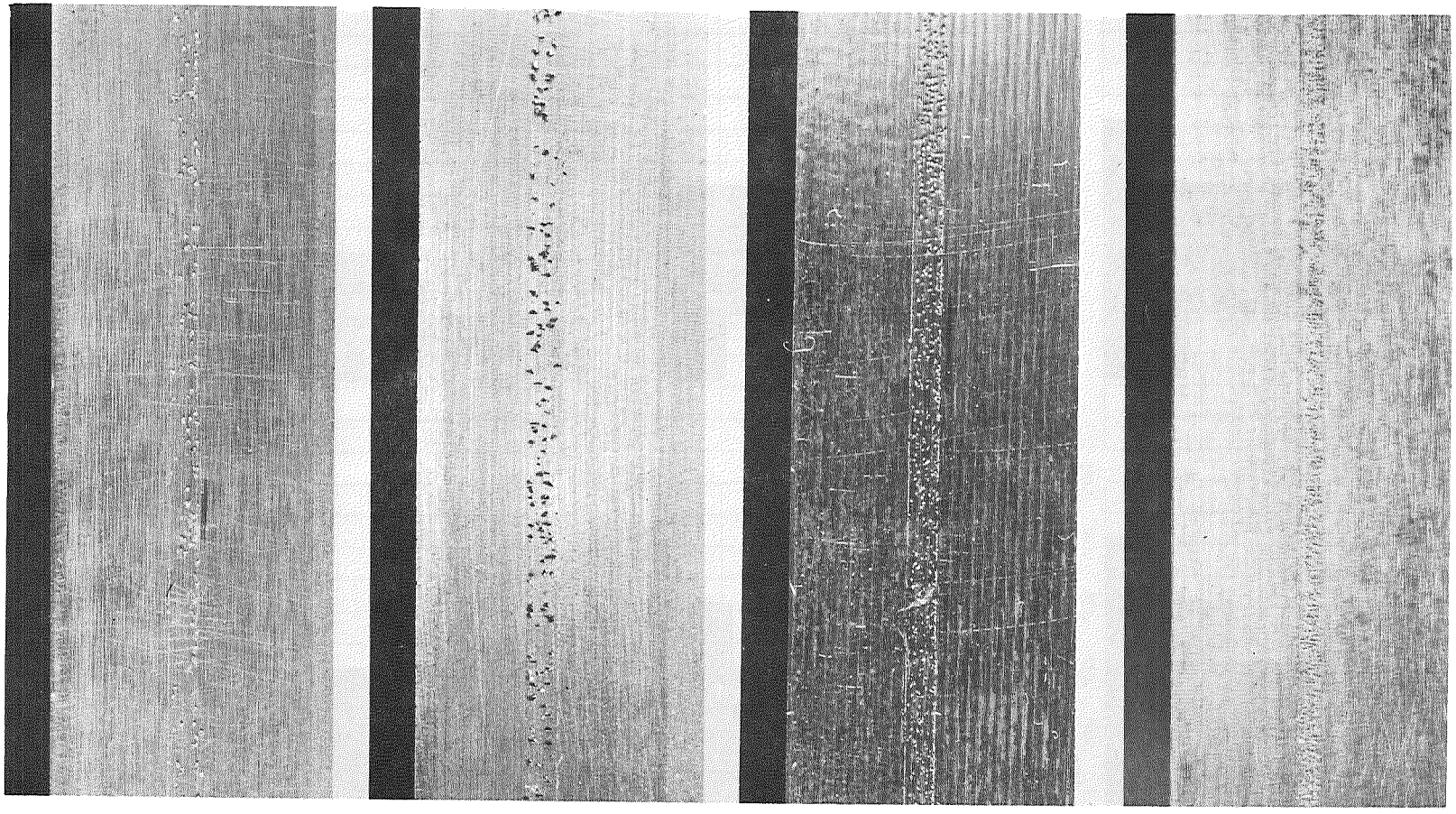

(e) Grit No. 120, sieved.

(f) Grit No. 120.

(g) Grit No. 240, sieved.

(h) Grit No. 240.

Figure 5.- Concluded.

L-69-5085

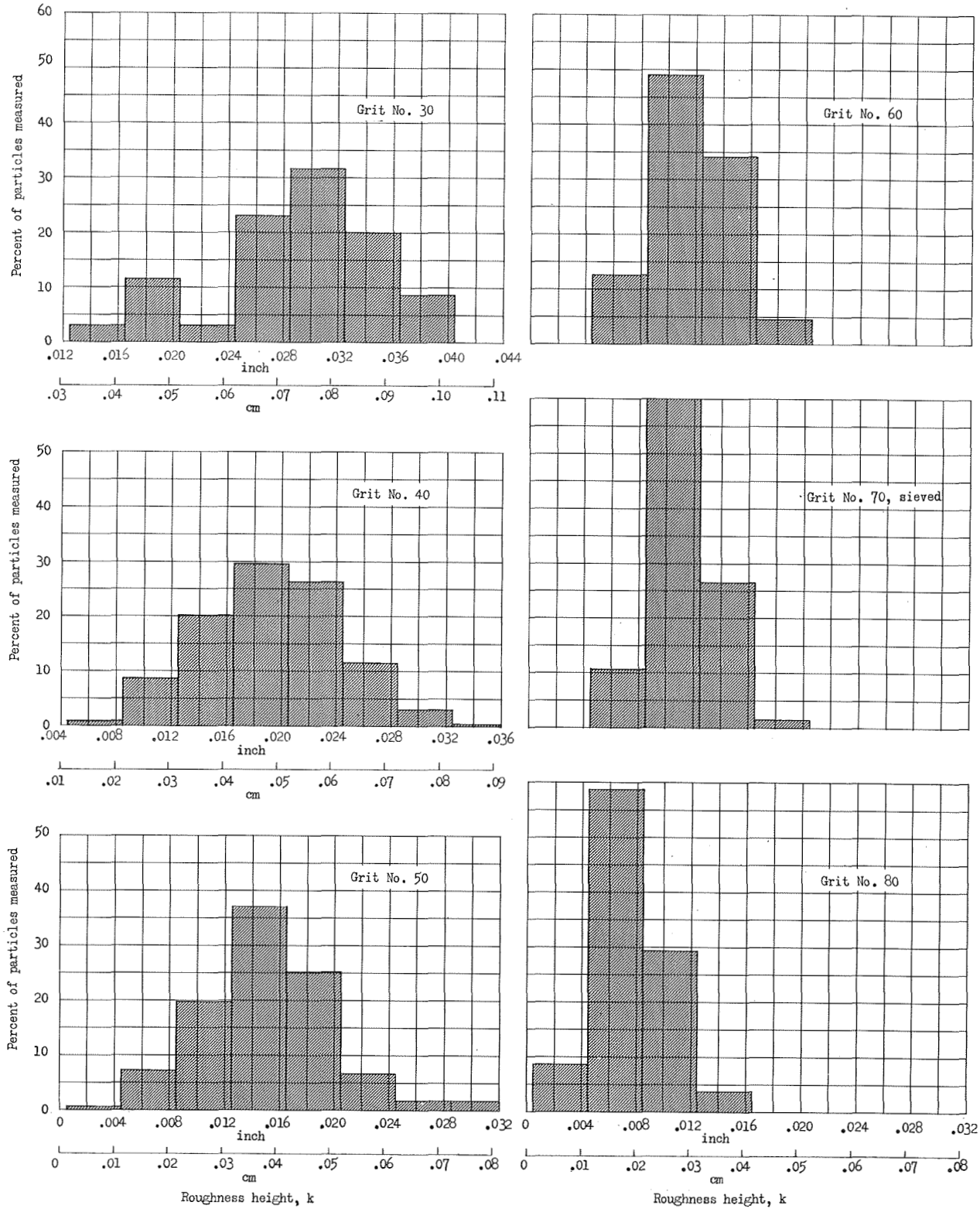

(a) Grit No. 30 – No. 80.

Figure 6.- Bar graphs showing distribution of measured heights of particles in a typical carborundum transition trip.

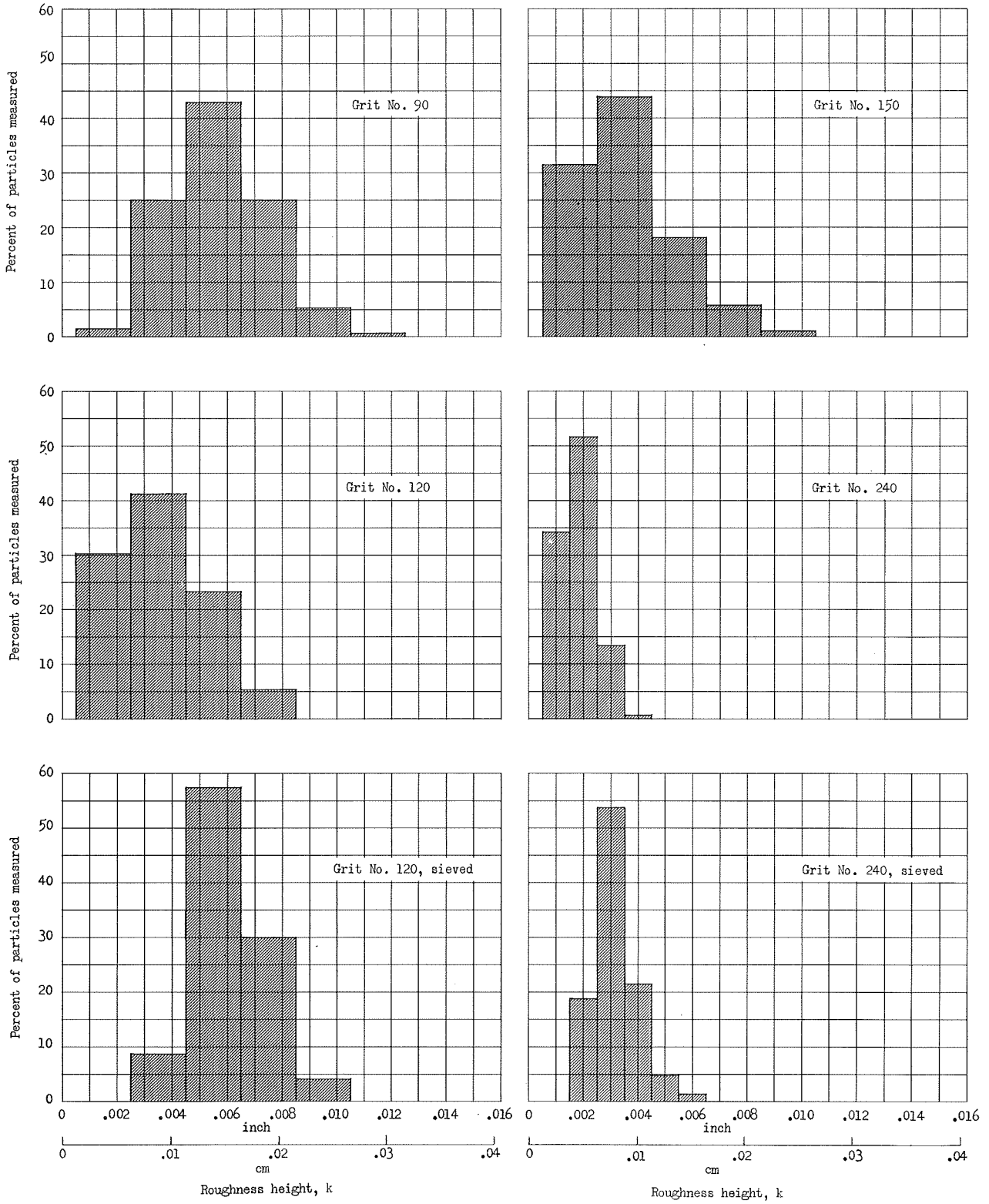

(b) Grit No. 90 – No. 240.

Figure 6.- Concluded.

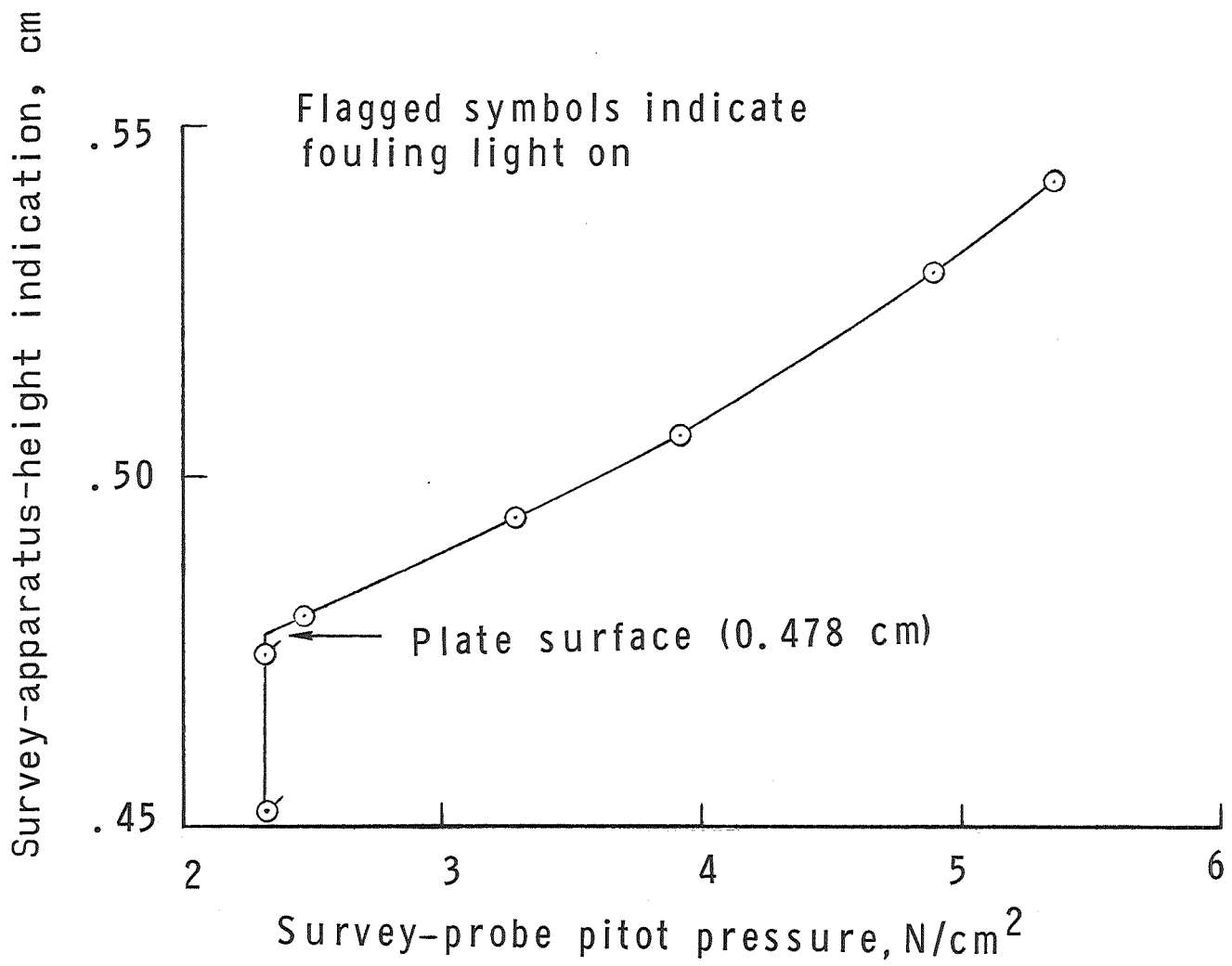

Figure 7.- Method used to determine position of plate surface.

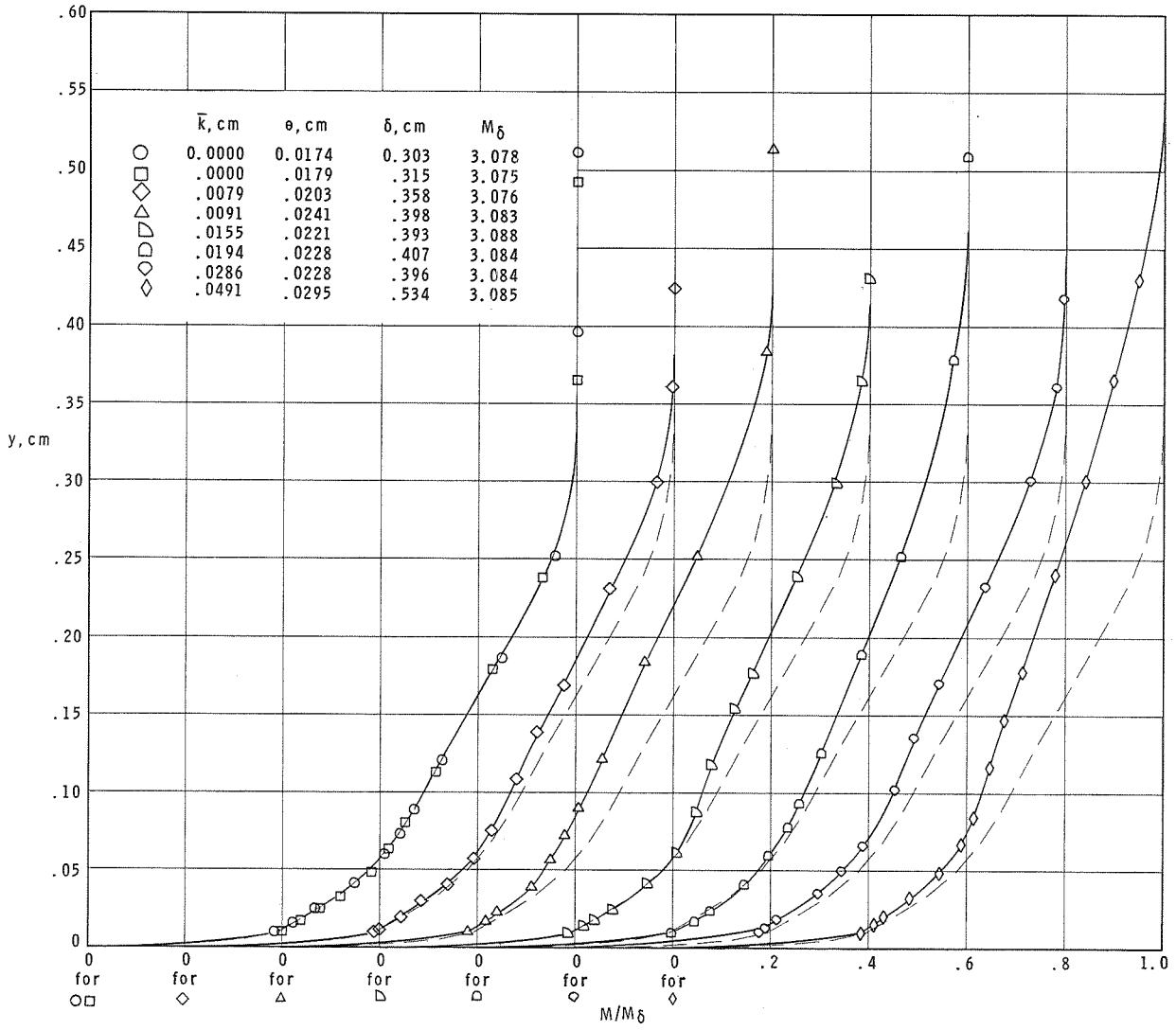

(a) x_k = 0.0 cm; w_k = 0.64 cm.

Figure 8.- Effect of trip size on boundary-layer profiles at x = 21.6 cm. M/M_δ as a function of y; M_δ = 3.

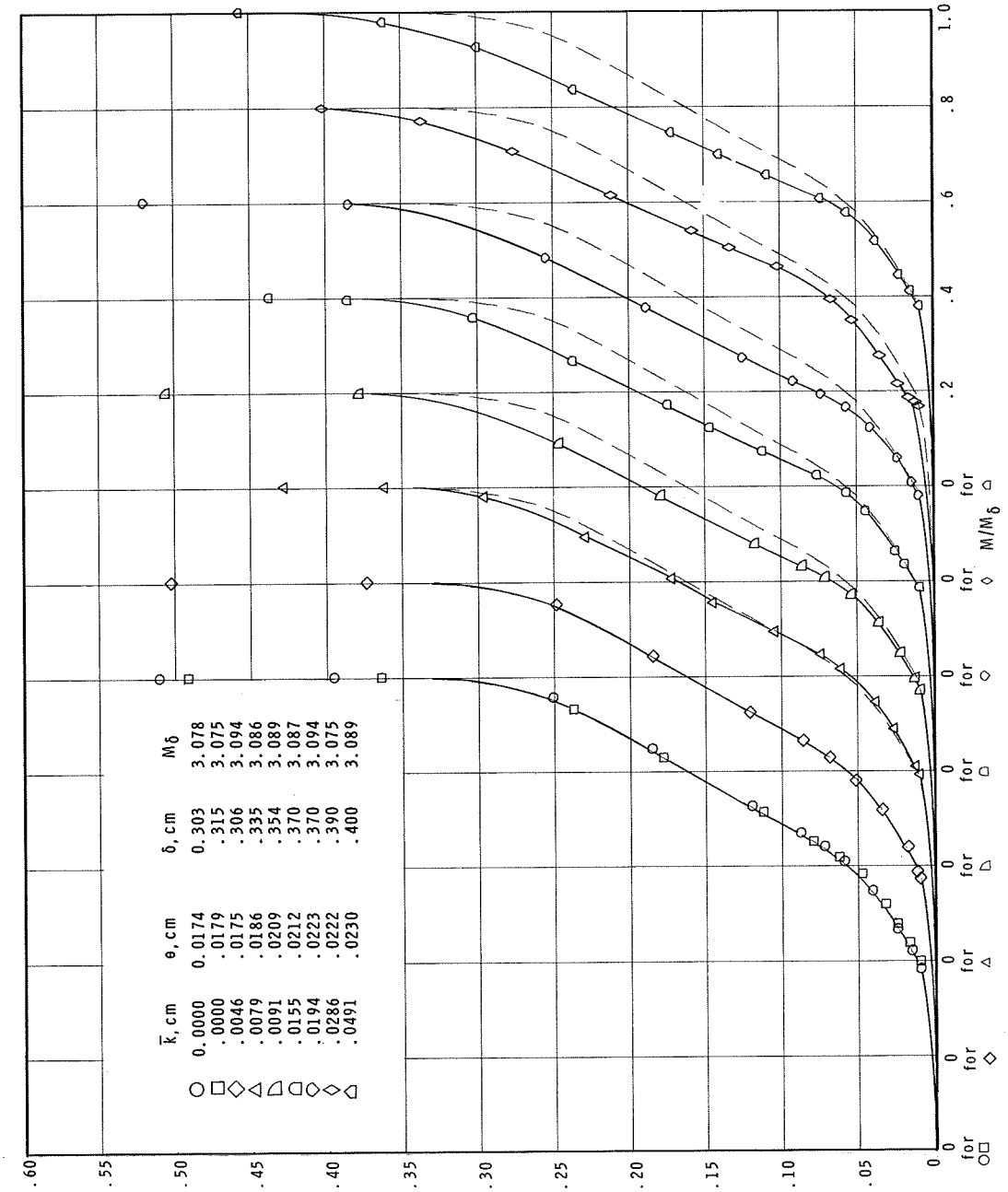

(b) x_k = 0.64 cm; w_k = 0.64 cm.

Figure 8.- Continued.

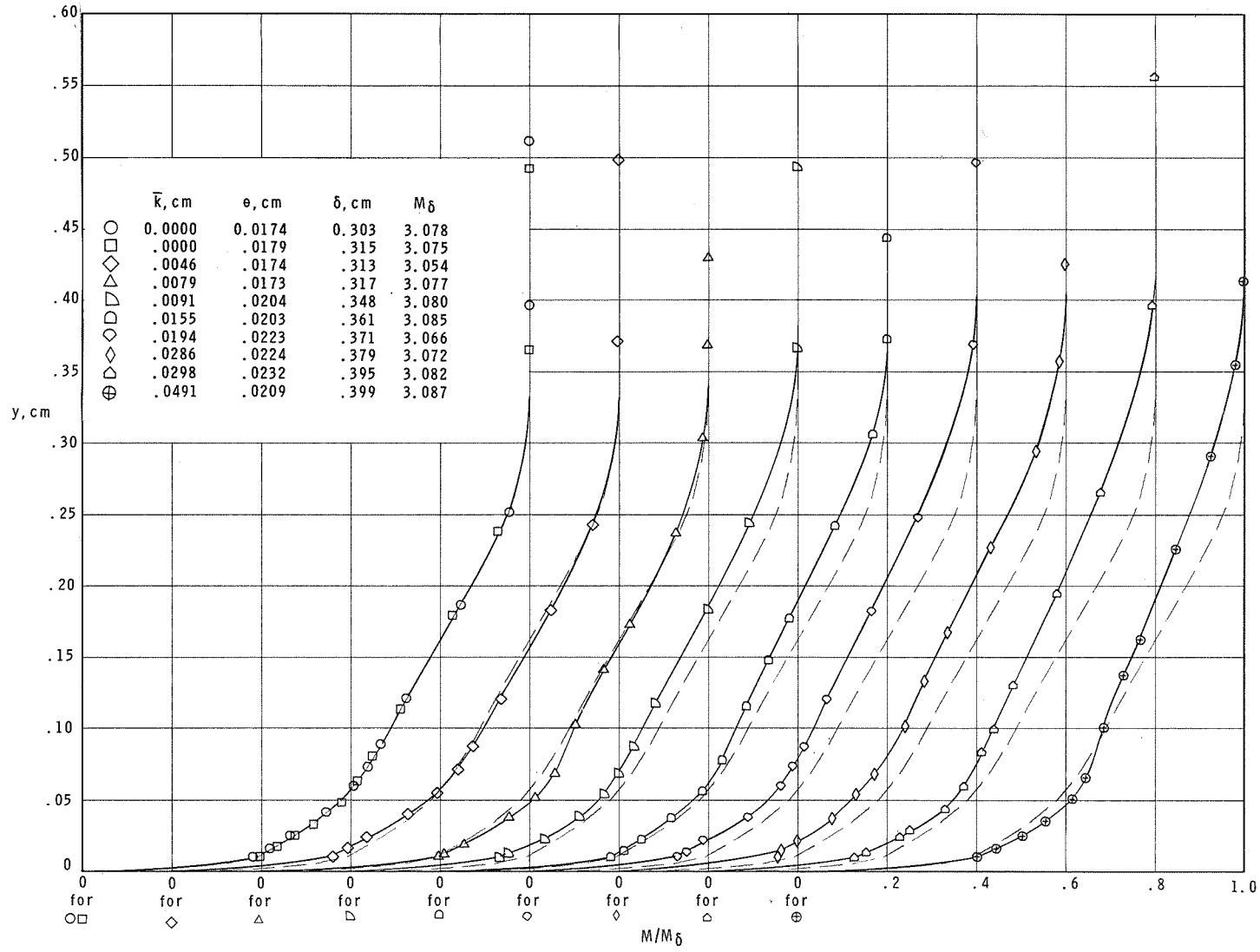

(c) x_k = 0.64 cm; w_k = 0.13 cm.

Figure 8.- Concluded.

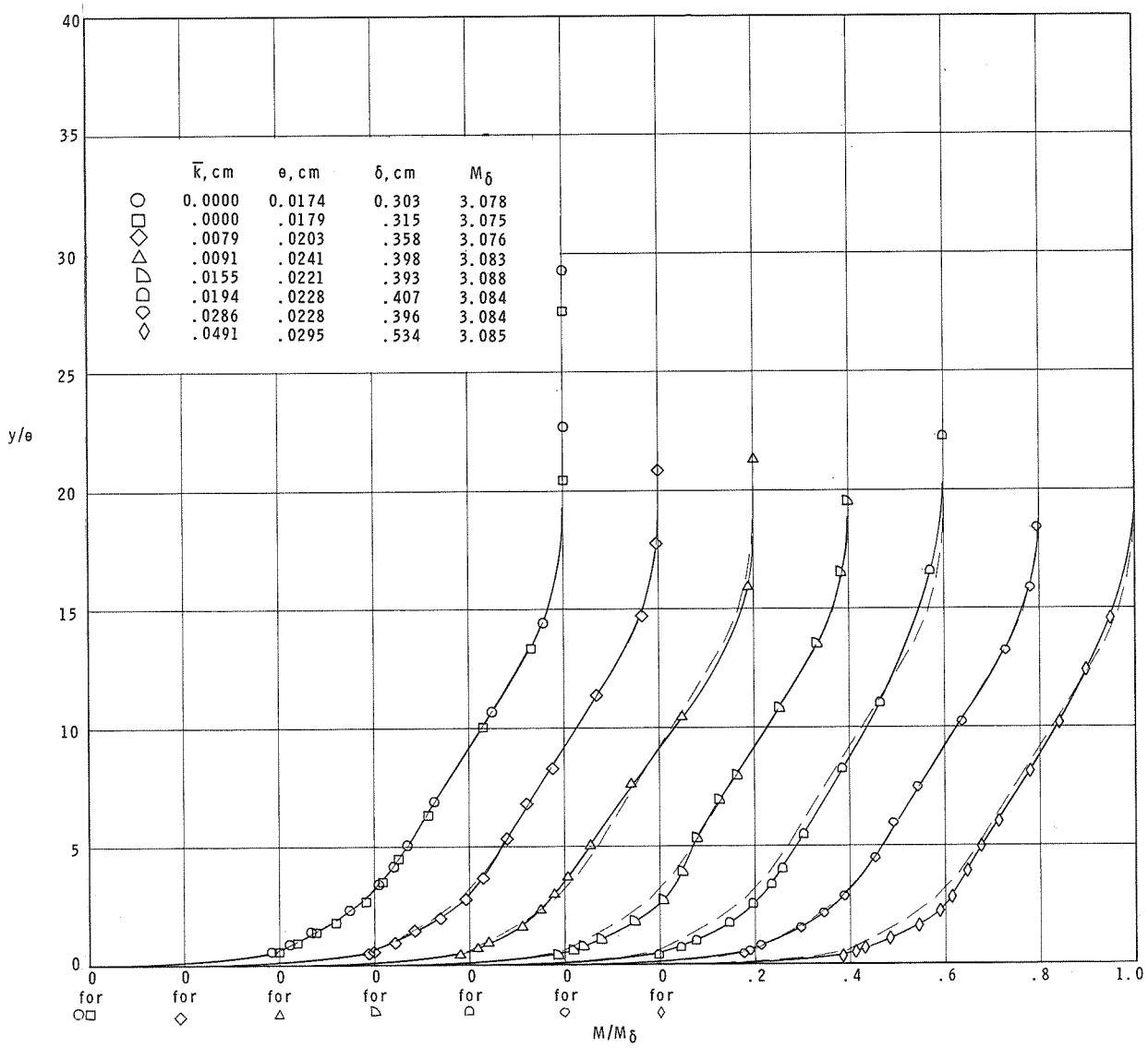

(a) x_k = 0.0 cm; w_k = 0.64 cm.

Figure 9.- Effect of trip size on boundary-layer profiles at x = 21.6 cm. M/M_δ as a function of y/θ; M_δ = 3.

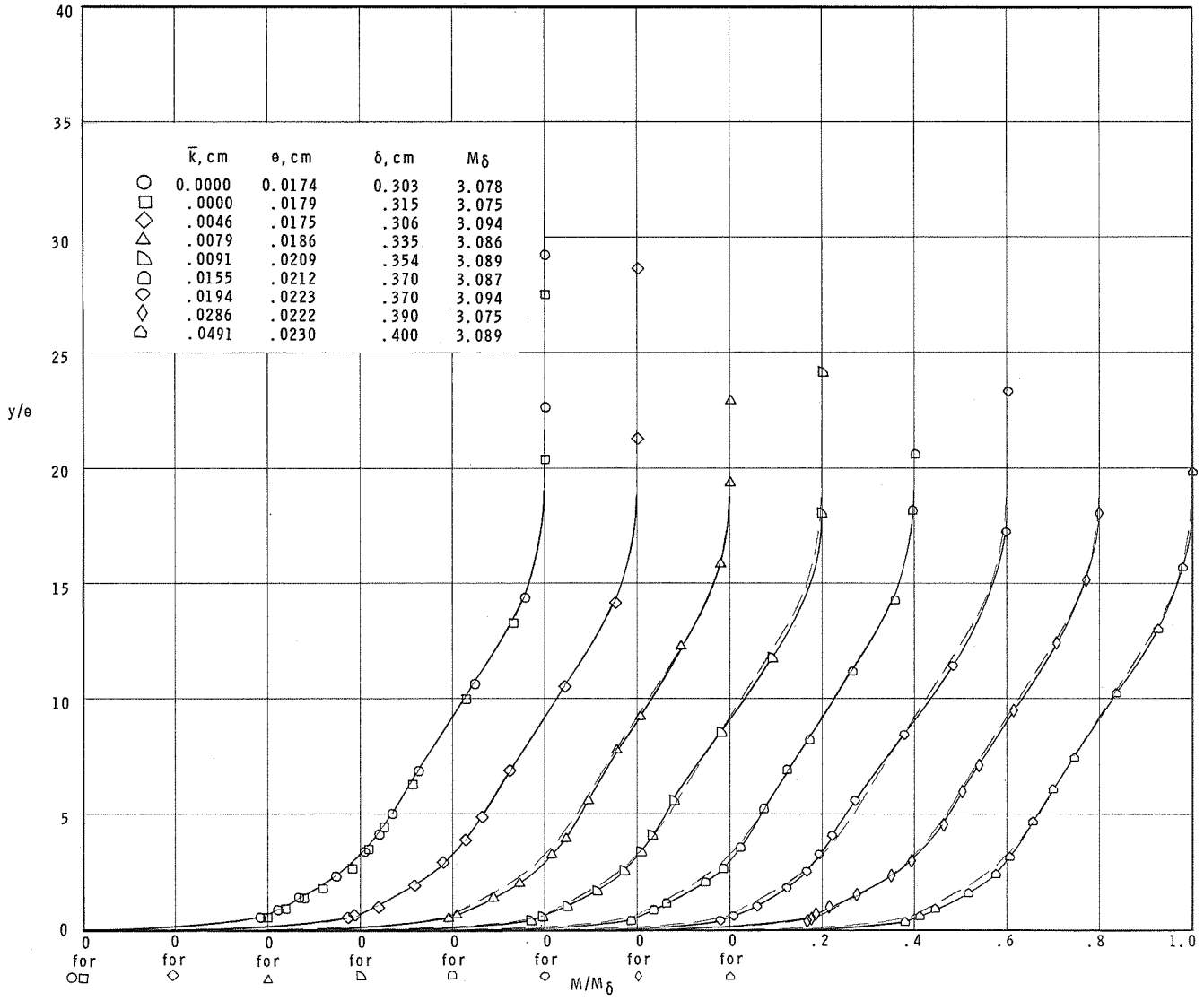

(b) x_k = 0.64 cm; w_k = 0.64 cm.

Figure 9.- Continued.

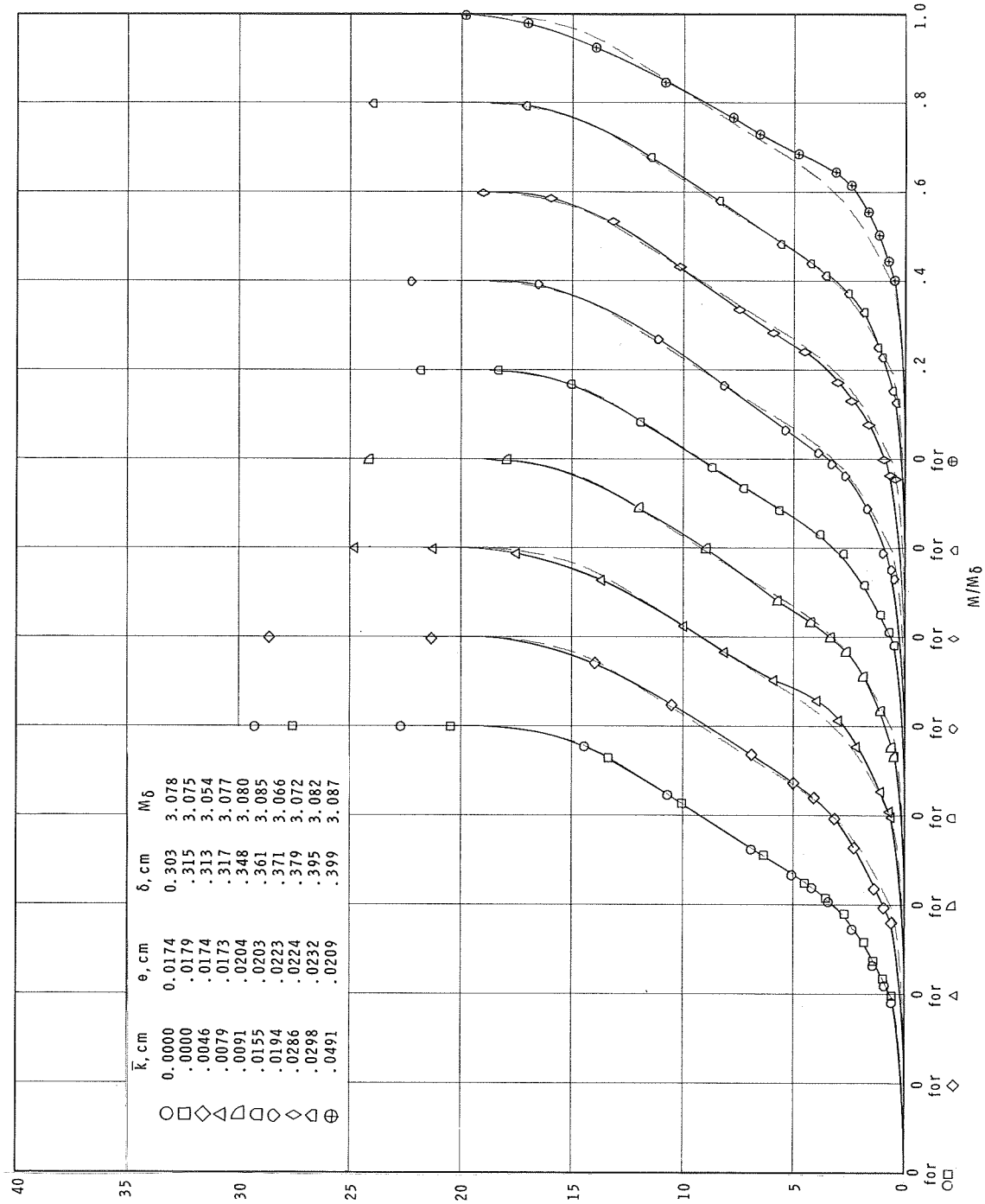

(c) x_k = 0.64 cm; w_k = 0.13 cm.

Figure 9.- Concluded.

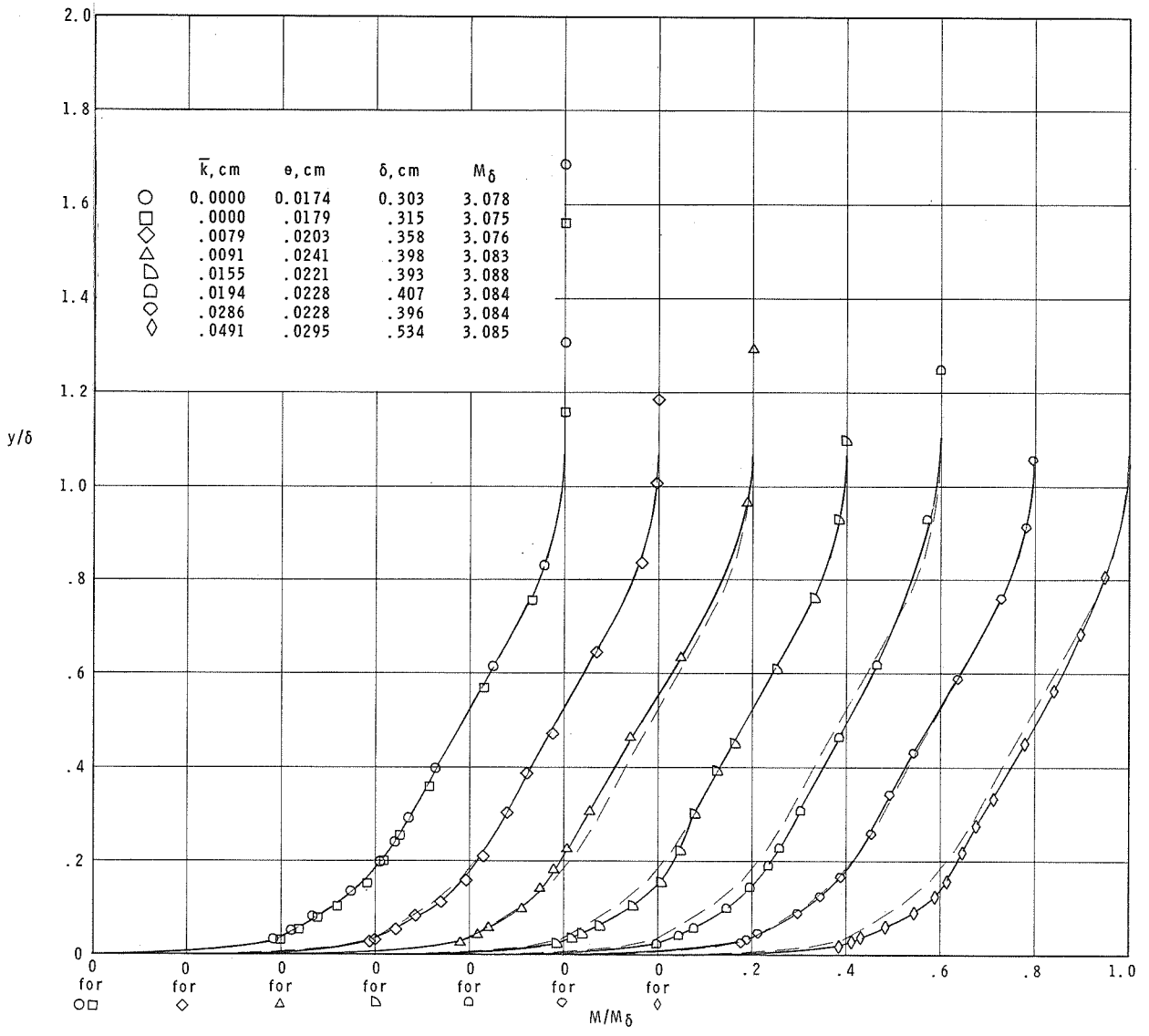

(a) x_k = 0.0 cm; w_k = 0.64 cm.

Figure 10.- Effect of trip size on boundary-layer profiles at x = 21.6 cm. M/M_δ as a function of y/δ; M_δ = 3.

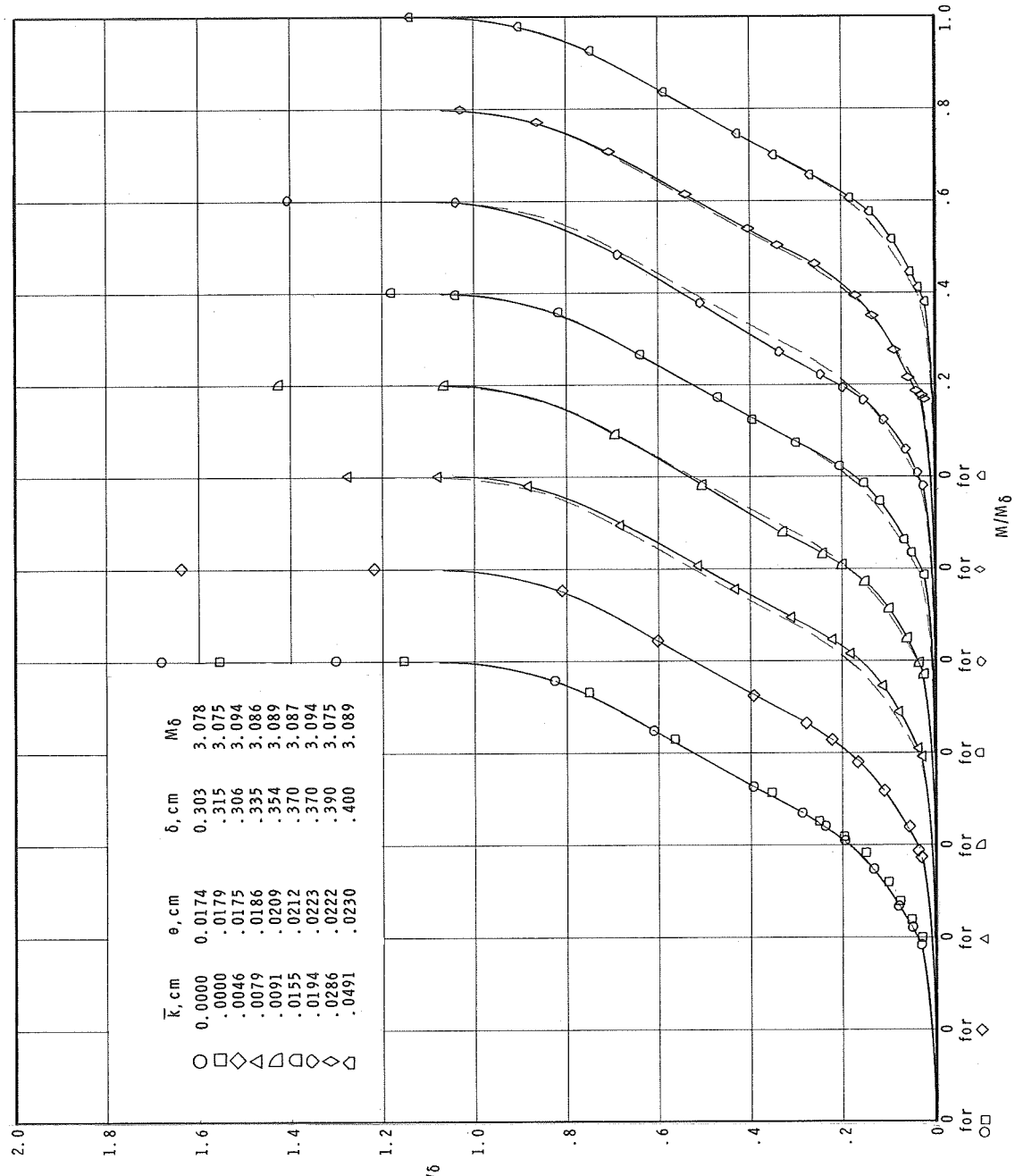

(b) x_k = 0.64 cm; w_k = 0.64 cm.

Figure 10.- Continued.

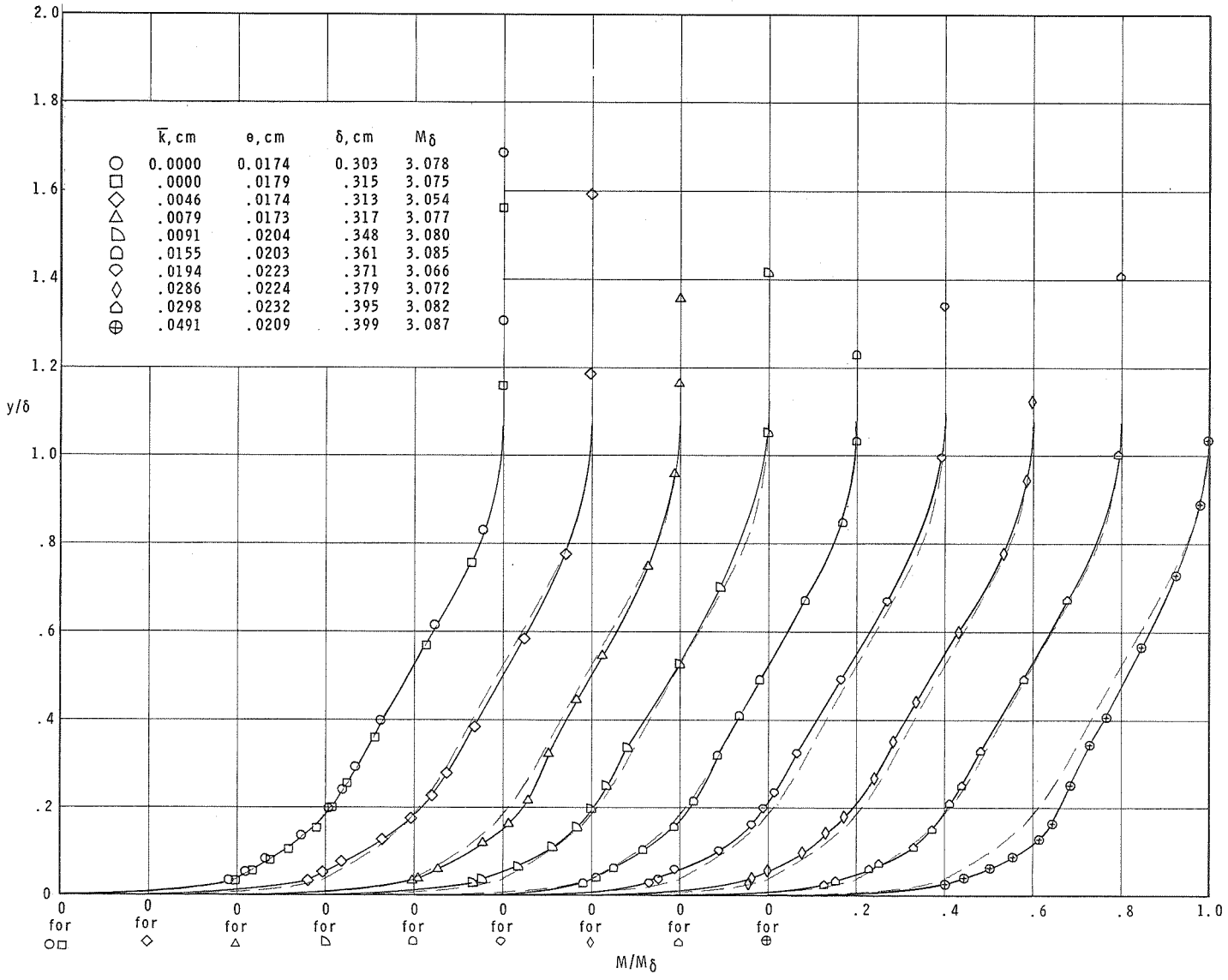

(c) x_k = 0.64 cm; w_k = 0.13 cm.

Figure 10.- Concluded.

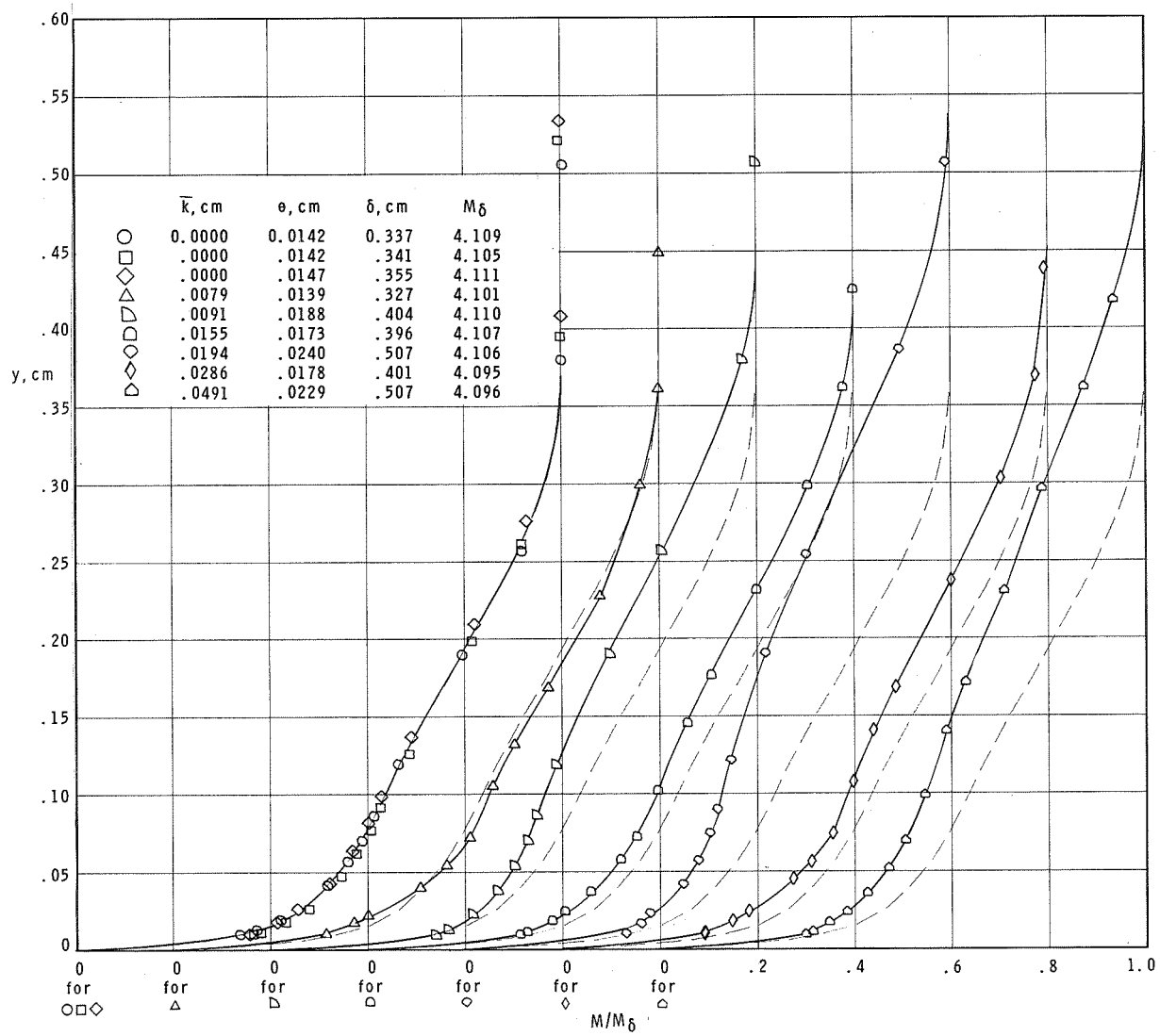

(a) x_k = 0.0 cm; w_k = 0.64 cm.

Figure 11.- Effect of trip size on boundary-layer profiles at x = 21.6 cm. M/M_δ as a function of y; M_δ = 4.

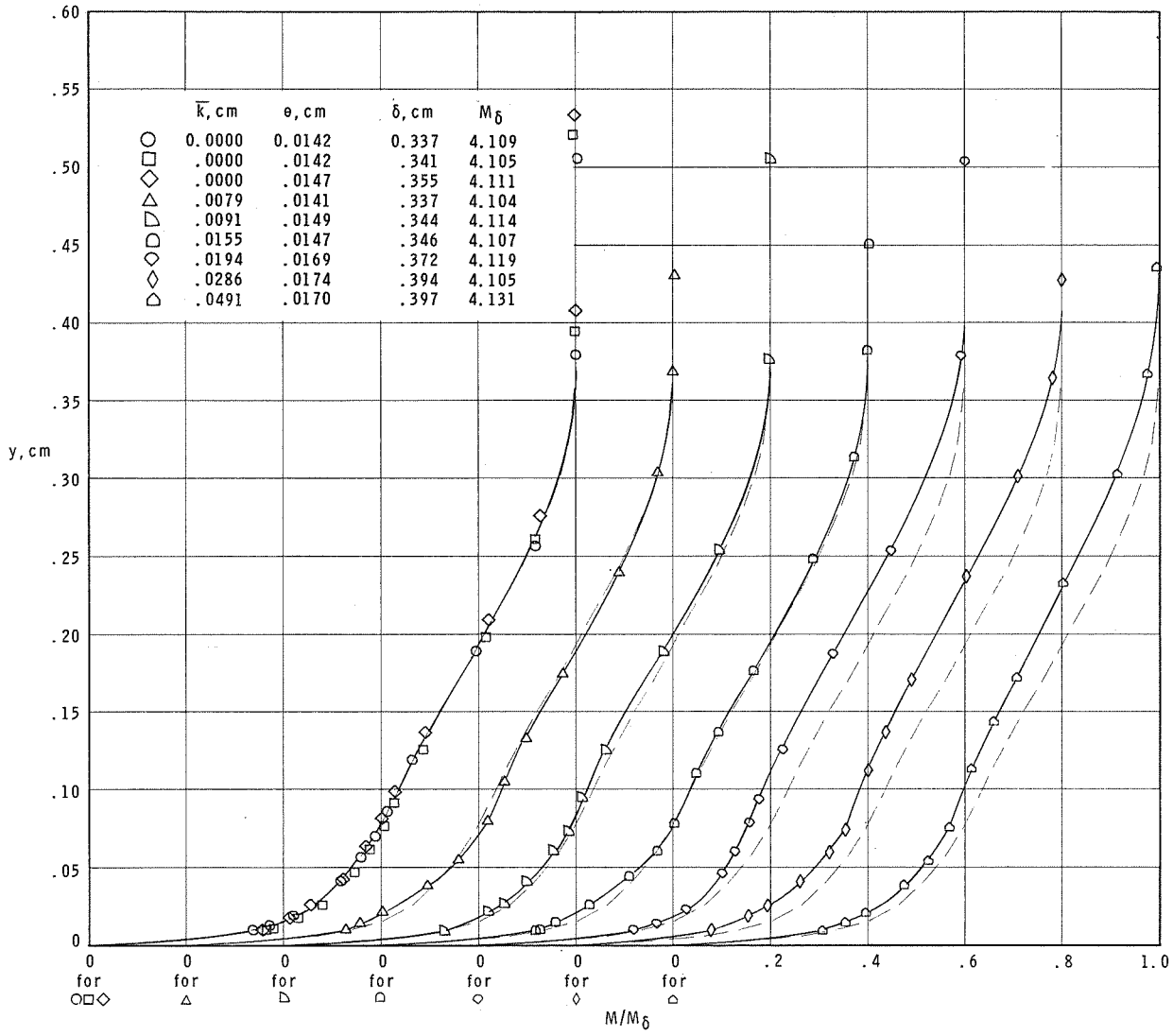

(b) x_k = 0.64 cm; w_k = 0.64 cm.

Figure 11.- Continued.

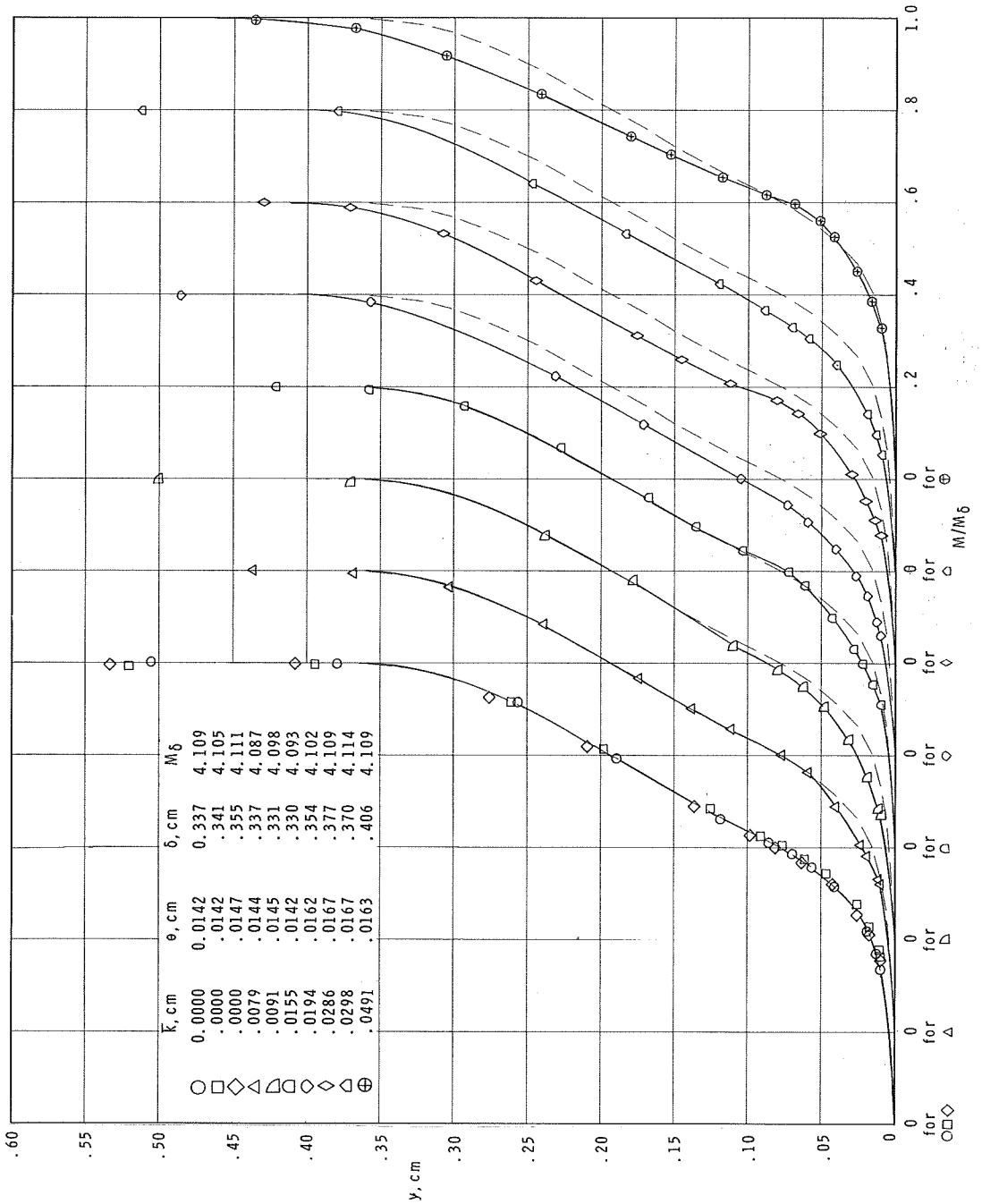

(c) x_k = 0.64 cm; w_k = 0.13 cm.

Figure 11.- Concluded.

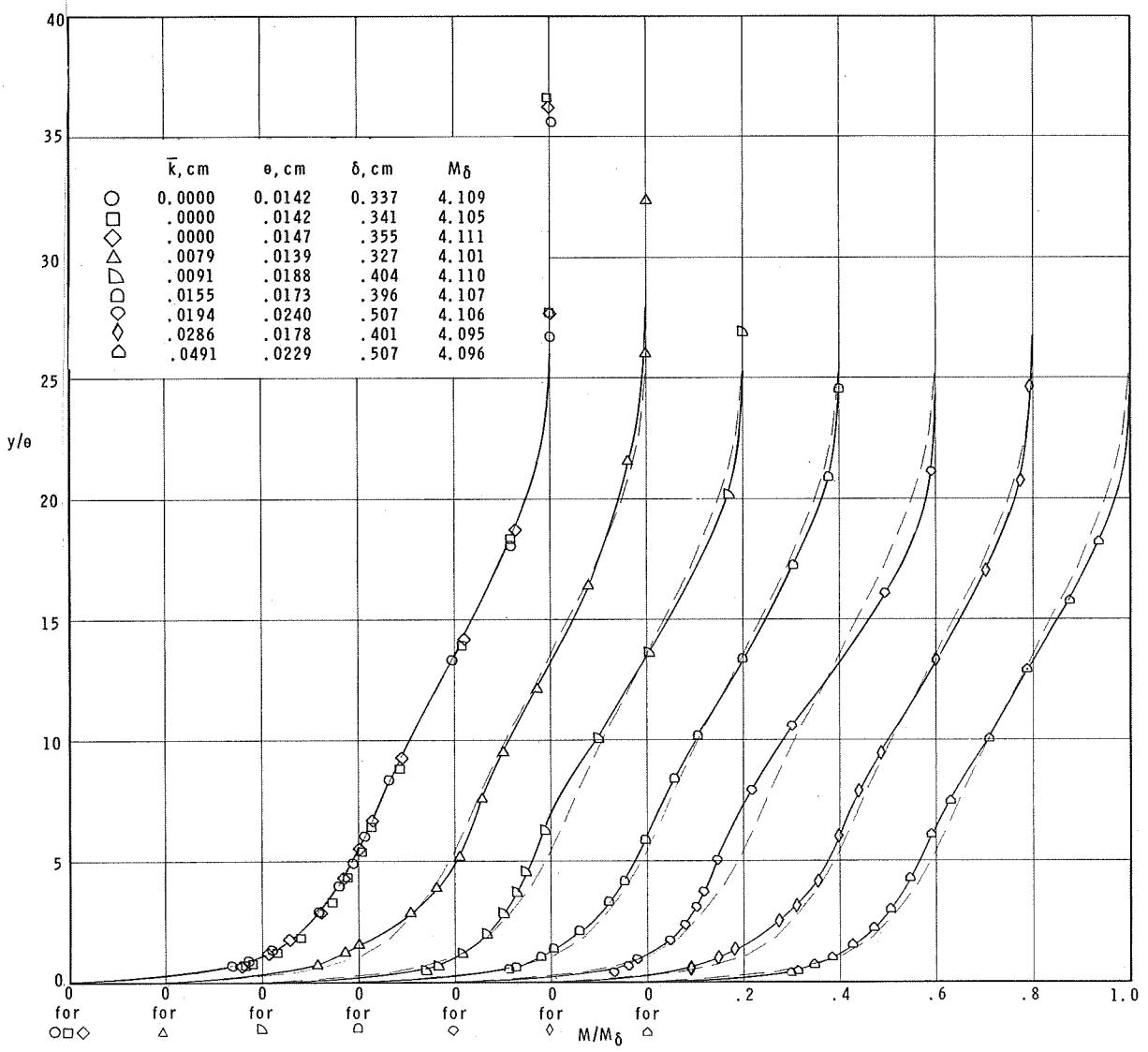

(a) x_k = 0.0 cm; w_k = 0.64 cm.

Figure 12.- Effect of trip size on boundary-layer profiles at x = 21.6 cm. M/M_δ as a function of y/θ; M_δ = 4.

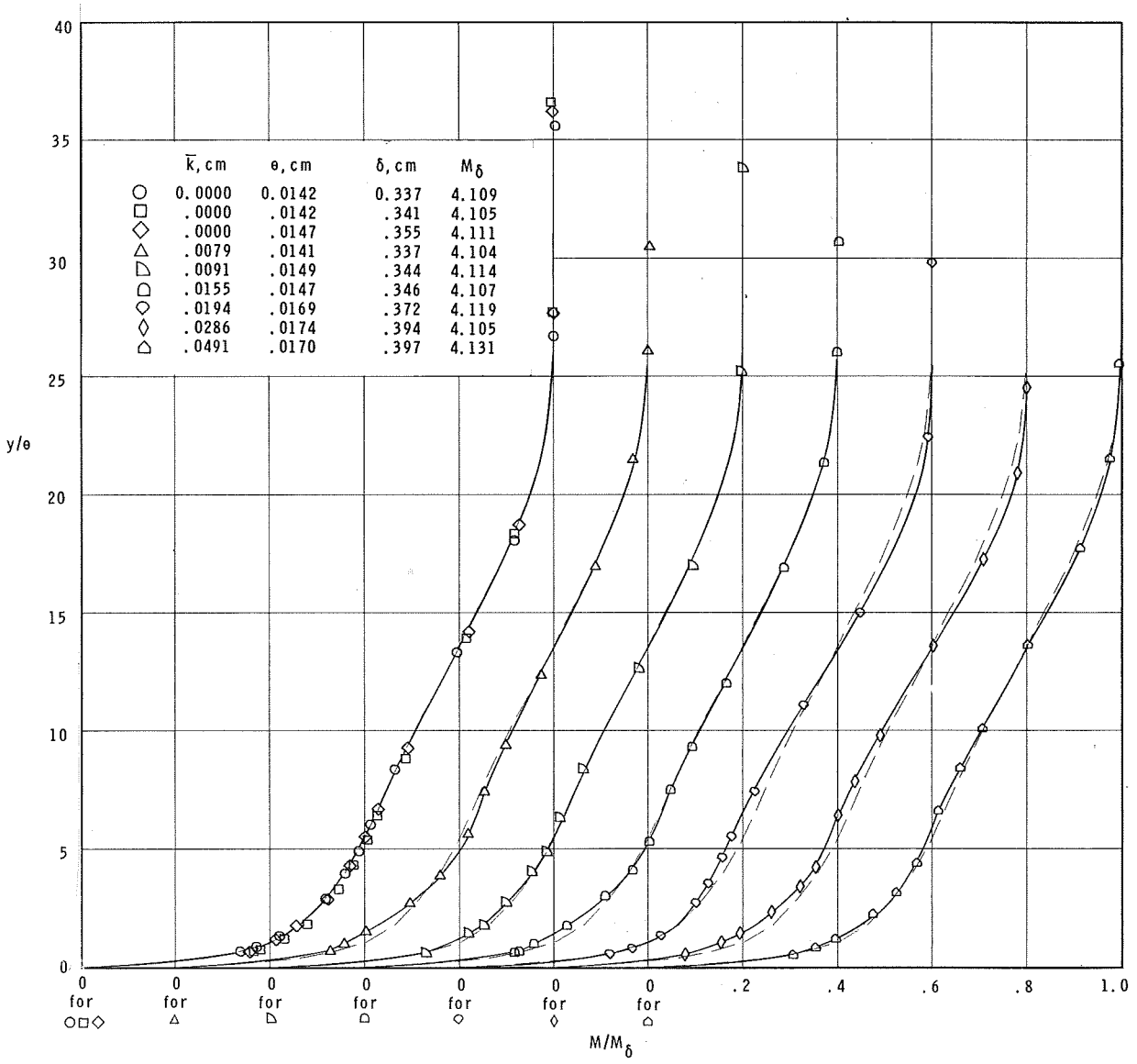

(b) x_k = 0.64 cm; w_k = 0.64 cm.

Figure 12.- Continued.

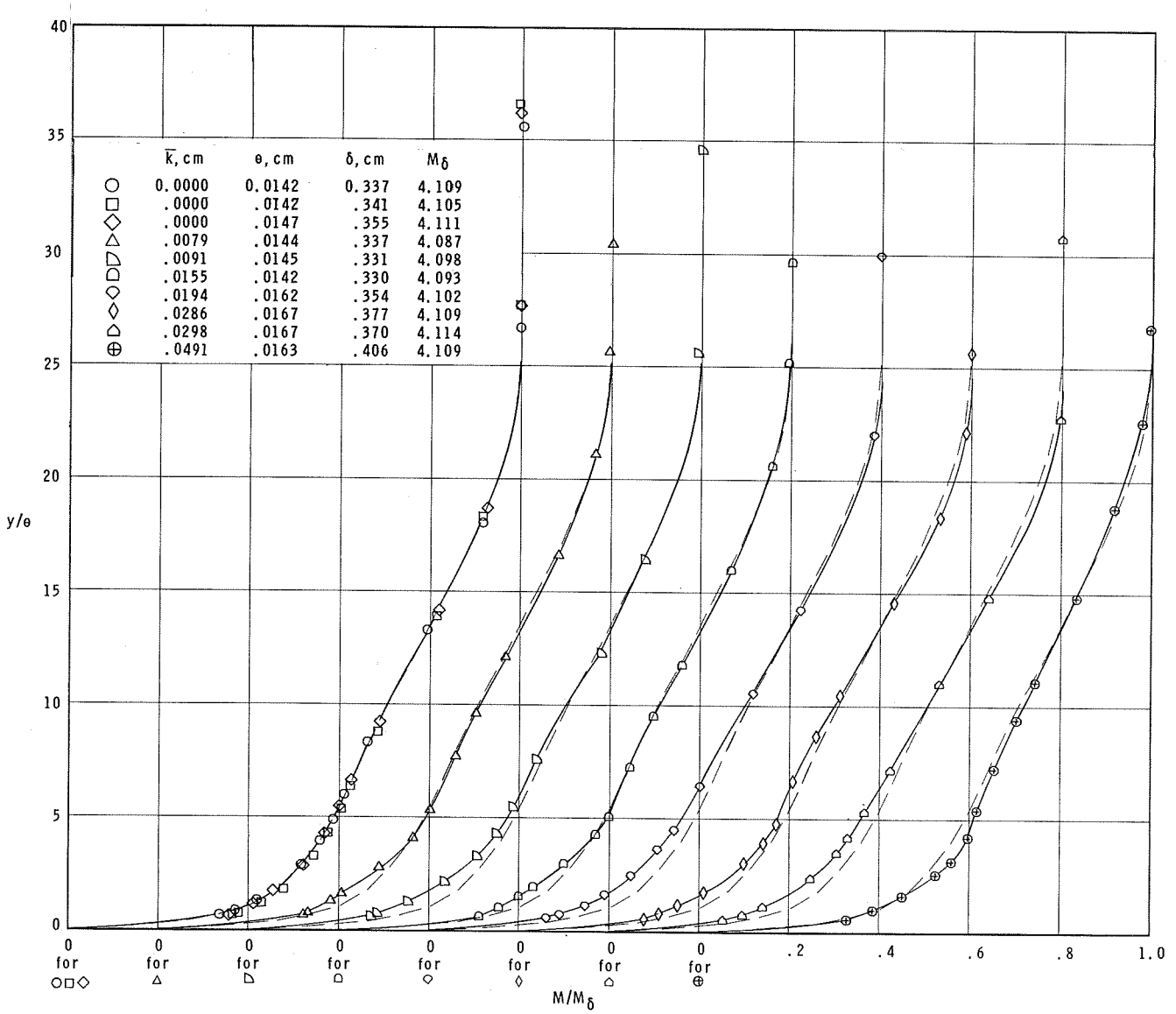

(c) x_k = 0.64 cm; w_k = 0.13 cm.

Figure 12.- Concluded.

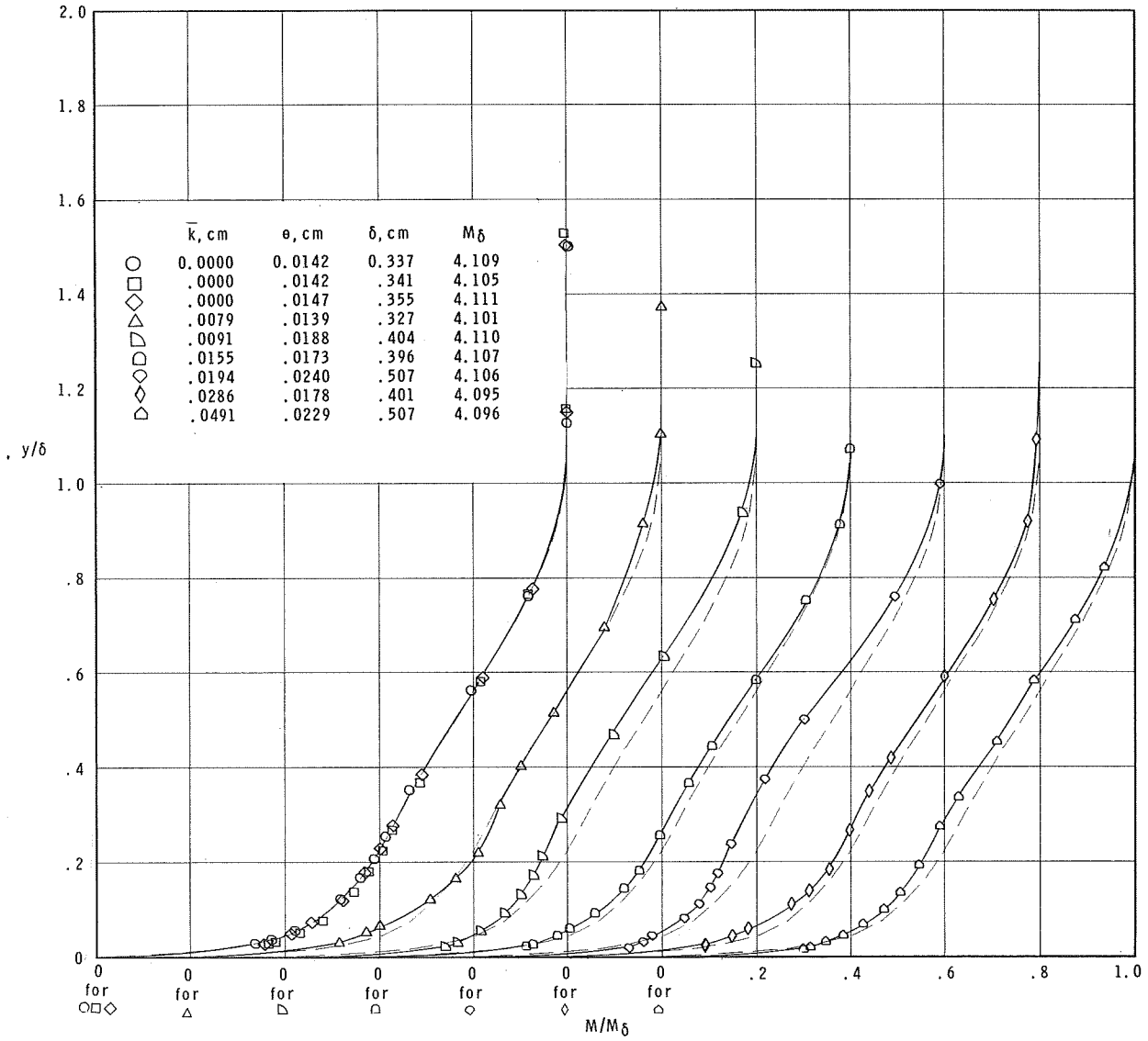

(a) x_k = 0.0 cm; w_k = 0.64 cm.

Figure 13.- Effect of trip size on boundary-layer profiles at x = 21.6 cm. M/M_δ as a function of y/δ; M_δ = 4.

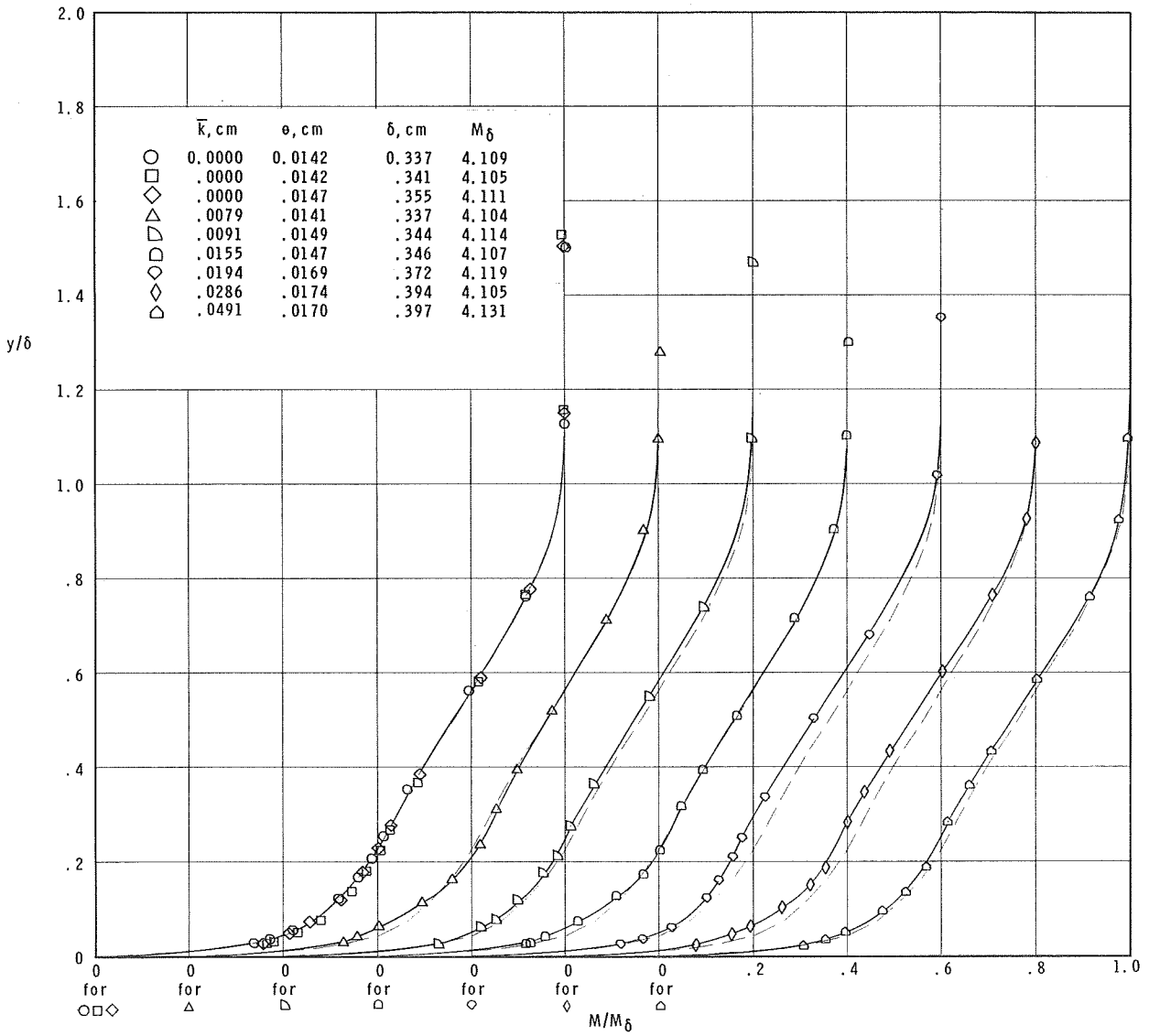

(b) x_k = 0.64 cm; w_k = 0.64 cm.

Figure 13.- Continued.

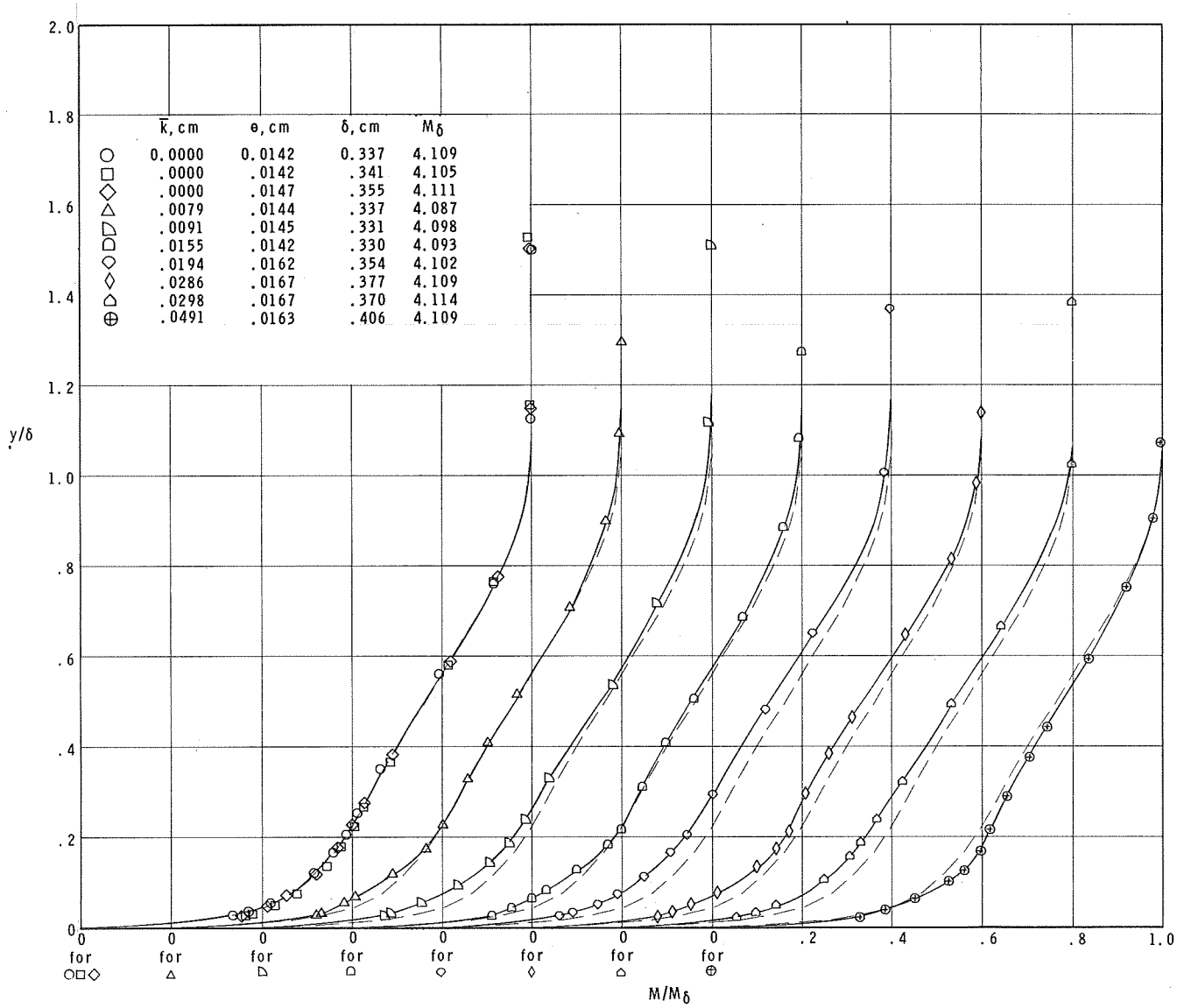

(c) x_k = 0.64 cm; w_k = 0.13 cm.

Figure 13.- Concluded.

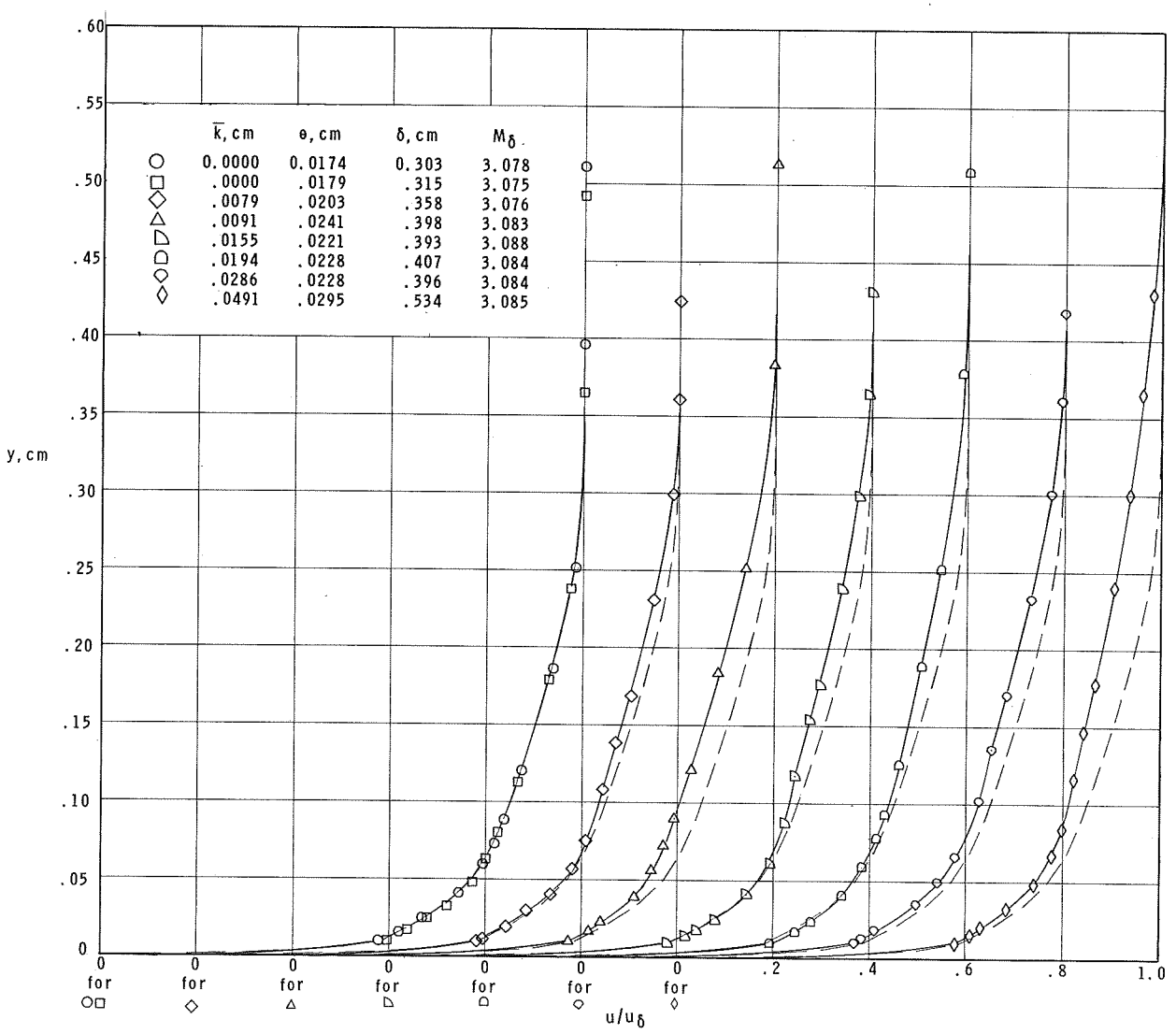

(a) x_k = 0.0 cm; w_k = 0.64 cm.

Figure 14.- Effect of trip size on boundary-layer profiles at x = 21.6 cm. u/u_δ as a function of y; M_δ = 3.

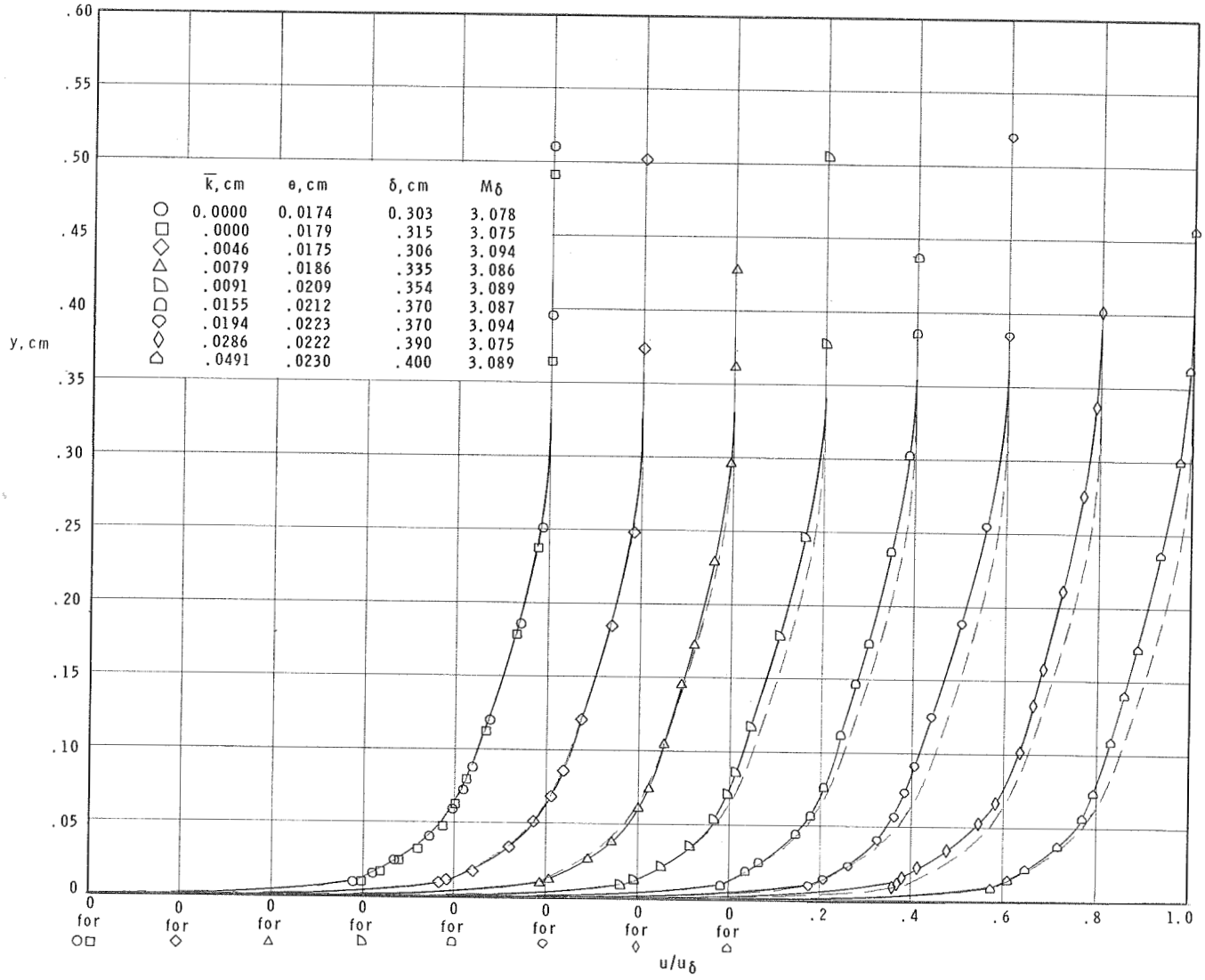

(b) x_k = 0.64 cm; w_k = 0.64 cm.

Figure 14.- Continued.

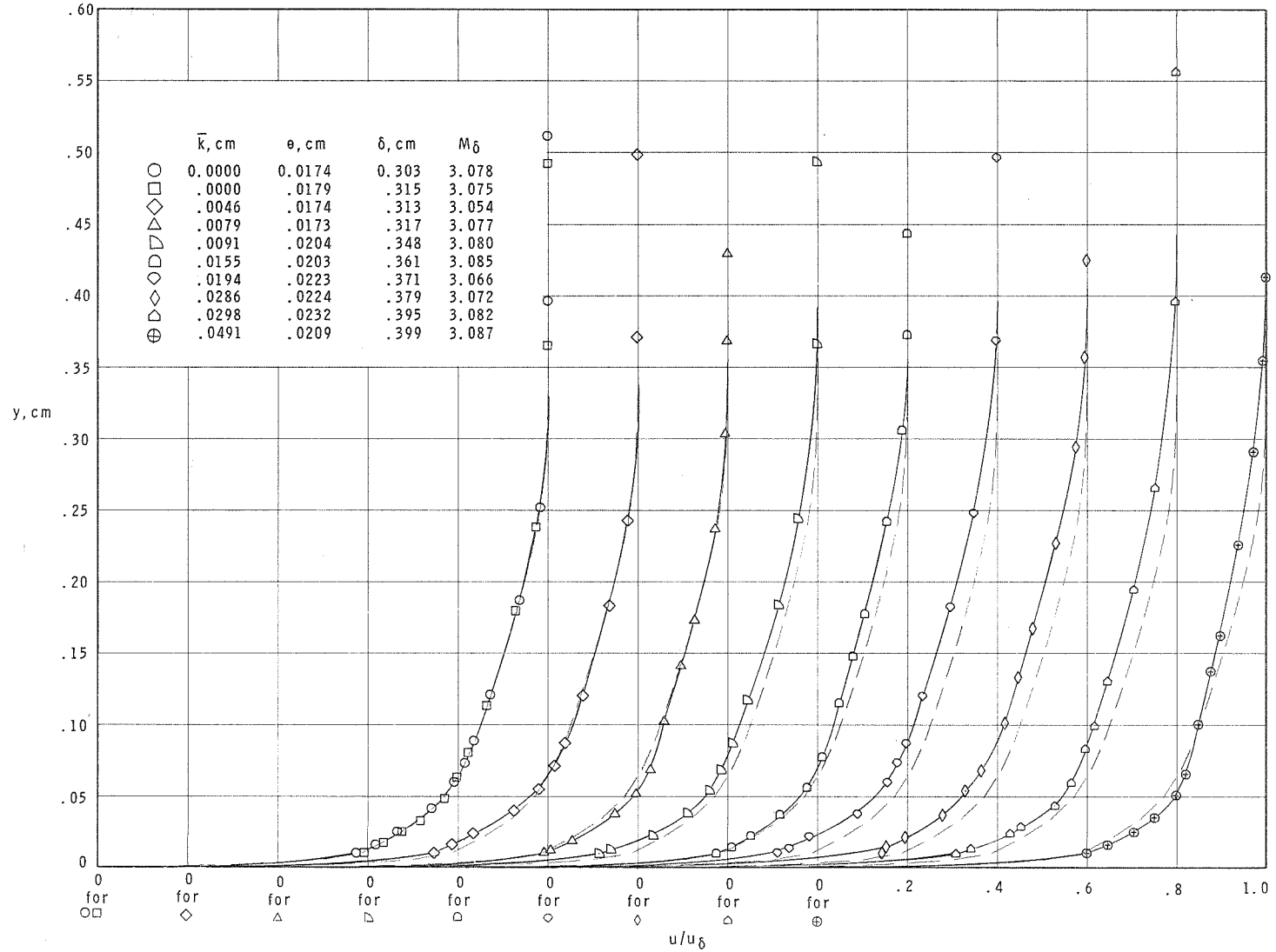

(c) x_k = 0.64 cm; w_k = 0.13 cm.

Figure 14.- Concluded.

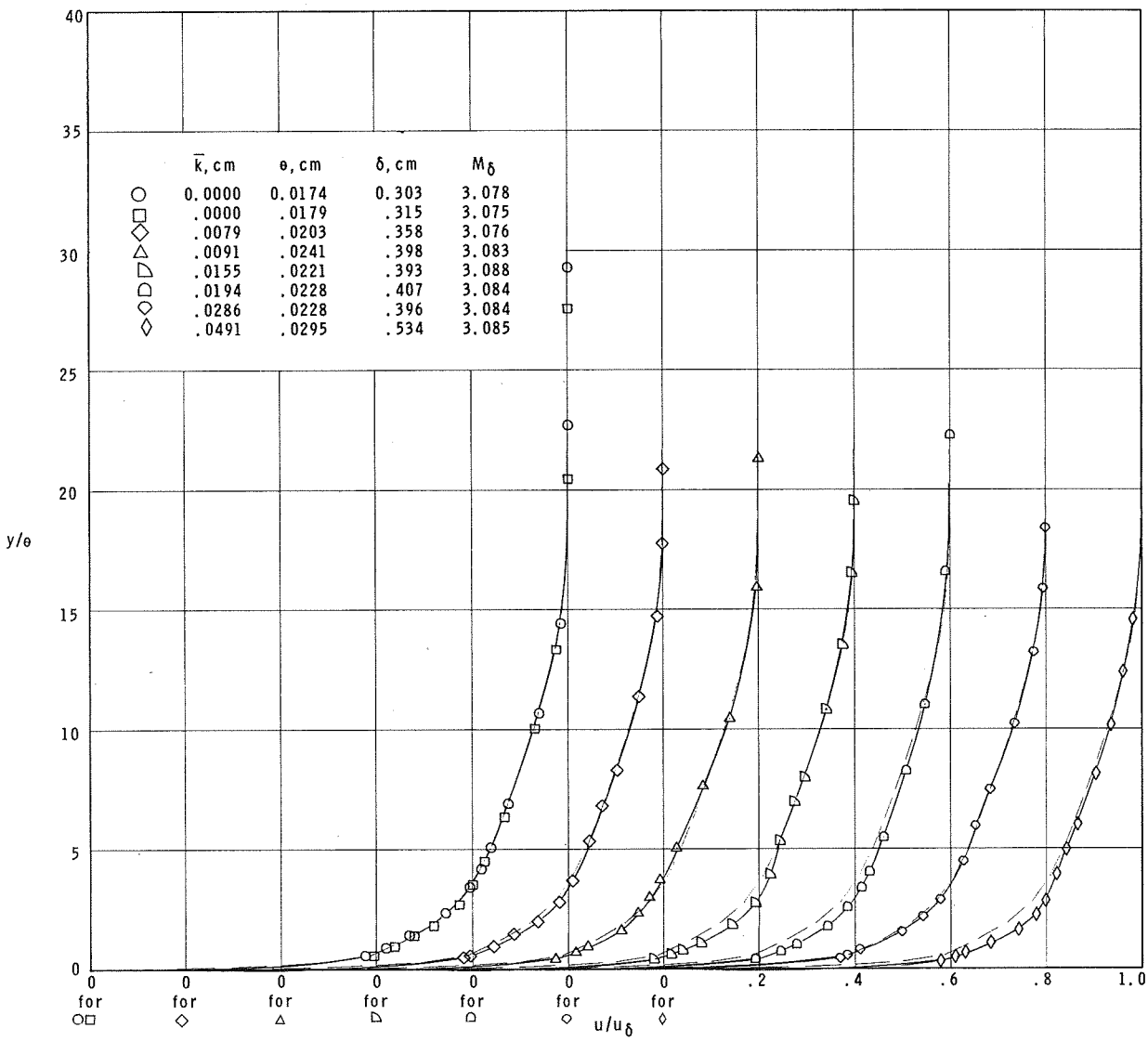

(a) x_k = 0.0 cm; w_k = 0.64 cm.

Figure 15.- Effect of trip size on boundary-layer profiles at x = 21.6 cm. u/u_δ as a function of y/θ; M_δ = 3.

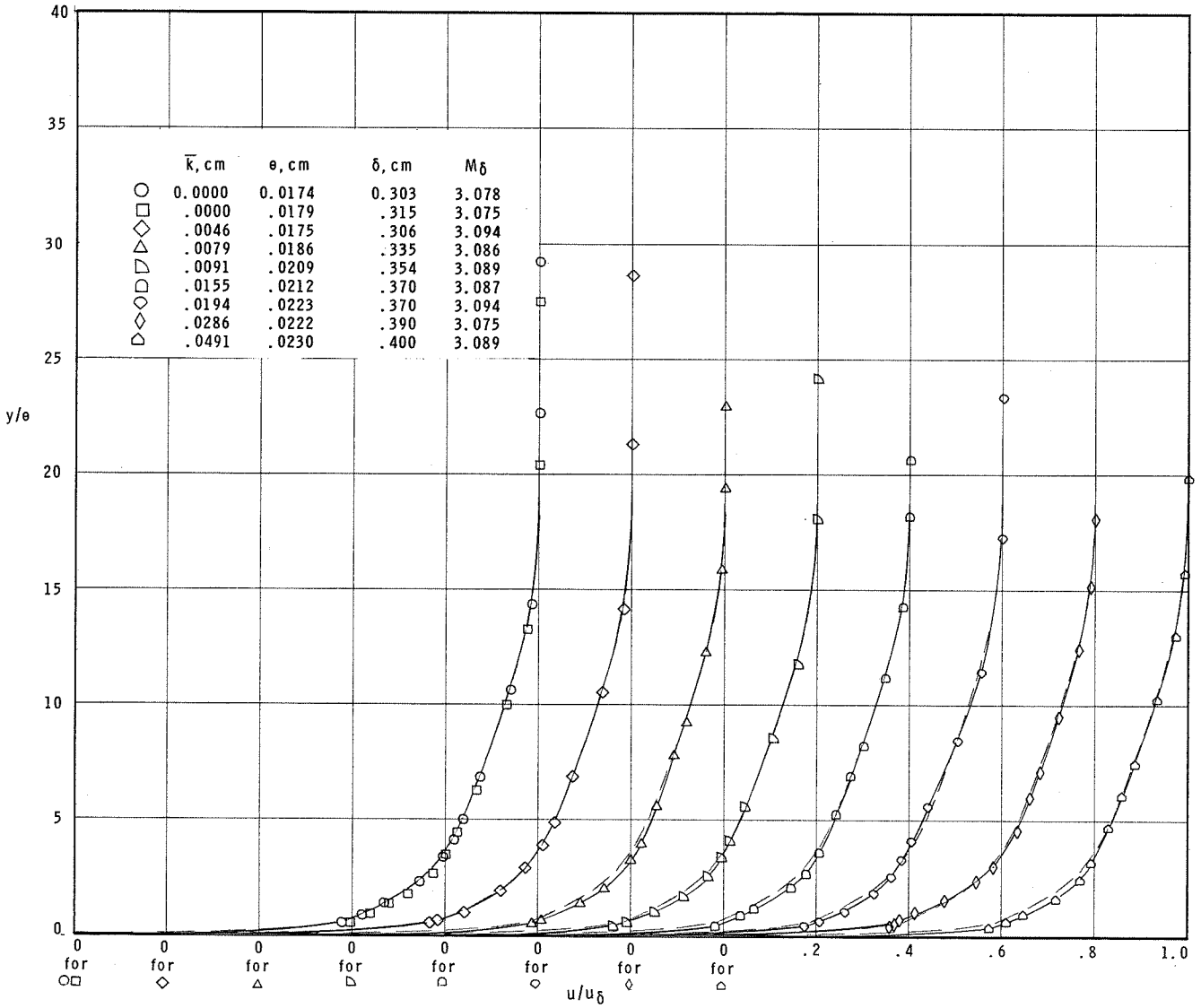

(b) x_k = 0.64 cm; w_k = 0.64 cm.

Figure 15.- Continued.

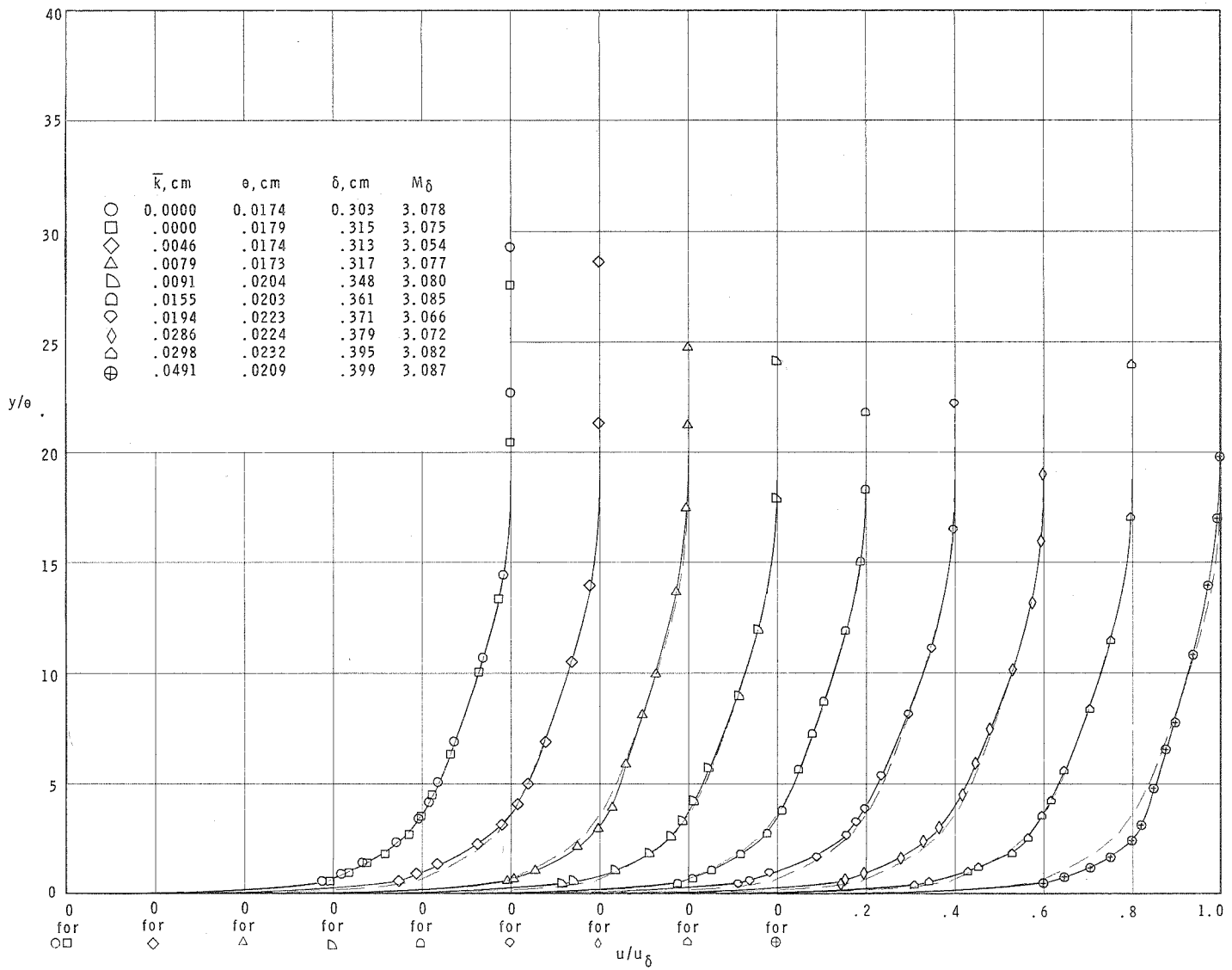

(c) x_k = 0.64 cm; w_k = 0.13 cm.

Figure 15.- Concluded.

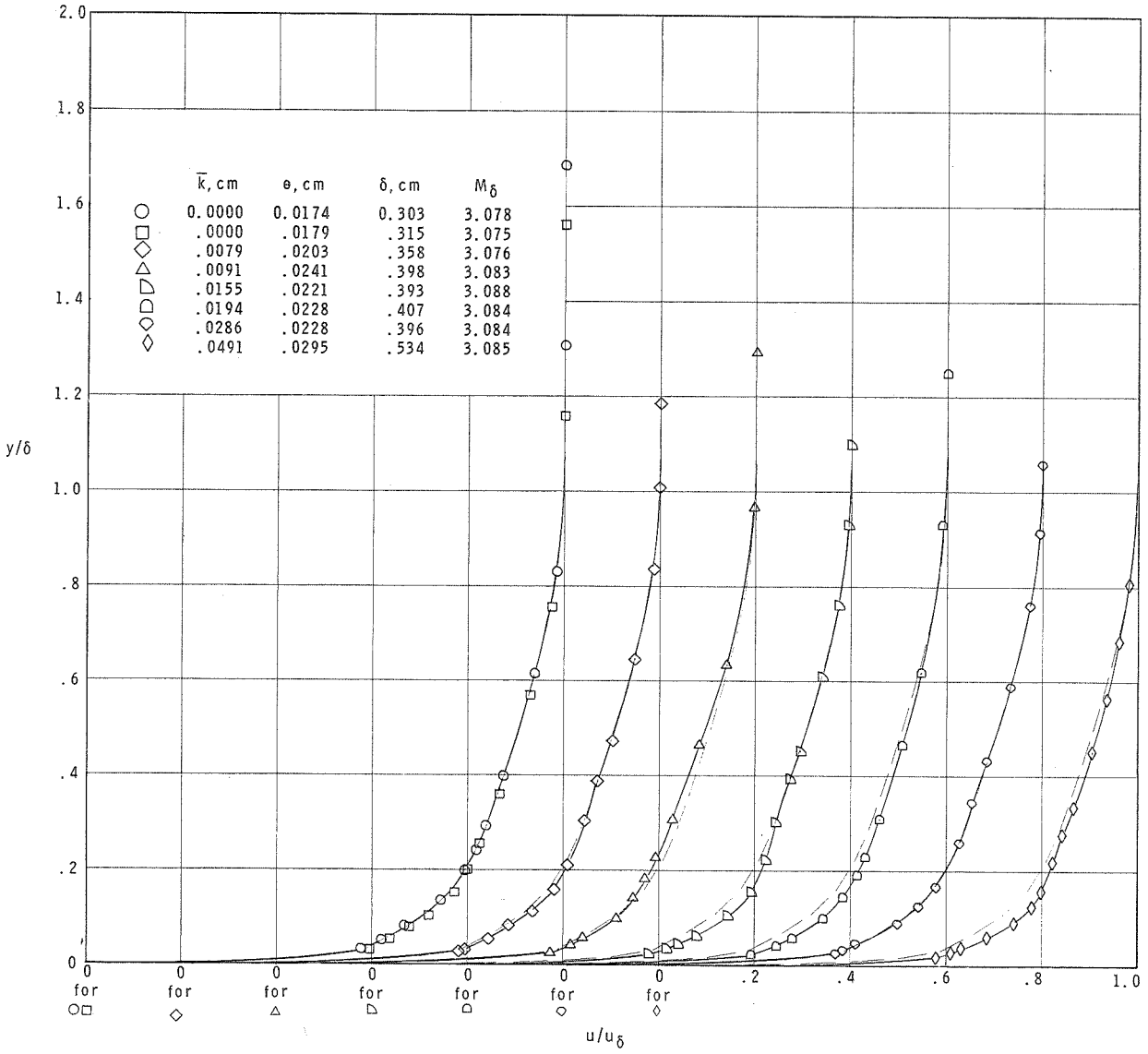

(a) x_k = 0.0 cm; w_k = 0.64 cm.

Figure 16.- Effect of trip size on boundary-layer profiles at x = 21.6 cm. u/u_δ as a function of y/δ; M_δ = 3.

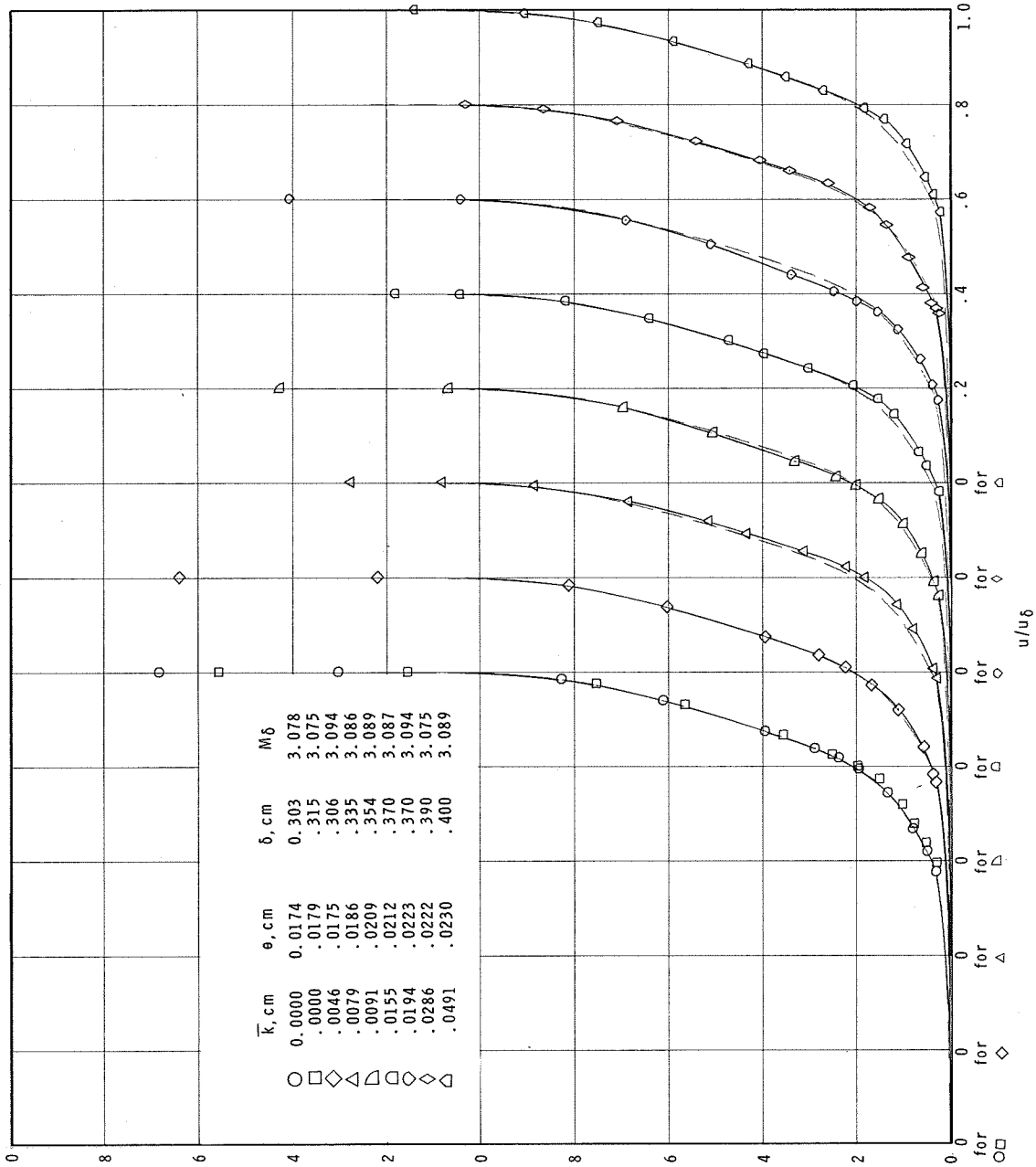

(b) x_k = 0.64 cm; w_k = 0.64 cm.

Figure 16.- Continued.

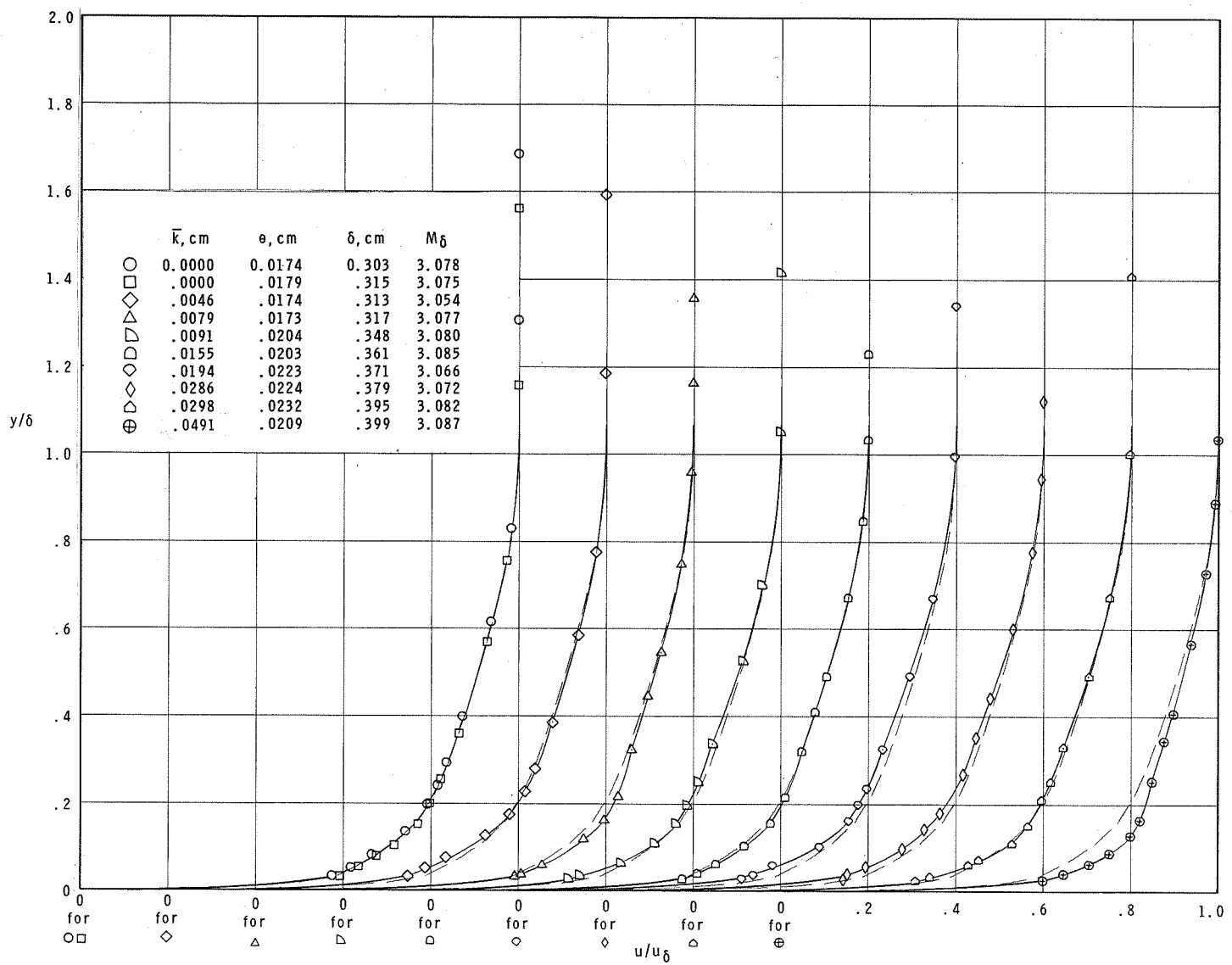

(c) x_k = 0.64 cm; w_k = 0.13 cm.

Figure 16.- Concluded.

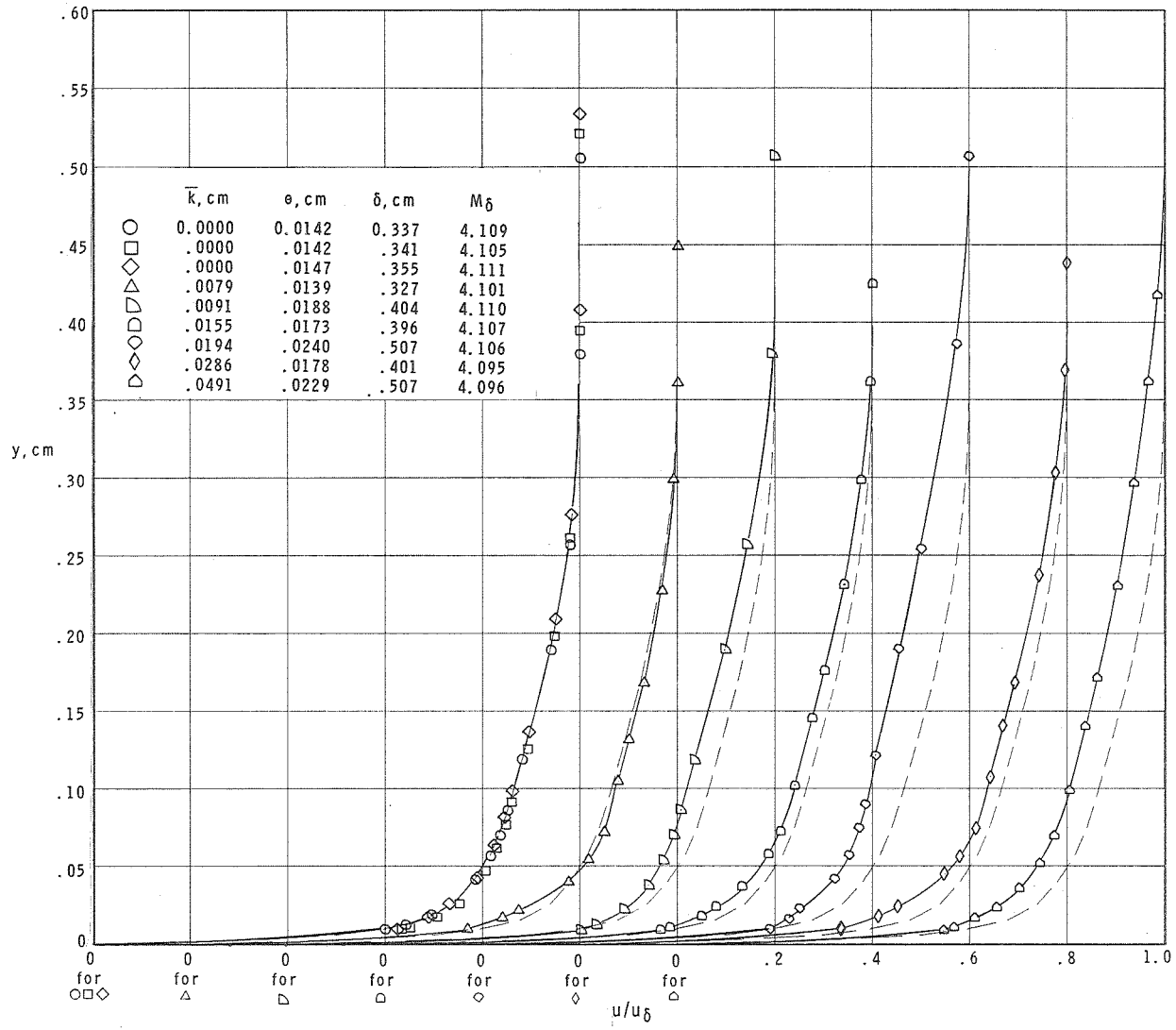

(a) x_k = 0.0 cm; w_k = 0.64 cm.

Figure 17.- Effect of trip size on boundary-layer profiles at x = 21.6 cm. u/u_δ as a function of y; M_δ = 4.

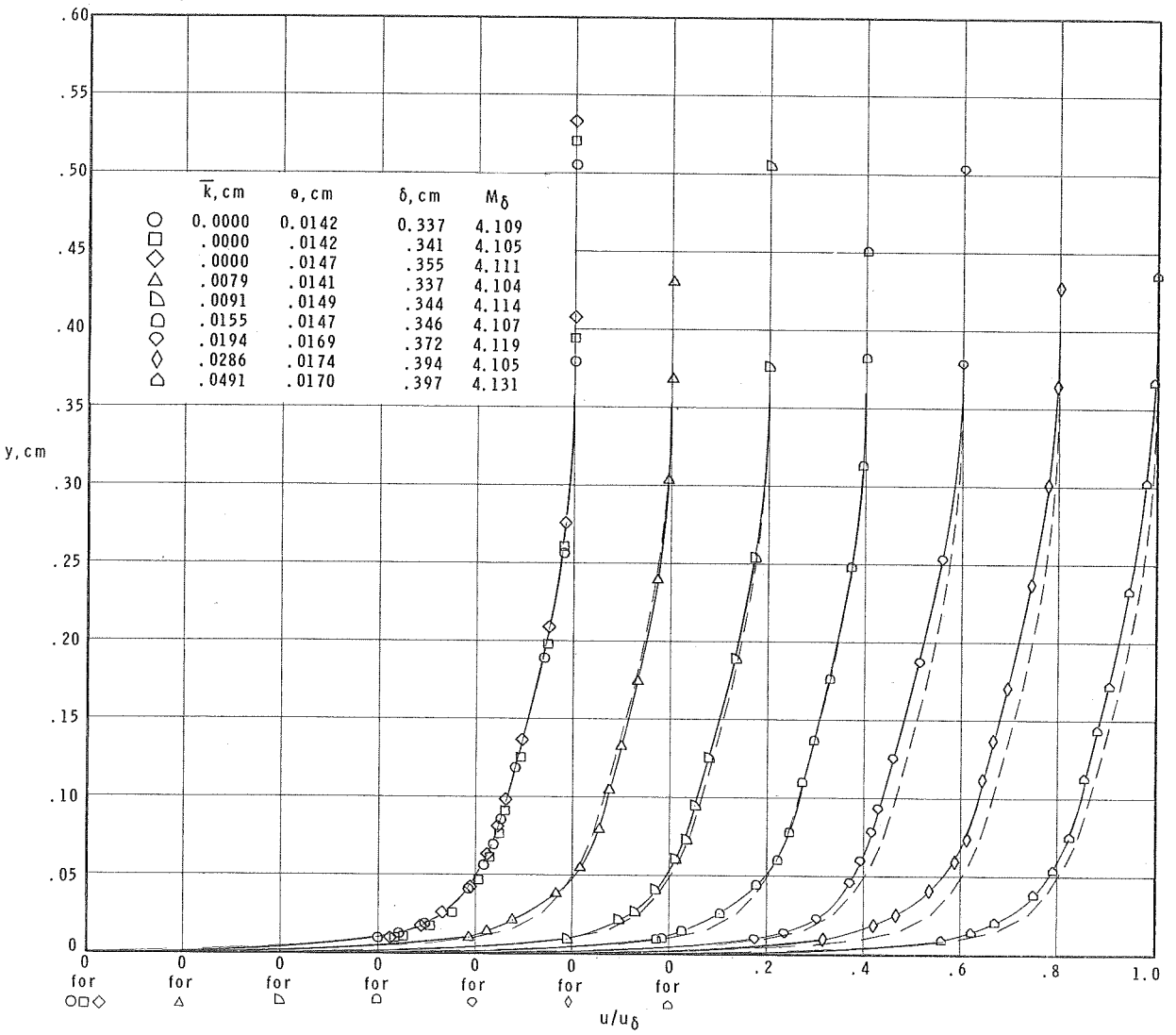

(b) x_k = 0.64 cm; w_k = 0.64 cm.

Figure 17.- Continued.

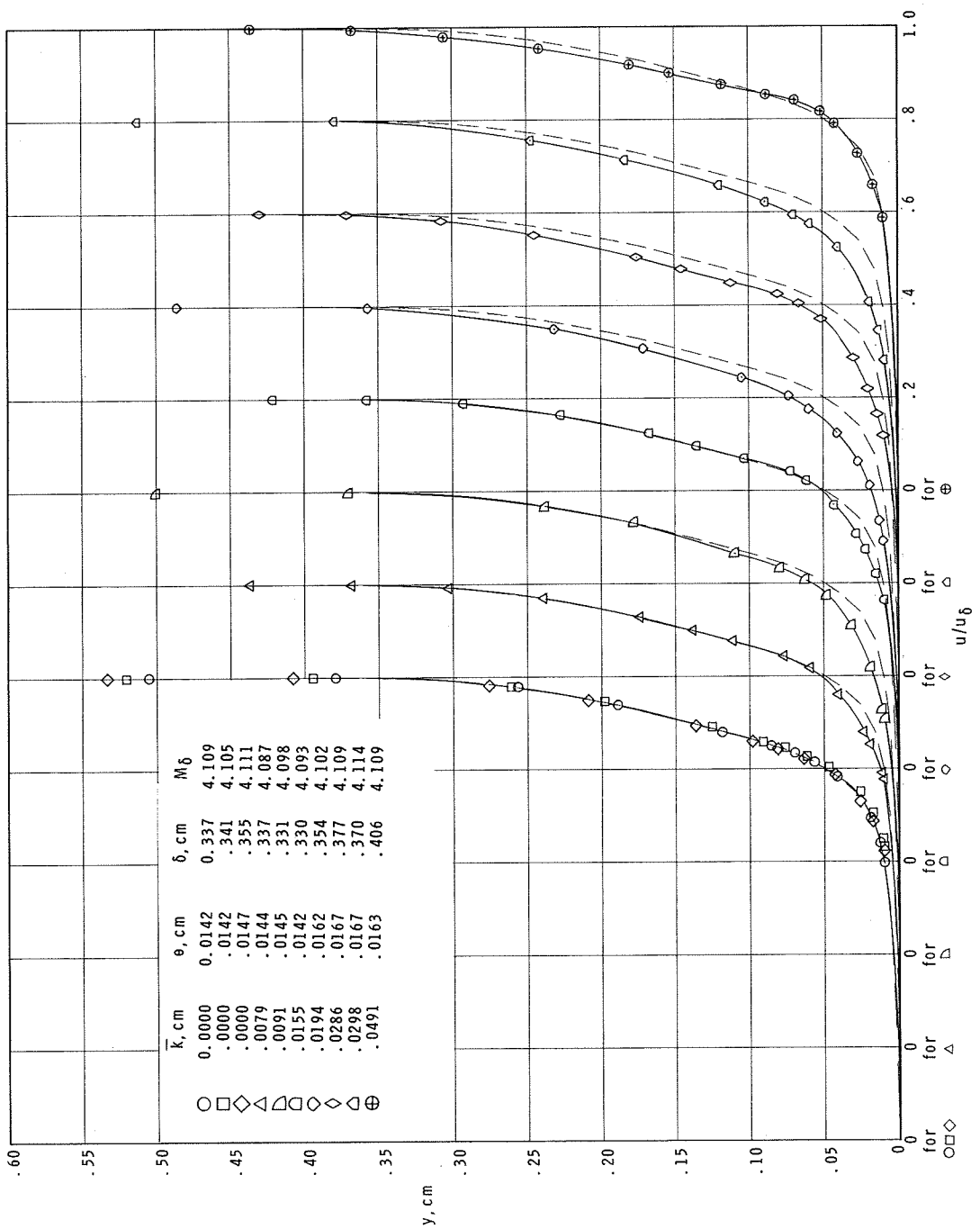

(c) x_k = 0.64 cm; w_k = 0.13 cm.

Figure 17.- Concluded.

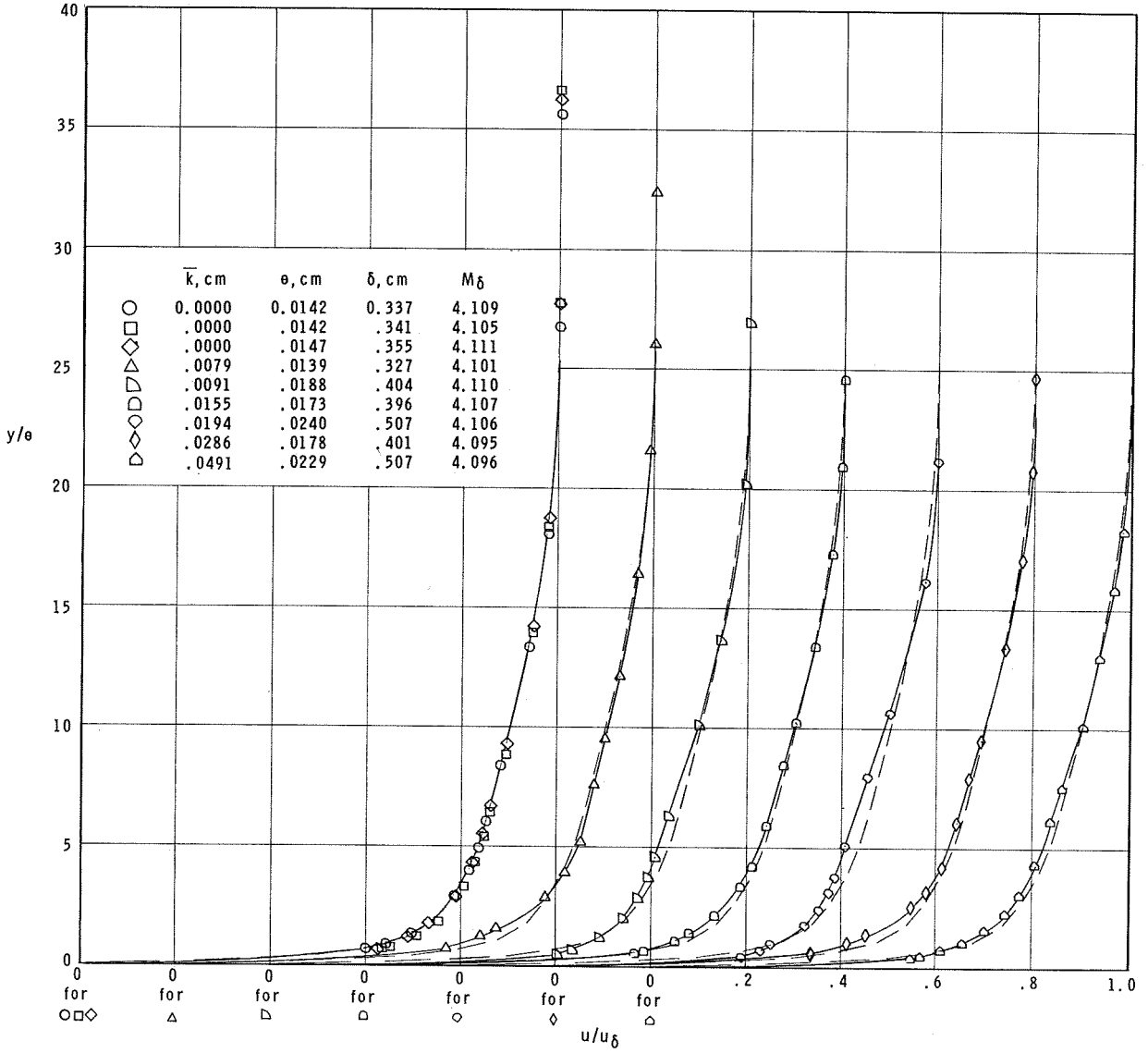

(a) x_k = 0.0 cm; w_k = 0.64 cm.

Figure 18.- Effect of trip size on boundary-layer profiles at x = 21.6 cm. u/u_δ as a function of y/θ; M_δ = 4.

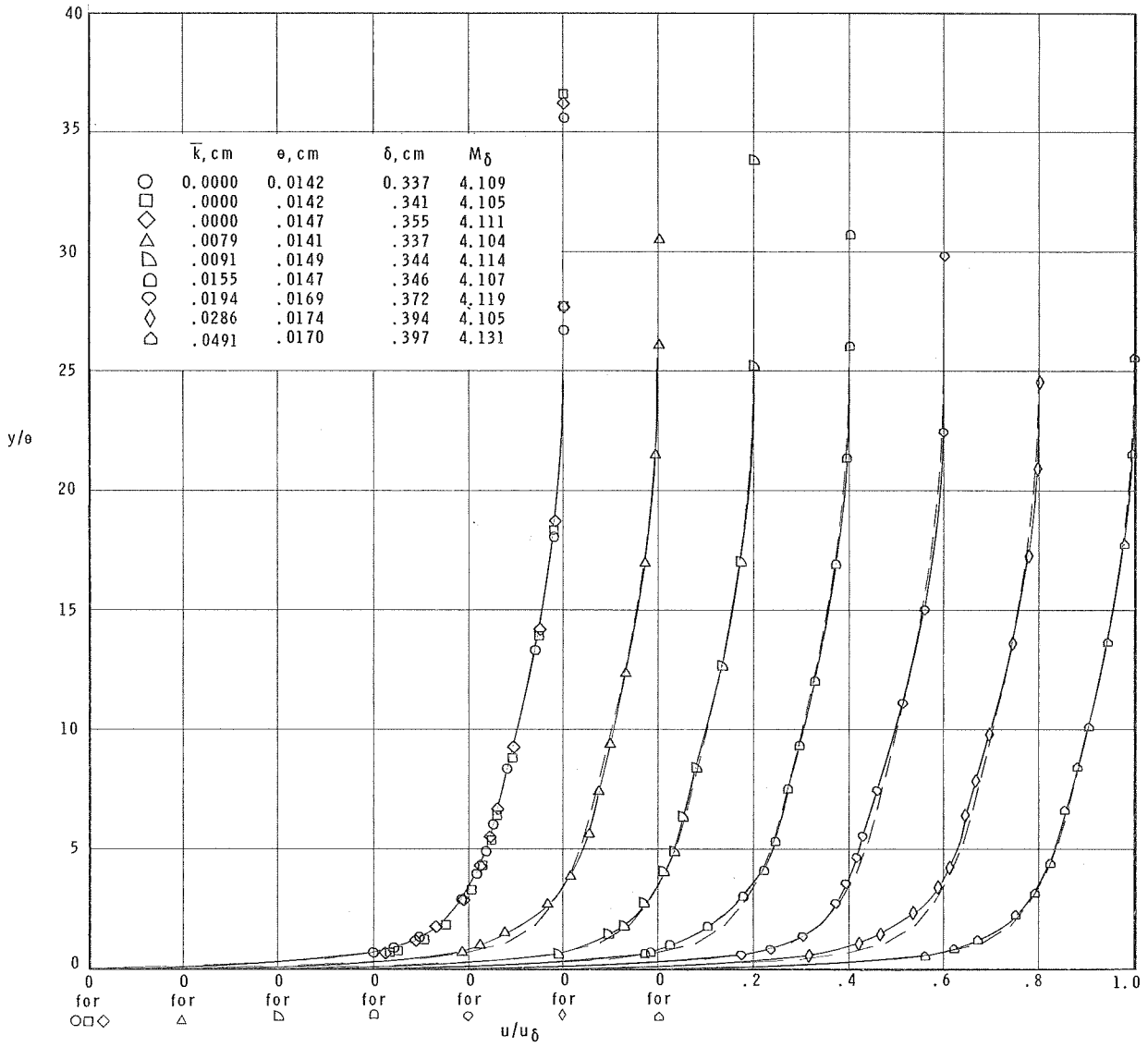

(b) x_k = 0.64 cm; w_k = 0.64 cm.

Figure 18.- Continued.

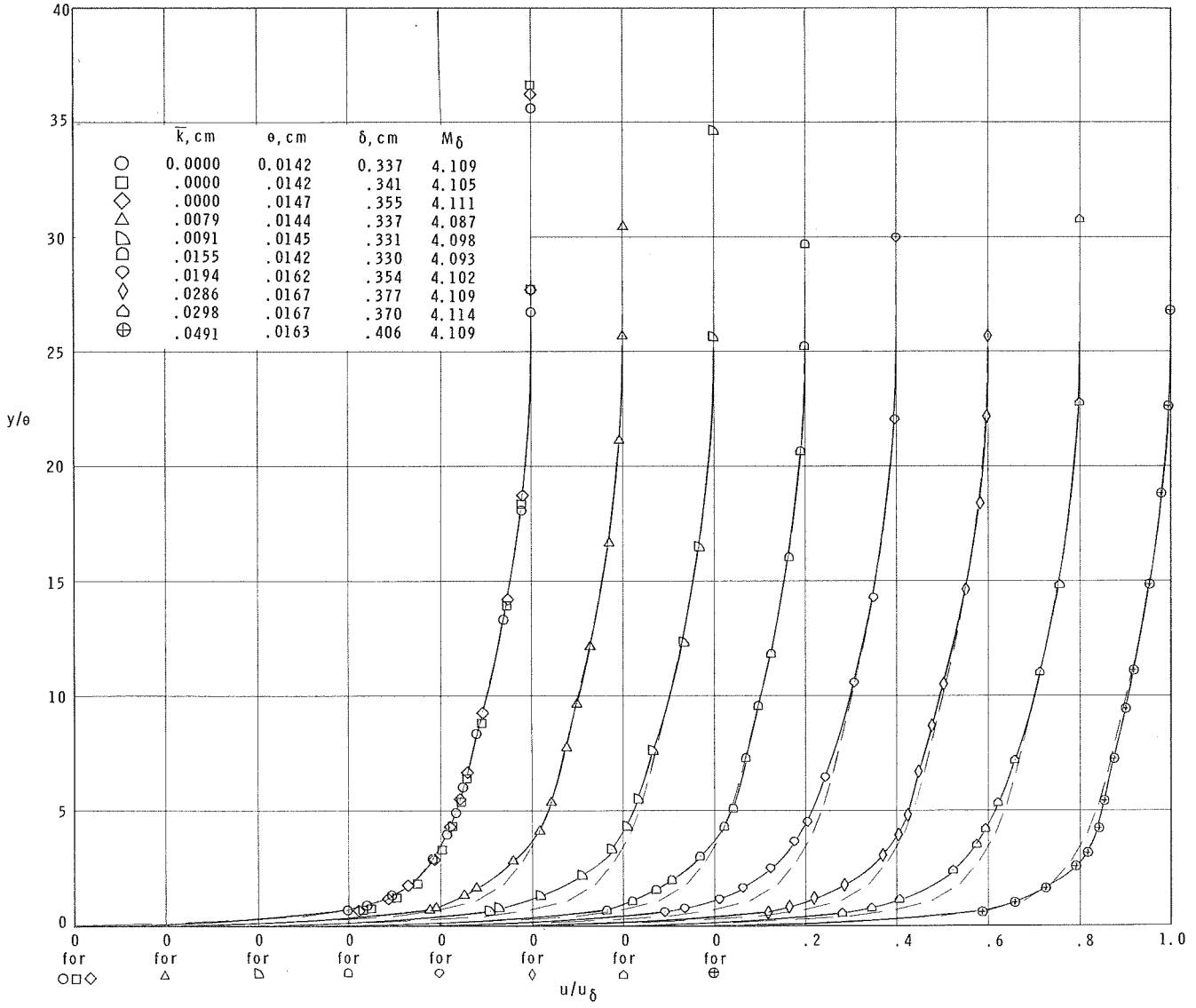

(c) x_k = 0.64 cm; w_k = 0.13 cm.

Figure 18.- Concluded.

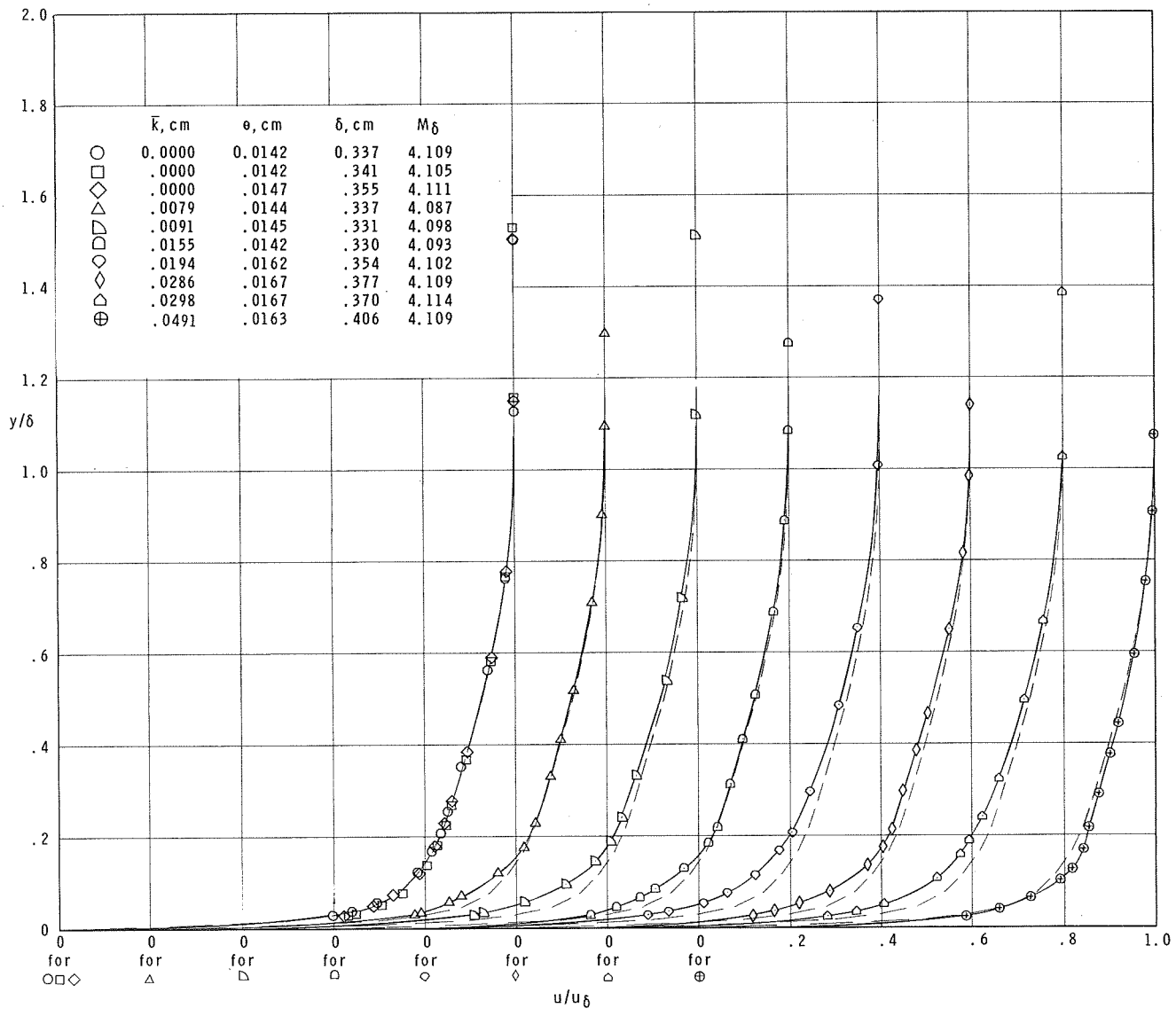

(a) x_k = 0.0 cm; w_k = 0.64 cm.

Figure 19.- Effect of trip size on boundary-layer profiles at x = 21.6 cm. u/u_δ as a function of y/δ; M_δ = 4.

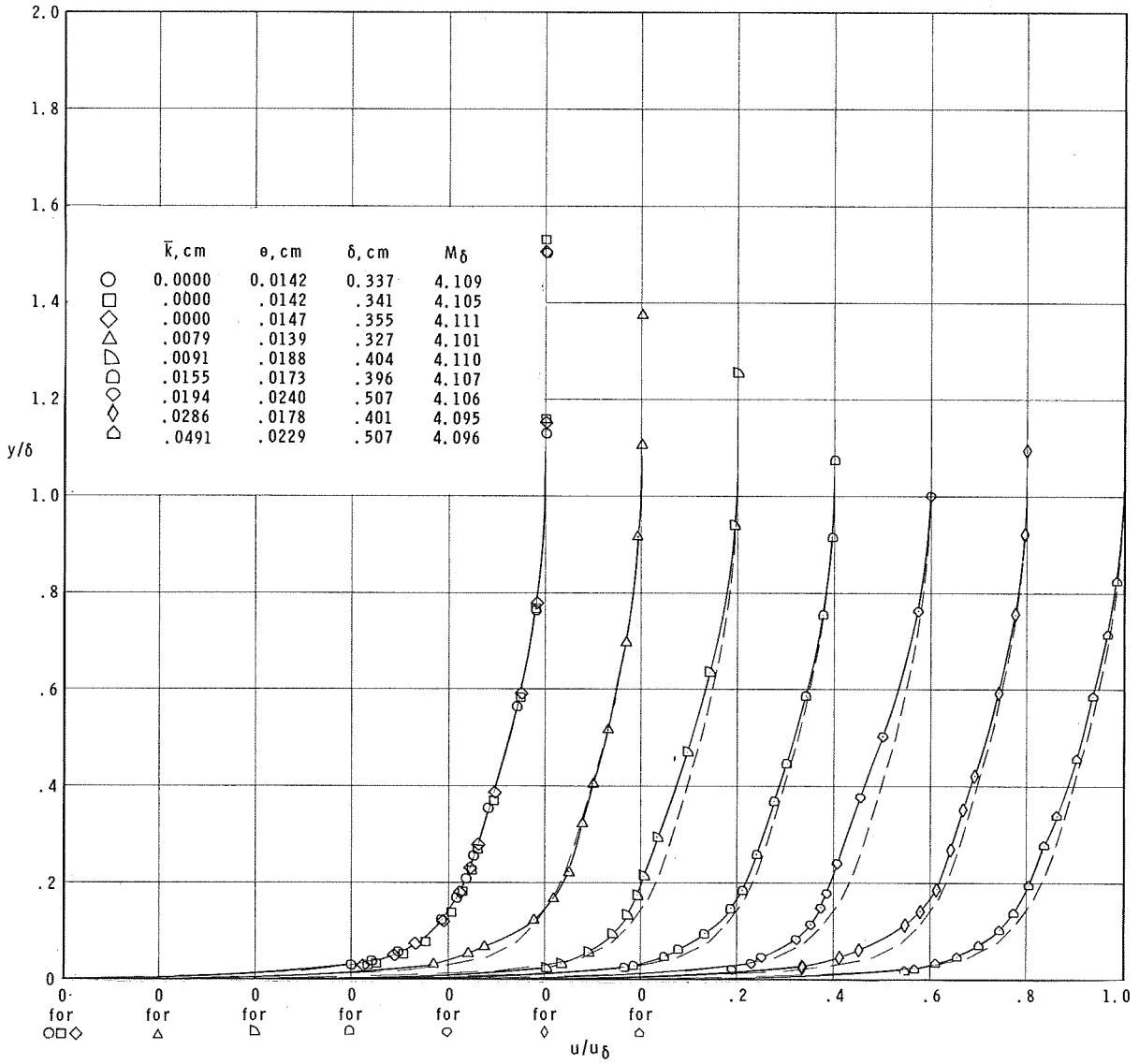

(b) x_k = 0.64 cm; w_k = 0.64 cm.

Figure 19.- Continued.

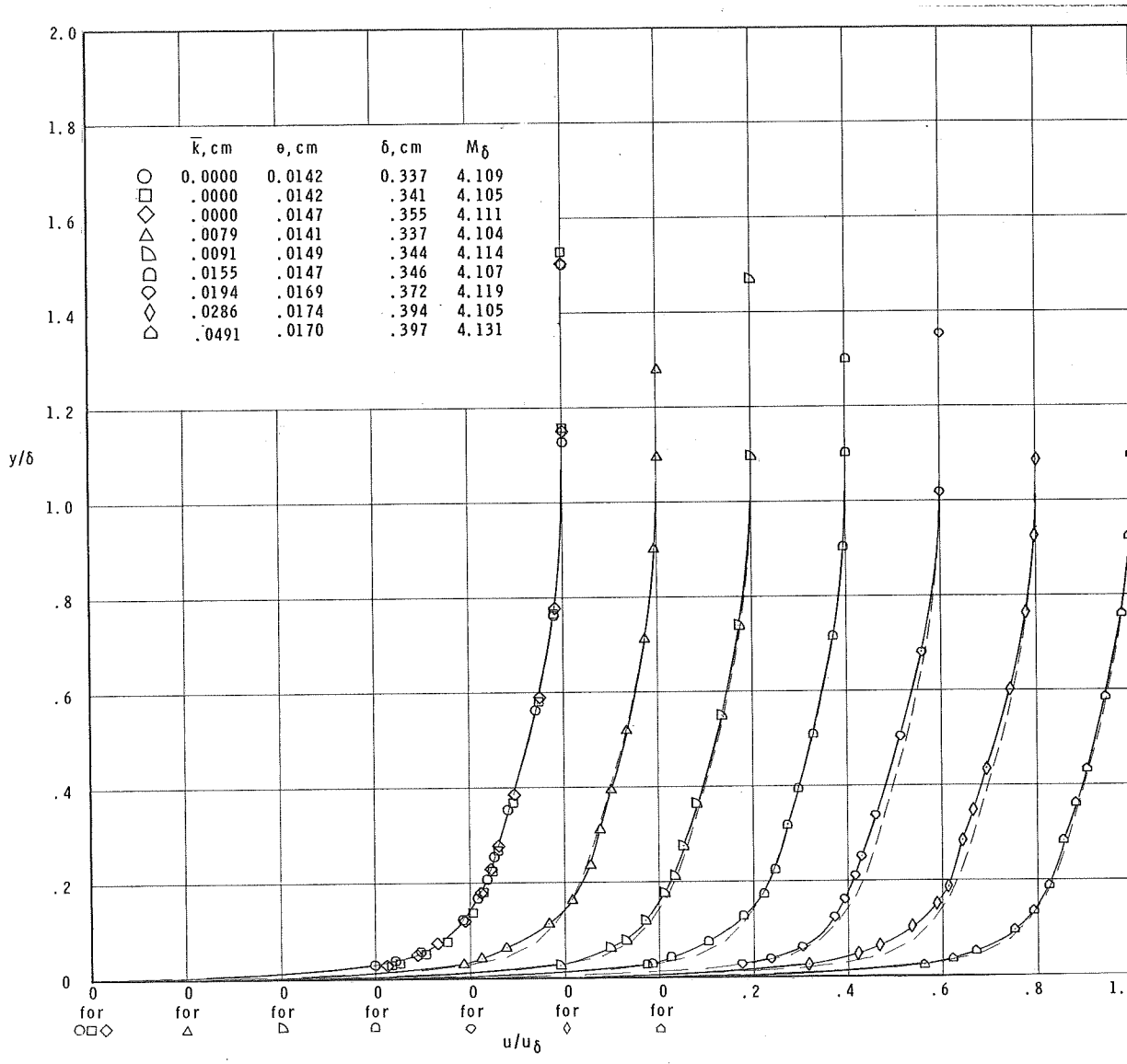

(c) x_k = 0.64 cm; w_k = 0.13 cm.

Figure 19.- Concluded.

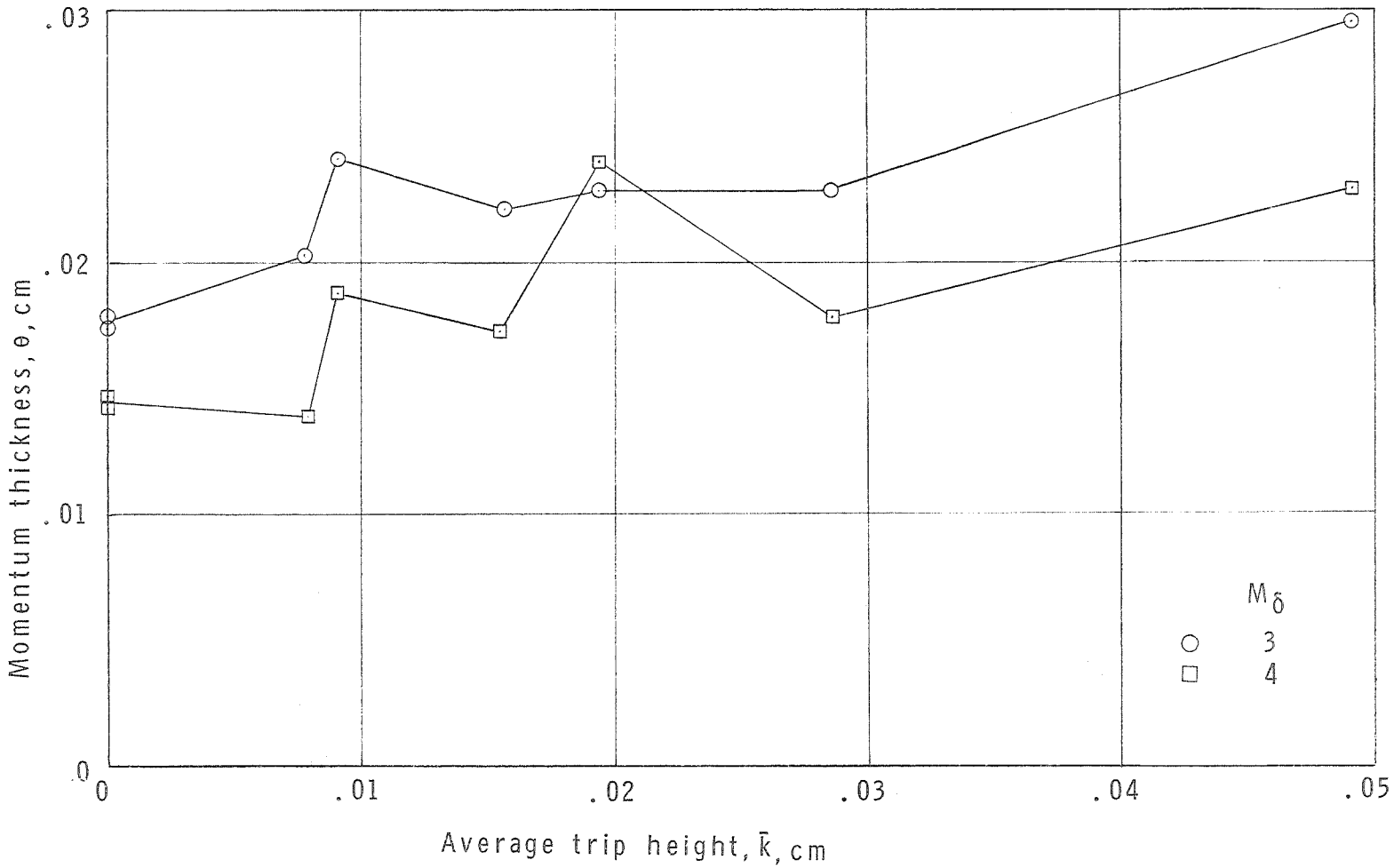

(a) x_k = 0.0 cm; w_k = 0.64 cm.

Figure 20.- Effect of trip height on boundary-layer momentum thickness.

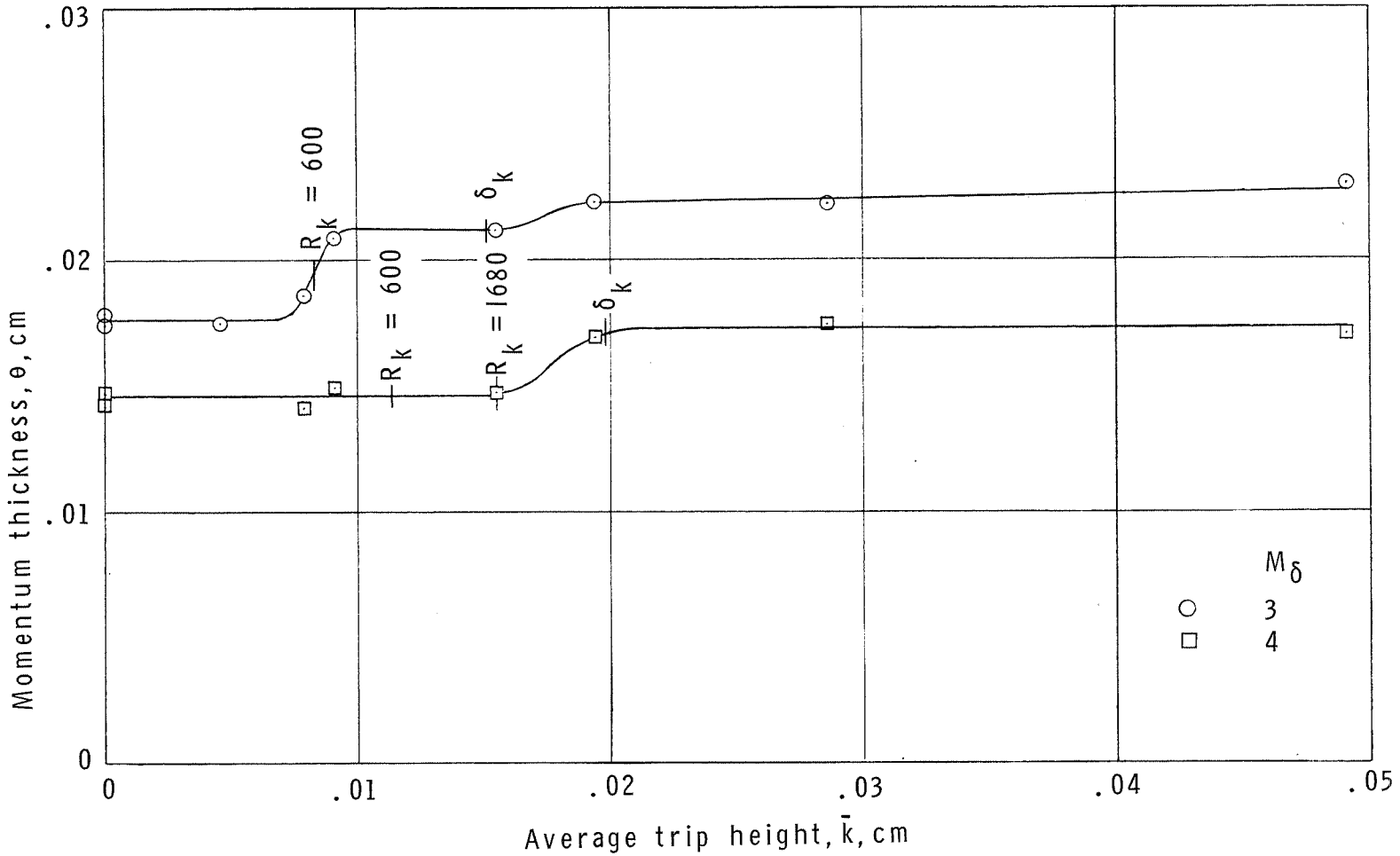

(b) x_k = 0.64 cm; w_k = 0.64 cm.

Figure 20.- Continued.

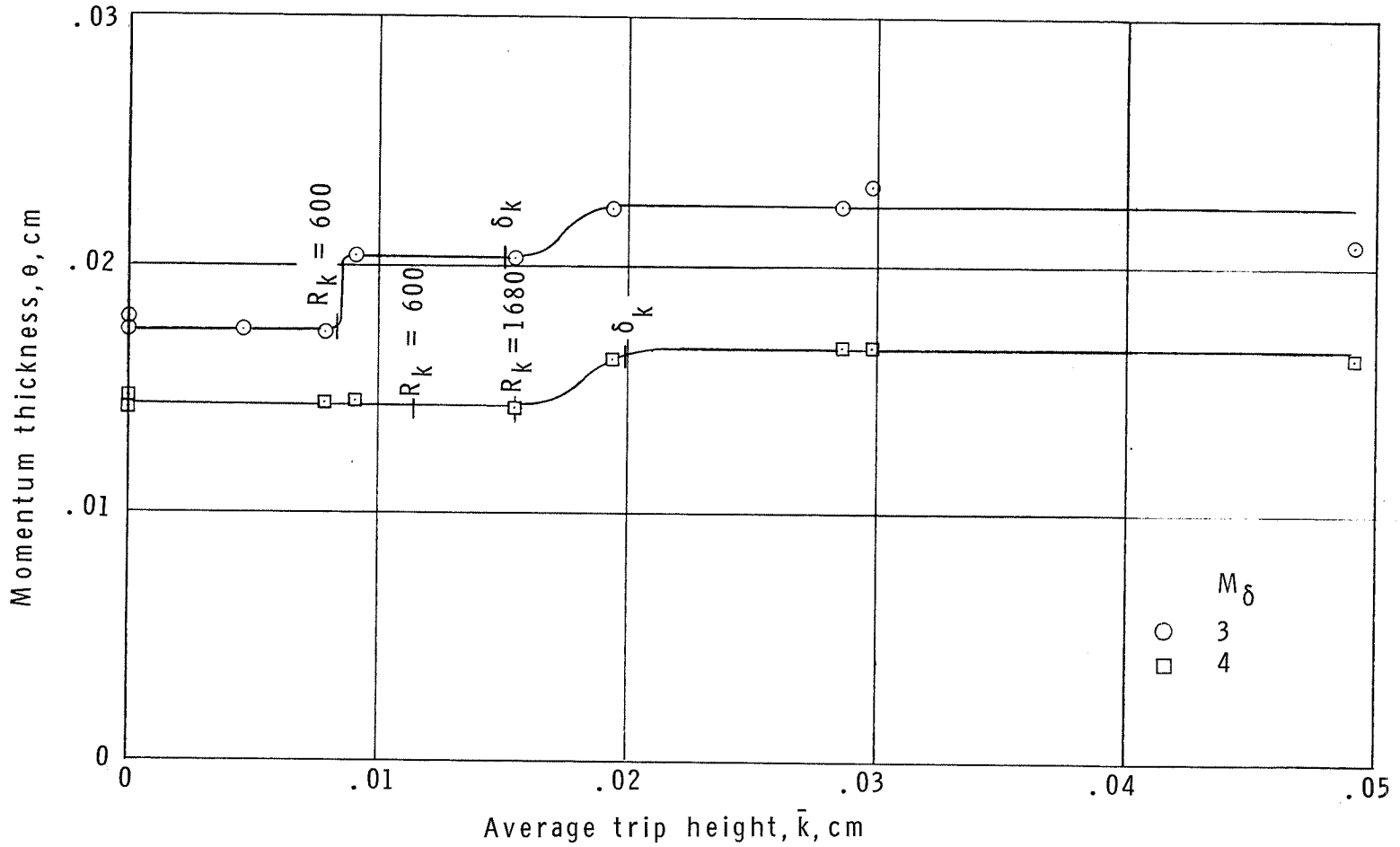

(c) x_k = 0.64 cm; w_k = 0.13 cm.

Figure 20.- Concluded.

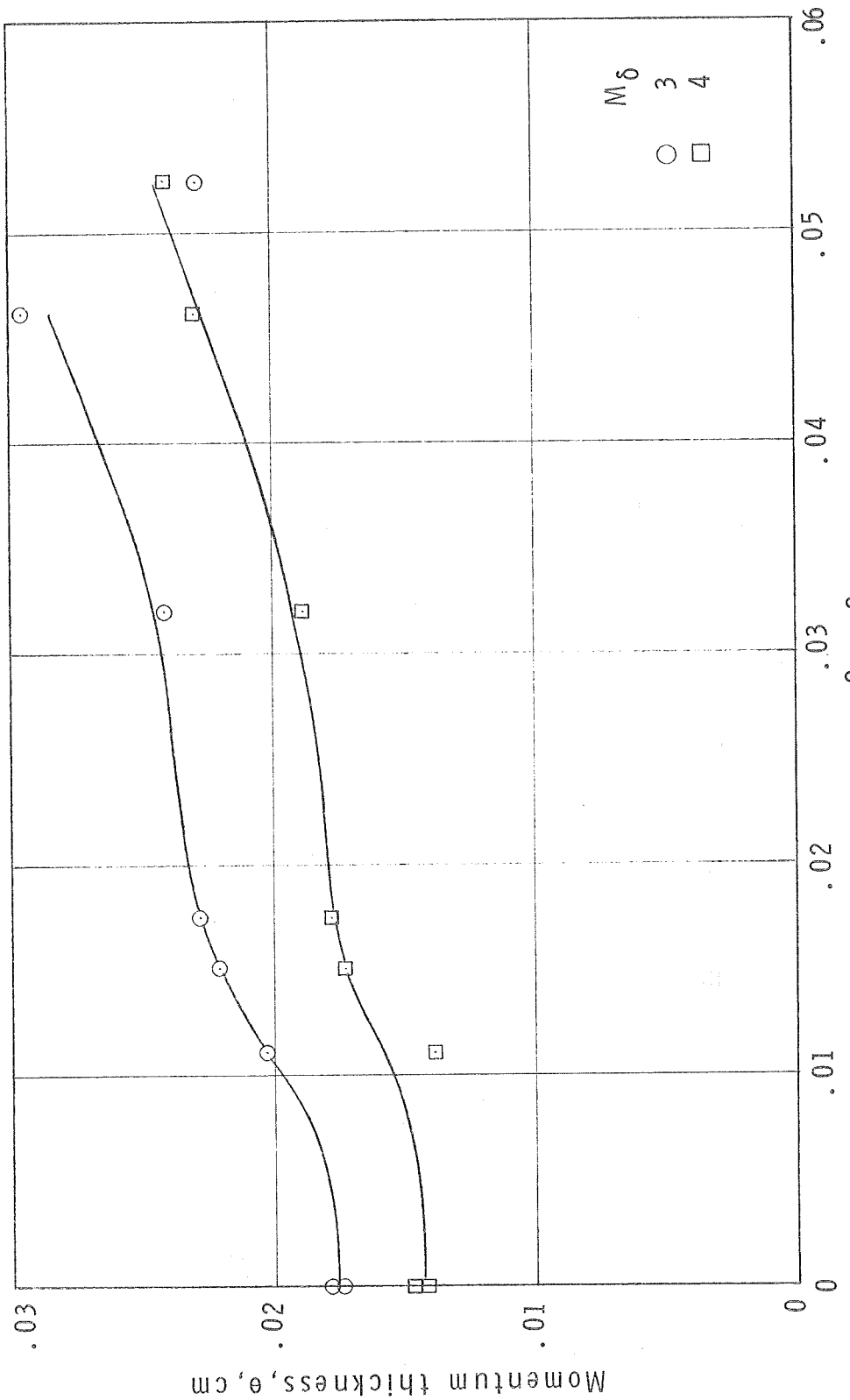

Figure 21.- Momentum thickness as a function of frontal area parameter $n\bar{k}^2$. x_k = 0.0 cm; w_k = 0.64 cm.

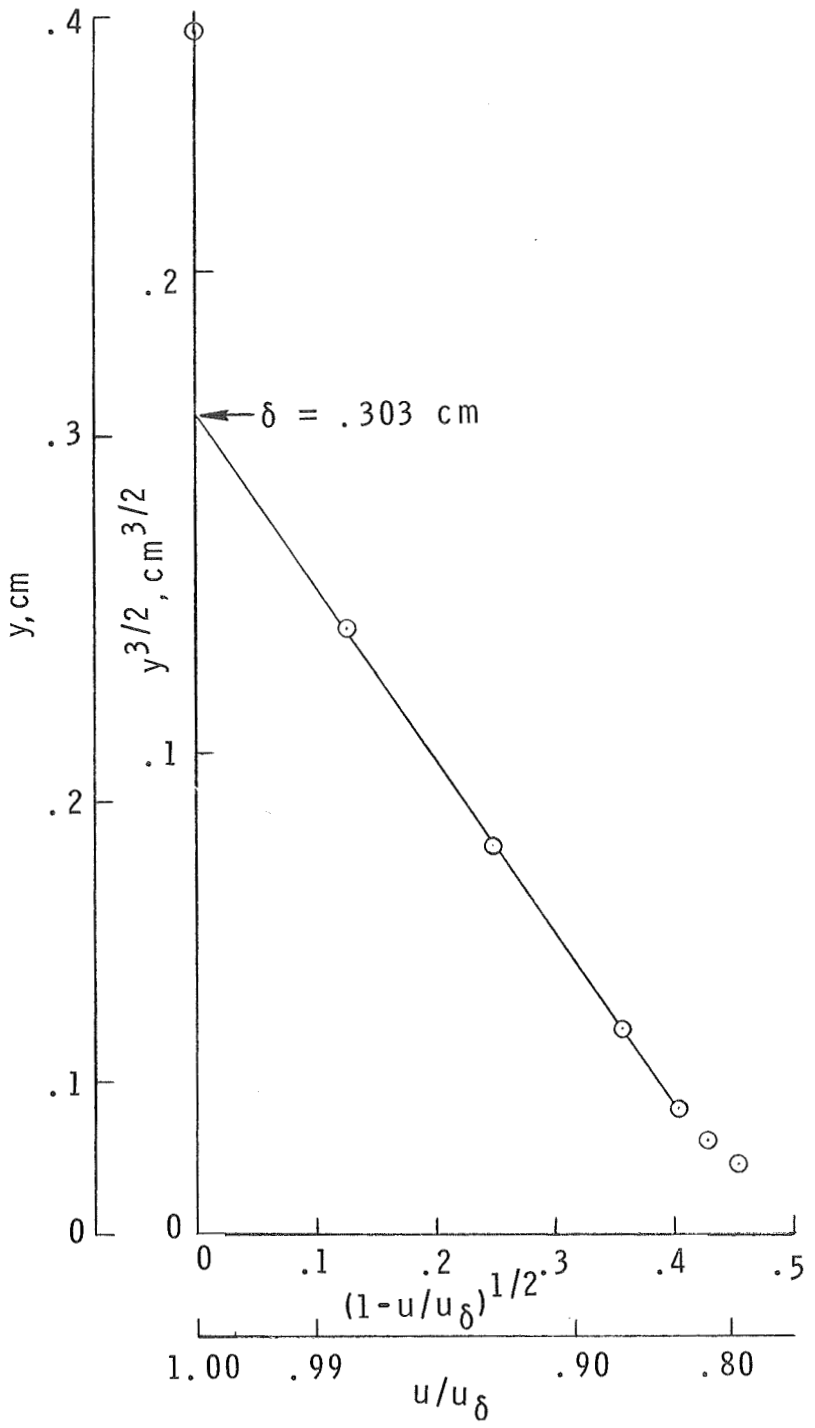

(a) Method used in this report. $y^{3/2}$ as a function of $\left(1 - \frac{u}{u_\delta}\right)^{1/2}$.

Figure 22.- Comparison of various methods of determining δ.

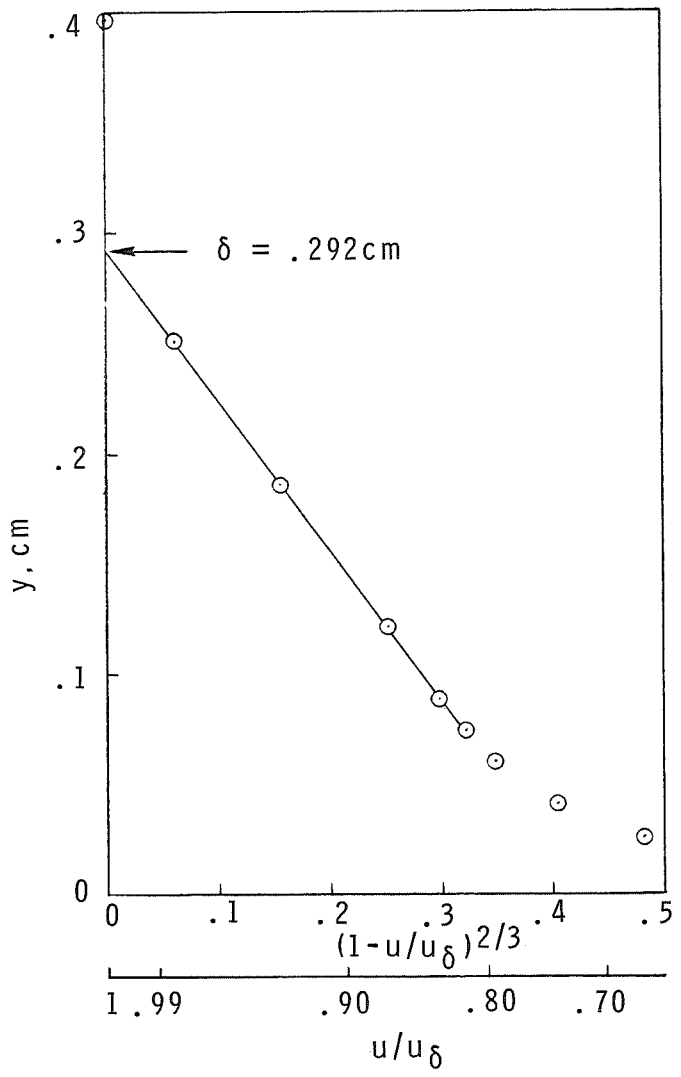

(b) Coles' method. y as a function of $\left(1 - \frac{u}{u_\delta}\right)^{2/3}$.

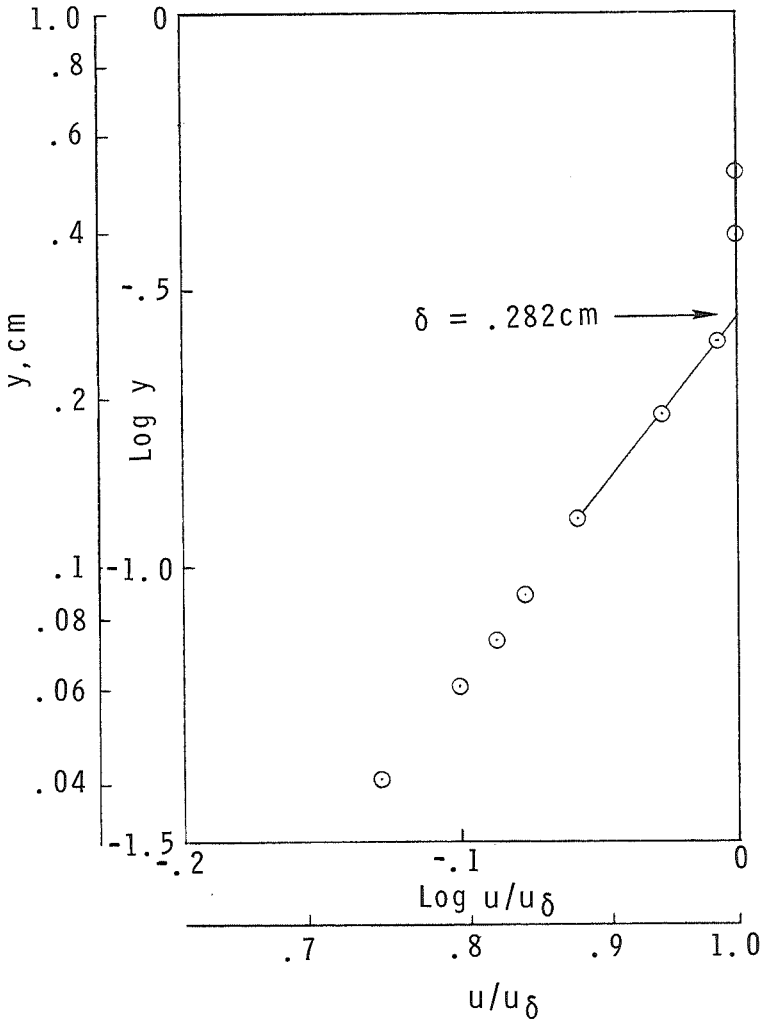

(c) Log method. Log y as a function of Log u/u_δ.

Figure 22.- Concluded.

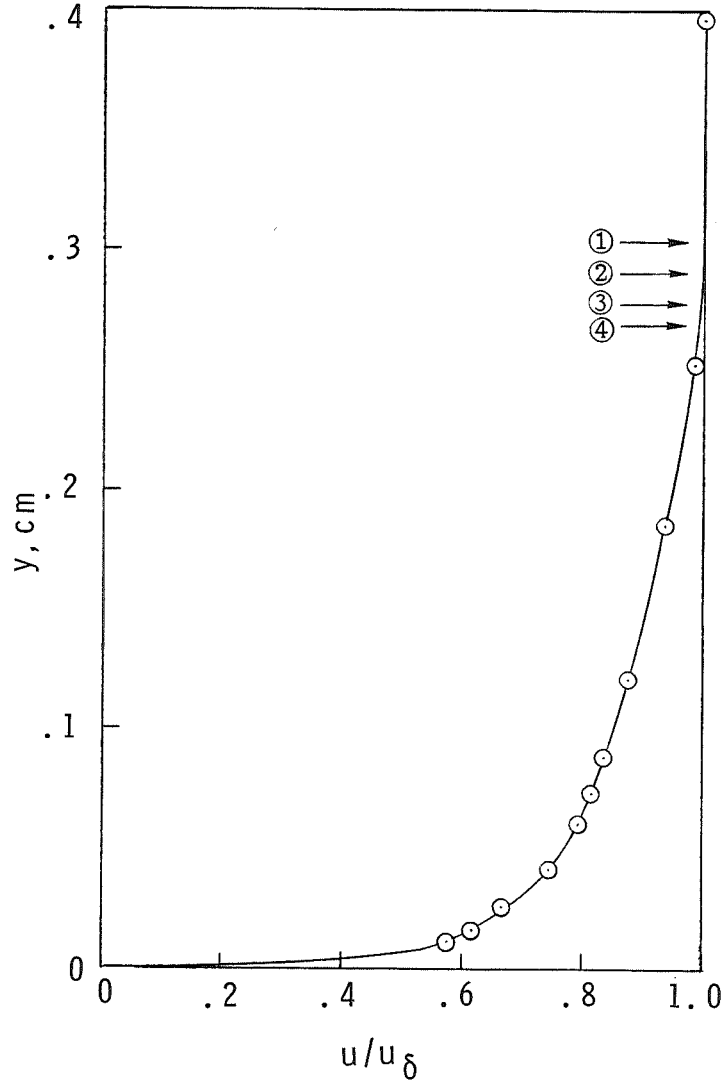

(a) Velocity profile.

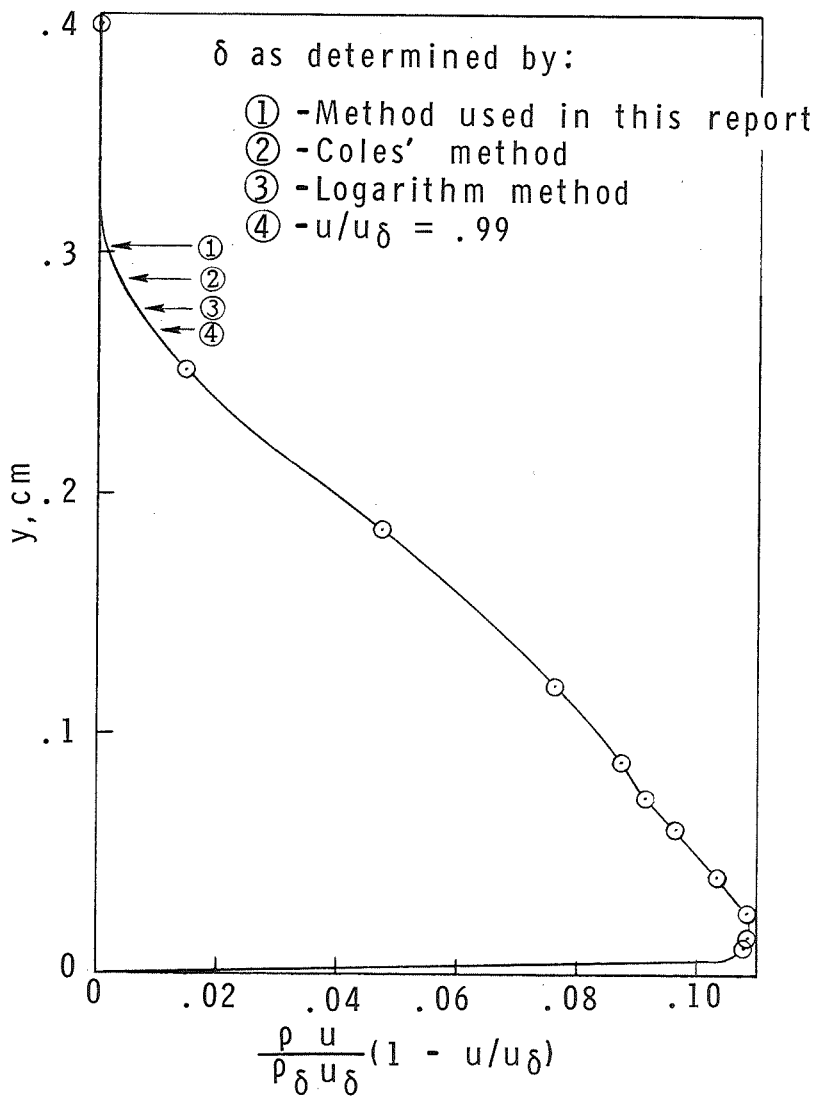

(b) Momentum-loss profile.

Figure 23.- Comparison of various δ's with velocity and momentum-loss profiles.

"The aeronautical and space activities of the United States shall be conducted so as to contribute . . . to the expansion of human knowledge of phenomena in the atmosphere and space. The Administration shall provide for the widest practicable and appropriate dissemination of information concerning its activities and the results thereof."

—NATIONAL AERONAUTICS AND SPACE ACT OF 1958

NASA SCIENTIFIC AND TECHNICAL PUBLICATIONS

TECHNICAL REPORTS: Scientific and technical information considered important, complete, and a lasting contribution to existing knowledge.

TECHNICAL NOTES: Information less broad in scope but nevertheless of importance as a contribution to existing knowledge.

TECHNICAL MEMORANDUMS: Information receiving limited distribution because of preliminary data, security classification, or other reasons.

CONTRACTOR REPORTS: Scientific and technical information generated under a NASA contract or grant and considered an important contribution to existing knowledge.

TECHNICAL TRANSLATIONS: Information published in a foreign language considered to merit NASA distribution in English.

SPECIAL PUBLICATIONS: Information derived from or of value to NASA activities. Publications include conference proceedings, monographs, data compilations, handbooks, sourcebooks, and special bibliographies.

TECHNOLOGY UTILIZATION PUBLICATIONS: Information on technology used by NASA that may be of particular interest in commercial and other non-aerospace applications. Publications include Tech Briefs, Technology Utilization Reports and Notes, and Technology Surveys.

Details on the availability of these publications may be obtained from:

SCIENTIFIC AND TECHNICAL INFORMATION DIVISION

NATIONAL AERONAUTICS AND SPACE ADMINISTRATION

Washington, D.C. 20546